New physics with low missing energy: identification and discrimination at the LHC

By

Satyanarayan Mukhopadhyay

Harish-Chandra Research Institute, Allahabad

Thesis submitted to the
Board of Studies in Physical Science Discipline
In partial fulfilment of the requirements
For the degree of
DOCTOR OF PHILOSOPHY
of

Homi Bhabha National Institute

March, 2012

Certificate

This is to certify that the Ph.D. thesis titled "New physics with low missing energy: identification and discrimination at the LHC" submitted by Satyanarayan Mukhopadhyay is a record of bona fide research work done under my supervision. It is further certified that the thesis represents independent work by the candidate and collaboration was necessitated by the nature and scope of the problems dealt with.

Date:

Biswarup Mukhopadhyaya
Thesis Adviser

Declaration

This thesis is a presentation of my original research work. Whenever contributions of others are involved, every effort is made to indicate this clearly, with due reference to the literature and acknowledgement of collaborative research and discussions.

The work is original and has not been submitted earlier as a whole or in part for a degree or diploma at this or any other Institution or University.

This work was done under the supervision of Professor Biswarup Mukhopadhyaya, at the Harish-Chandra Research Institute, Allahabad, India.

Date:

Satyanarayan Mukhopadhyay
Ph.D. Candidate

Acknowledgements

I would like to thank Biswarup Mukhopadhyaya for supervising my thesis work. His guidance at every step was invaluable. In addition to being a very good teacher and a wonderful collaborator, he has encouraged me to think and work independently all along.

I have learnt a lot from all my collaborators and have thoroughly enjoyed working with them. I take this opportunity to thank Andreas Nyffeler, Kirtiman Ghosh, Soumitra SenGupta, Raj Gandhi, Atri Bhattacharya and Kaoru Hagiwara for working with me and for teaching me many aspects of particle physics.

I would like to acknowledge the financial support I have received from the Regional Centre for Accelerator-based Particle Physics (RECAPP), HRI. I also acknowledge the warm hospitality of the theory groups at Indian Association for the Cultivation of Science (IACS), Kolkata, and High Energy Accelerator Research Organization (KEK), Japan, where part of this research work was carried out.

I thank all my friends at HRI, seniors, batchmates and juniors alike, for their support and encouragement. They have helped me stay balanced in the midst of high demands of research work. I would like to especially thank Sanjoy Biswas, Atri Bhattacharya, Dhiraj Hazra, Subhaditya Bhattacharya and Paramita Dey for their understanding, numerous help, and constant encouragement. Sanjoy'da taught me a lot of collider physics, and Atri helped me out whenever I got into trouble with computer related problems, both of which were instrumental for carrying out my work.

Finally, I am indebted beyond measure to my parents for taking up many hardships so that I could pursue my own dreams, to Rabindra Nath Sarkar for being a constant source of inspiration, and my sister and her family, who took care of everything else while I was working on this thesis.

List of Publications

(This thesis is based on the papers marked with an asterisk.)

* 1. *Dilepton and Four-Lepton Signals at the LHC in the Littlest Higgs Model with T-parity Violation*
Satyanarayan Mukhopadhyay, Biswarup Mukhopadhyaya, Andreas Nyffeler
Published in **JHEP 1005:001,2010**

* 2. *Same-sign trileptons and four-leptons as signatures of new physics at the Large Hadron Collider*
Biswarup Mukhopadhyaya, Satyanarayan Mukhopadhyay
Published in **Phys.Rev.D82:031501,2010 (Rapid Communications)**.

* 3. *Discrimination of low missing energy look-alikes at the LHC*
Kirtiman Ghosh, Satyanarayan Mukhopadhyay, Biswarup Mukhopadhyaya
Published in **JHEP 1010:096,2010**

* 4. *Same-sign trileptons at the LHC: A Window to lepton-number violating supersymmetry*
Satyanarayan Mukhopadhyay, Biswarup Mukhopadhyaya
Published in **Phys.Rev.D84:095001,2011**

5. *Low-scale SUSY breaking by modular fields and Higgs mass bounds*
Satyanarayan Mukhopadhyay, Biswarup Mukhopadhyaya, Soumitra SenGupta
E-print: **arXiv:1103.3678 [hep-ph]**

6. *Re-analysing the implications of CPT and unitarity for baryogenesis and leptogenesis*
Atri Bhattacharya, Raj Gandhi, Satyanarayan Mukhopadhyay
E-print: **arXiv:1109.1832 [hep-ph]**

Synopsis

- **Name: Satyanarayan Mukhopadhyay**
- **Thesis Title: New physics with low missing-energy : identification and discrimination at the LHC**
- **Supervisor: Professor Biswarup Mukhopadhyaya**
- **Submitted to Homi Bhabha National Institute (HBNI)**

The Large Hadron Collider (LHC) marks the beginning of an era where physics at the TeV scale can be probed at an unprecedented level. One important goal of such investigations is to see whether the standard model (SM) of elementary particles is embedded within a set of new laws which make their presence felt at the TeV scale. Several proposals of such new physics have been put forward, with motivations ranging from the naturalness problem of the Higgs mass to solving the dark matter puzzle.

One distinguishing criterion for new physics, often used in these searches, is a large amount of missing transverse energy, carried away by weakly interacting massive particles. However, this criterion may not be fulfilled in a number of well-motivated theoretical scenarios. We have considered several such situations, their characteristic signatures in the form of multiple leptons, and the criteria for distinguishing among various scenarios of this kind. In this connection, we emphasize the usefulness of one type of signals, namely, same-sign trileptons and four-leptons, not only as a clean discovery mode for new physics but also as a probe to the underlying dynamics of supersymmetry with lepton number violation. We elaborate on the specific studies included in the thesis in the following.

In the presence of the T-parity violating Wess-Zumino-Witten (WZW) anomaly term, the otherwise stable heavy photon A_H in the Littlest Higgs model with T-parity (LHT) decays to either Standard Model (SM) gauge boson pairs, or to SM fermions via loop diagrams. We make a detailed study of the collider signatures where the A_H can be reconstructed from invariant mass peaks in the opposite sign same flavour dilepton or the four-lepton channel. This enables us to obtain information about the fundamental symmetry breaking scale f in the LHT and thereby the low-lying mass spectrum of the theory. In addition, indication of the presence of the WZW term gives us hints of the possible UV completion of

the LHT via strong dynamics. The crucial observation is that the sum of all production processes of heavy T-odd quark pairs has a sizeable cross-section at the LHC and these T-odd particles eventually all cascade decay down to the heavy photon A_H. We show that for certain regions of the parameter space with either a small f of around 500 GeV or relatively light T-odd quarks with a mass of around 400 GeV, one can reconstruct the A_H even at the previously planned LHC run with $\sqrt{s} = 10$ TeV and a modest integrated luminosity of $200\,\text{pb}^{-1}$. At $\sqrt{s} = 14$ TeV and with an integrated luminosity of $30\,\text{fb}^{-1}$, it is possible to cover a large part of the typical parameter space of the LHT, with the scale f up to 1.5 TeV and with T-odd quark masses almost up to 1 TeV. In this region of the parameter space, the mass of the reconstructed A_H ranges from 66 GeV to 230 GeV.

In two subsequent studies, we point out that same-sign multilepton events, not given due attention yet for new physics search, can be extremely useful at the LHC. After showing the easy reducibility of the standard model backgrounds, we demonstrate the viability of same-sign trilepton (SS3ℓ) signals for R-parity breaking supersymmetry, at both 7 and 14 TeV. We find that same-sign four-leptons (SS4ℓ), too, can have appreciable rates. Same-sign trileptons are also expected, for example, in Little Higgs theories with T-parity broken by anomaly terms. For the case of lepton-number (L) violating supersymmetry (SUSY), we demonstrate the efficacy of these signals for both minimal supergravity as well as a more general phenomenological SUSY model. Furthermore, we show that it is extremely unlikely to ever achieve similar rates in R-parity conserving SUSY. In addition, we show how SS3ℓ and SS4ℓ, in conjunction with the mixed-sign trilepton and four-lepton channels, can be used to extract dynamical information about the underlying SUSY theory, namely, the Majorana character of the decaying lightest neutralino and the nature of L-violating couplings. We define suitable variables and relationships between them which can be verified experimentally and which are largely independent of the SUSY production cross-sections and the cascade decay branching fractions. These theoretical predictions are validated by Monte Carlo simulations including detector and background effects.

This thesis also includes a study on the so-called LHC inverse problem. The problem of discriminating possible scenarios of TeV scale new physics with large missing energy signature at the LHC has received some attention in the recent past. We consider the complementary, and yet unexplored, case of theories predicting much softer missing energy spectra. As there is enough scope for

such models to fake each other by having similar final states at the LHC, we have outlined a systematic method based on a combination of different kinematic features which can be used to distinguish among different possibilities. These features often trace back to the underlying mass spectrum and the spins of the new particles present in these models. As examples of "low missing energy look-alikes", we consider Supersymmetry with R-parity violation, Universal Extra Dimensions with both KK-parity conserved and KK-parity violated and the Littlest Higgs model with T-parity violated by the Wess-Zumino-Witten anomaly term. Through detailed Monte Carlo analysis of the four and higher lepton final states predicted by these models, we show that the models in their minimal forms may be distinguished at the LHC, while non-minimal variations can always leave scope for further confusion. We find that, for strongly interacting new particle mass-scale $\sim$ 600 GeV (1 TeV), the simplest versions of the different theories can be discriminated at the LHC running at $\sqrt{s} = 14$ TeV within an integrated luminosity of 5 (30) fb^{-1}.

Contents

Part I.

Introduction

Chapter 1.

The Standard Model and Beyond

1.1. Introduction

The Standard Model (SM) of particle physics [1] encompasses our current understanding of elementary particles and three of the four fundamental interactions. In the SM, the matter sector consists of six quarks, three charged leptons and their associated neutrinos, all of which are represented by fermionic quantum fields. The quanta of the gauge fields, which mediate the interactions between the matter particles are known as gauge bosons. There are eight massless gauge bosons, called gluons (g), which mediate the strong interactions among quarks, three massive gauge bosons mediating the weak interactions, known as $W^{\pm}$ and Z, and finally one massless gauge boson responsible for the electromagnetic interactions, named photon (γ). The interactions among matter fields and gauge bosons are described by the principle of local gauge invariance. The gauge group of the SM is known to be $SU(3)_C \times SU(2)_L \times U(1)_Y$, which describes the three fundamental interactions of nature , where strong interactions are described by $SU(3)_C$ while electromagnetic and weak interactions are governed by $SU(2)_L \times U(1)_Y$. Gravitational interaction among elementary particles of very tiny mass, which become relevant only near the so called Planck energy scale of around 10^{19} GeV, is not a part of SM.

The transformation properties of the SM matter fields under the above gauge

group are determined by their respective charges under the gauge groups. The quark fields transform as triplets of the $SU(3)_C$ gauge group, while the leptons and neutrinos do not have colour charge, and hence they do not participate in strong interactions. Under $SU(2)_L$ the left-handed fields transform as doublets (where the left-handed projection of a field q is defined as $q_L = \frac{1}{2}(1-\gamma_5)q$), while the right handed ones ($q_R = \frac{1}{2}(1+\gamma_5)q$) are singlets. The quark doublets in the SM are

$$\begin{pmatrix} u \\ d \end{pmatrix}_L, \begin{pmatrix} c \\ s \end{pmatrix}_L, \begin{pmatrix} t \\ b \end{pmatrix}_L$$

while the lepton doublets are given by

$$\begin{pmatrix} \nu_e \\ e \end{pmatrix}_L, \begin{pmatrix} \nu_\mu \\ \mu \end{pmatrix}_L, \begin{pmatrix} \nu_\tau \\ \tau \end{pmatrix}_L$$

If T_3 are the eigenvalues of the third component of $SU(2)_L$ generators, and Q denotes the electric charge of the fields, then the transformation under $U(1)_Y$ is determined in terms of the hypercharge quantum numbers (Y), which are defined by the relation:

$$Q = T_3 + \frac{Y}{2} \tag{1.1}$$

Once the gauge charges are thus fixed, one can write down the gauge-invariant kinetic term in the Lagrangian for each field in the matter sector as (the fermion mass term will be discussed later)

$$L_{matter} = \overline{\psi} i \gamma^\mu D_\mu \psi \tag{1.2}$$

where the covariant derivative D_μ acts on the fermion fields as

$$D_\mu \psi = (\partial_\mu + i g T^a A^a_\mu)\psi \tag{1.3}$$

Here T^a are the generators of the corresponding gauge group in the representation in which the fermion fields transform, A^a_μ denote the gauge fields carrying the gauge index a, and g is the coupling strength. The kinetic term of the gauge fields, which also encodes the self-interaction of non-abelian gauge fields, is given by

$$L_{gauge} = -\frac{1}{4} F^{\mu\nu a} F^{a}_{\mu\nu}, \tag{1.4}$$

where $F^{a}_{\mu\nu}$ is the anti-symmetric field-strength tensor corresponding to each generator of the gauge group, written as

$$F^{a}_{\mu\nu} = \partial_\mu A^{a}_{\nu} - \partial_\nu A^{a}_{\mu} - g f^{abc} A^{b}_{\mu} A^{c}_{\nu} \tag{1.5}$$

f_{abc} are called the structure constants of the group.

Gauge symmetry forbids any mass term for the gauge fields. But the gauge bosons, mediating the short-range weak interactions, namely $W^{\pm}$ and Z are required to be massive. Furthermore, since the left and right handed fermion fields transform differently under the electroweak gauge group $SU(2)_L \times U(1)_Y$, we cannot write any gauge-invariant mass term (of the form $m\overline{\psi}\psi$) for them which necessarily mixes the left and right handed components. Therefore, the mechanism for mass generation is a matter of special concern in the SM, which is solved by the concept of spontaneous symmetry breaking (SSB) [2, 3]. In SSB, although the Lagrangian of the theory is invariant under gauge transformations, the choice of vacuum breaks the symmetry. It has been shown that a spontaneously broken gauge theory is renormalizable [4], thereby giving us a predictive quantum field theory where masses of gauge bosons and fermions can be successfully generated. In the SM, the Glashow-Salam-Weinberg (GSW) model [5] proposes to achieve the spontaneous breaking of the electroweak gauge group by postulating the existence of an $SU(2)_L$ doublet complex scalar field, which takes an appropriate vacuum expectation value (VEV) to break the symmetry spontaneously. We describe this model briefly in the following.

1.2. The Glashow-Salam-Weinberg Model

As mentioned before, the masses for the $W^{\pm}$ and Z bosons, as well those of quarks and leptons are generated by the mechanism of spontaneous symmetry breaking. In the SM, since electric charge is conserved, and therefore the gauge group of electromagnetism, $U(1)_{EM}$, is an exact symmetry, we require the following pattern of SSB:

$$SU(2)_L \times U(1)_Y \longrightarrow U(1)_{EM} \tag{1.6}$$

In order to achieve the spontaneous breaking of electroweak symmetry, in the GSW model, one introduces a complex $SU(2)_L$ doublet scalar field Φ with hypercharge $Y_\Phi = +1$:

$$\Phi = \begin{pmatrix} \phi^+ \\ \phi^0 \end{pmatrix} \tag{1.7}$$

The Lagrangian density for Φ is given by:

$$L_\Phi = D^\mu \Phi^\dagger D_\mu \Phi - V(\Phi, \Phi^\dagger), \tag{1.8}$$

where, the gauge-invariant potential is chosen to be

$$V(\Phi, \Phi^\dagger) = m^2 \Phi^\dagger \Phi + \lambda (\Phi^\dagger \Phi)^2 \tag{1.9}$$

For $m^2 < 0$, the potential has degenerate minima with

$$\Phi^\dagger \Phi = \frac{v^2}{2}; \qquad v = \sqrt{\frac{-m^2}{\lambda}} \tag{1.10}$$

Without a loss of generality, by utilizing the freedom of $SU(2)_L$ gauge transformations, we can choose the VEV of Φ to be real and entirely in the electrically neutral component of the Higgs field:

$$\langle 0|\Phi|0\rangle = \begin{pmatrix} 0 \\ v/\sqrt{2} \end{pmatrix} \tag{1.11}$$

This choice of VEV achieves the required breaking of $SU(2)_L \times U(1)_Y \longrightarrow U(1)_{EM}$. The $W^\pm$ and Z boson masses are generated from the kinetic term of the Higgs field, Eqn. 1.8. The mass terms for the fermion fields can be generated starting from gauge-invariant Yukawa couplings between the Higgs field and fermion fields. For example, for electron, we can have the following term:

$$L_{Yukawa} = -y_e(\overline{\nu_e}, \overline{e_L}) \begin{pmatrix} \phi^+ \\ \phi^0 \end{pmatrix} e_R + h.c. \tag{1.12}$$

After the Higgs field gets a VEV, Eqn.1.12 gives rise to a term of the form

$$L_{Yukawa} = -\frac{y_e}{\sqrt{2}}(v + h)\bar{e}e, \tag{1.13}$$

where the first term can be interpreted as electron mass with the value

$$m_e = \frac{y_e v}{\sqrt{2}} \tag{1.14}$$

Here, of course, the Yukawa couplings are free parameters of the theory. The masses for the other fermions can be generated in a similar manner. Note that, although neutrinos have been found to have a tiny mass, in the SM, their masses are not incorporated. Thus neutrino masses can be thought of as a first hint of physics beyond the SM.

Out of the four degrees of freedom of the complex scalar doublet field Φ, only one real scalar component, h, is a physical scalar particle, known as the Higgs boson. The other three components, the so called would-be Nambu-Goldstone bosons generate the longitudinal components of the $W^{\pm}$ and Z bosons. Note that, before SSB, the W and Z bosons, being massless, have two transverse polarization degrees of freedom each, while after SSB, they become massive, thereby gaining a third longitudinal mode.

The predictions of the standard model have been tested to high accuracies in experiments carried out at both high-energy colliders like the LEP and Tevatron, as well as in low-energy experiments of flavour physics. In almost all cases, experimental data are consistent with the predictions of GSW model. In this connection, we should mention that there is a persisting discrepancy of about 3 standard deviations between the SM prediction of the anomalous magnetic moment of the muon, and the corresponding measurement for it [6]. However, some uncertainty in the theory prediction, caused by strong interaction effects, still remain.

No experimental evidence for the Higgs boson has been found yet, whose discovery would validate the GSW model of electroweak symmetry breaking. Previous collider experiments like LEP have placed lower bounds on its mass, while the Tevatron and the ongoing LHC experiments continue to make these bounds more stringent.

1.3. New Physics Beyond the SM : Motivations

Apart from finding the Higgs boson, all the predictions of the SM have been successfully verified. The two pieces of experimental findings suggesting the existence of physics beyond the SM are the evidence for neutrino masses (observed

in the form of neutrino oscillations) [7] and the astrophysical evidence for non-baryonic dark matter in the universe. Although neutrino masses can be easily accommodated in the SM framework by postulating the existence of right-handed neutrinos, the nature of neutrino masses is largely still unknown. Moreover, the extreme smallness of their masses perhaps calls for a deeper explanation of why they are so many orders of magnitude below all the other fermion masses, including even the mass of particles belonging to the same $SU(2)_L$ multiplets, namely the charged leptons. Also inexplicable is the mixing pattern of the neutrinos which differs drastically from what is observed in the quark sector. If neutrinos are found to be of Majorana nature, then lepton number would be violated by their mass terms, thereby signalling the presence of physics beyond the SM. Several proposals for explaining the nature of neutrino masses have been made, starting from see-saw mechanisms [8] largely motivated by high-scale grand unified theories (GUT) [9], to low-scale models like supersymmetry with lepton-number violation [10].

Astrophysical evidences in the form of anomalous behaviours of galaxy rotation curves [11] first led to the proposition that non-baryonic dark matter exists in the universe. Thereafter, this proposal has received support from various other pieces of evidence coming from astrophysics and standard big-bang cosmology. Currently, a cosmological model with cold (non-relativistic) dark matter and a positive cosmological constant fits the cosmological data very well [12] (most importantly the cosmic microwave background radiation (CMBR) data from WMAP [13] and also the requirements of structure formation in the universe in the form of galaxies and galaxy clusters). Furthermore, the recent observation of colliding galaxy clusters, known as bullet clusters, is being considered as a very direct evidence for collisionless cold dark matter [14]. These findings largely rely on X-ray observations by the Chandra X-ray telescope and gravitational lensing methods, the later being subject to significant uncertainties.

Apart from the experimental evidence, there have been theoretical considerations motivating the existence of new physics beyond the SM. The primary problem here is the phenomenon of electroweak symmetry breaking. In the SM, no dynamic explanation is given for the form of the Higgs potential. And the parameters of the potential are subject to large radiative corrections, if we have new physics coming in at some high scales (like the GUT or Planck scales). In particular, the mass of the Higgs boson will be very sensitive to the higher scale where

the SM ceases to be a valid description of nature. The radiative corrections to the Higgs mass due to loops of, for example, top quarks, are quadratically sensitive to the cut-off scale. It will then require a large fine-tuning of parameters to keep the value of Higgs mass at the weak scale. This so called hierarchy problem [15] has motivated the proposal of several new physics scenarios, the most novel one being the existence of supersymmetry (SUSY), a symmetry relating bosonic and fermionic degrees of freedom. This postulates the existence of a mirror world of the SM, where we have a partner for every SM particle whose spin differs by half a unit. Other possibilities include the Higgs being a pseudo Nambu-Goldstone boson, and its mass being protected from radiative corrections by a shift symmetry. This possibility has been realized in several models, including the so called little Higgs models. Finally, one can have extra dimensions coming in at different length scales, thereby bringing the scale of new physics to a lower value, and removing the hierarchy problem. In the next chapter, we consider these possibilities in a more detailed manner.

Finally, we must mention that the SM, although a very successful and predictive theory of elementary particles, is not satisfactory in itself. There are several parameters whose values can only be fixed by experiments, and the SM offers no explanation for them. The most important point in this connection is the hierarchy of fermion masses. Excluding the neutrinos, the fermion masses vary from 0.5 MeV to 175 GeV, a span of about five orders of magnitude. The Higgs mechanism does not offer any explanation for this, since the Yukawa couplings are free parameters. It should be noted that the most commonly suggested extensions of the SM do not offer any explanation for the fermion Yukawas either, and in many cases, they introduce a even larger set of unknown parameters. The mixing angles in the quark and lepton sectors are also found to be widely different. Thus not only the electroweak sector of the SM requires further theoretical explorations, the flavour sector is also not sufficiently well understood.

Bibliography

[1] For an introduction, see, for example, F. Halzen and A.D. Martin, *Quarks and Leptons: An introductory course in modern particle physics*, (John Wiley, 1984); T.P. Cheng and L.F. Li, *Gauge theory of elementary particle physics*, (Oxford Univ. Press, 1984), and references therein.

[2] Y. Nambu and G. Jona-Lasinio, Phys. Rev. **122**, 345 (1961). Y. Nambu and G. Jona-Lasinio, Phys. Rev. **124**, 246 (1961); J. Goldstone, Nuovo cimento **19**, 154 (1961) J. Goldstone, A. Salam and S. Weinberg, Phys. Rev. **127**, 965 (1962)

[3] F. Englert and R. Brout, Phys. Rev. Lett. **13**, 321 (1964); P. W. Higgs, Phys. Rev. Lett. **13**, 508 (1964); G. S. Guralnik, C. R. Hagen and T. W. B. Kibble, Phys. Rev. Lett. **13**, 585 (1964); P. W. Higgs, Phys. Rev. **145**, 1156 (1966); T. W. B. Kibble, Phys. Rev. **155**, 1554 (1967).

[4] G. 't Hooft, Nucl. Phys. B **35**, 167 (1971); G. 't Hooft and M. J. G. Veltman, Nucl. Phys. B **44**, 189 (1972).

[5] S. L. Glashow, Nucl. Phys. **22**, 579 (1961); S. Weinberg, Phys. Rev. Lett. **19**, 1264 (1967); A. Salam, Proceedings of 8th Nobel Symposium, Ed. N. Svartholm (1968).

[6] F. Jegerlehner and A. Nyffeler, Phys. Rept. **477**, 1 (2009).

[7] For reviews, see R. N. Mohapatra *et al.*, Rept. Prog. Phys. **70**, 1757 (2007); A. Strumia and F. Vissani, arXiv:hep-ph/0606054.

[8] P. Minkowski, Phys. Lett. **B67**, 421 (1977); T. Yanagida, *Proceedings of the Workshop on the Unified Theory and the Baryon Number in the Universe*, O. Sawada and A. Sugamoto *(eds.)*, KEK, Tsukuba, Japan, 1979, p. 95; M. Gell-Mann, P. Ramond and R. Slansky, *Supergravity*, P. van Nieuwenhuizen *et al. (eds.)*, North Holland, Amsterdam, 1980, p. 315; R.N. Mohapatra and G. Senjanovic, Phys. Rev. Lett. **44**, 912 (1980).

[9] H. Georgi and S. L. Glashow, Phys. Rev. Lett. **32**, 438 (1974); For reviews, see for example P. Langacker, "Grand Unified Theories And Proton Decay," Phys. Rept. **72** (1981) 185; *Grand Unified Theories* by G. Ross(1984), Westview Press.

[10] See, for example, B. Mukhopadhyaya, arXiv:hep-ph/0301278, and references therein.

[11] F. Zwicky, Astrophys. J. **86**, 217 (1937).

[12] For a review, see V. Trimble, Ann. Rev. Astron. Astrophys. **25**, 425 (1987).

[13] E. Komatsu *et al.* [WMAP Collaboration], Astrophys. J. Suppl. **192**, 18 (2011).

[14] D. Clowe *et al.*, Astrophys. J. **648**, L109 (2006).

[15] E. Gildener and S. Weinberg, Phys. Rev. D **13**, 3333 (1976); E. Gildener, Phys. Rev. D **14**, 1667 (1976); G. 't Hooft, in *Recent developments in gauge theories*, Proceedings of the NATO Advanced Summer Institute, Cargese 1979, (Plenum, 1980).

Chapter 2.

Physics beyond the SM: a brief overview of some possible scenarios

In this chapter we shall consider some possible scenarios of new physics beyond the SM, whose motivations, as discussed in the previous chapter, range from the naturalness problem of the electroweak scale to solving puzzles posed by the existence of dark matter and tiny neutrino masses. In the following, we discuss some of these possibilities whose phenomenology at the LHC has been further explored in the later chapters of the thesis. We start with supersymmetry (SUSY), the very well known prototype of new physics, and then move on to universal extra dimensions (UED). We end this chapter with an overview of little Higgs scenarios, in particular the littlest Higgs model with T-parity (LHT). In each one of these cases, we also consider the possibility of violation of the often imposed discrete Z_2-type symmetries, viz., R-parity in SUSY, KK-parity in UED and T-parity in LHT.

2.1. Supersymmetry

2.1.1. Introduction

Weak-scale supersymmetry [1–5] provides a natural solution to the gauge-hierarchy problem discussed in the previous chapter. In the minimal supersymmetric ver-

sion of the standard model (MSSM), one postulates the existence of a new bosonic degree of freedom corresponding to each fermionic degree of freedom in the SM and vice versa, all other quantum numbers remaining the same. Thus there are new scalar particles, known as sleptons, squarks and sneutrinos, as well as new fermions, known as gauginos. If SUSY is exact, then the quadratically divergent contributions to the Higgs mass, due to the top quark, say, is cancelled by the contribution of the top squarks (there are two of them, corresponding to the left and right handed top quark components), thereby ameliorating the hierarchy problem altogether. However, exact SUSY also predicts that the masses of the superpartners will be the same as that of their SM counterparts. This is not allowed experimentally, since then we should have already observed, for example, a scalar particle with the same mass and charge as that of the electron. Thus, if it exists, SUSY must be a broken symmetry of nature. If it is broken in the Lagrangian by terms whose co-efficients are not dimensionless (the so-called soft SUSY breaking terms), then it can still be shown that the residual radiative correction to the Higgs mass squared depends only logarithmically on the cut-off scale, and the quadratic contributions still cancel out [6]. This is one of the primary reasons which prompted the acceptance of MSSM with soft SUSY breaking as a viable candidate of physics beyond the standard model. It should be mentioned that there are a number of other attractive features of MSSM, two of which deserve mention. As we know, if one considers the running of gauge couplings in the SM, they tend to unify at a very high energy scale of about 10^{15} GeV, although they do not quite meet at a point at this scale. This fact is related to the quest for grand unified theories where the SM gauge groups are embedded in one single larger gauge group, which is then spontaneously broken at a higher energy scale. The running of gauge couplings is modified when we include the contributions due to the superparticles also, and one finds that the convergence of the couplings to a single value is much better achieved in this case [7]. Another attractive feature that can be built into SUSY models is the radiative mechanism of electroweak symmetry breaking. As we have seen in section 1.2, the potential for the Higgs field is proposed in an ad hoc manner in the SM, and no explanation is provided for the negative sign of the mass-squared term in the scalar potential. In high-scale models of SUSY breaking, one can start with positive mass-squared values at a higher scale, and then radiative effects can give rise to a negative mass squared for the Higgs field at the weak-scale, thereby trigger-

ing spontaneous electroweak symmetry breaking (EWSB). It must be mentioned that apart from all these nice features of weak scale supersymmetric versions of the SM, there are a number of other wonderful mathematical properties of SUSY quantum field theories that are worth studying in themselves [8, 9].

2.1.2. A brief review of MSSM

In the MSSM [1, 2], each of the known fundamental particles belong to either a chiral or gauge supermultiplet, containing its superpartner with spin differing by half a unit. In the SM, the left and right handed components of the quarks and leptons are two component Weyl fermions with different gauge transformation properties. Therefore, each must have its own complex scalar partner, known as left and right chiral squarks and sleptons. For example, the superpartners of the left and right handed electron fields are named left and right chiral selectrons, and denoted by $\tilde{e}_L$ and $\tilde{e}_R$. Similarly, we have two smuons and staus each. Since the neutrinos are massless in the SM, and are always left-handed, their superpartners, the sneutrinos, are denoted by $\tilde{\nu}_e$, $\tilde{\nu}_\mu$ and $\tilde{\nu}_\tau$, corresponding to three different flavours. We also have the squarks denoted by $\tilde{q}_L$ and $\tilde{q}_R$, with q running over all the six flavours. From the conditions of anomaly cancellation, and also in order to give masses to both the up and down type quarks (and leptons) while complying with a requirement coming from the structure of the SUSY Lagrangian (namely, holomorphicity of the superpotential), one is required to introduce two complex Higgs doublets in the MSSM, one with hypercharge $Y = +1$ and the other with $Y = -1$, denoted as H_u and H_d respectively. The fermionic partners of the Higgs scalar fields are known as higgsinos, denoted by $\tilde{H}_u$ and $\tilde{H}_d$. We summarize the particle content of the chiral supermultiplets along with their gauge quantum numbers in Table 2.1.

We now turn to the gauge supermultiplets, which contain the SM gauge bosons and their spin-1/2 counterparts, known as gauginos. The spin-1/2 colour-octet partner of the gluon is known as the gluino ($\tilde{g}$). The partners of W-bosons, $W^\pm$ and W^0, are called winos, and are denoted as $\tilde{W}^\pm$ and $\tilde{W}^0$. Similarly, the partner of the $U(1)_Y$ gauge boson is called the bino, $\tilde{B}$. We summarize the gauge supermultiplets along with their quantum numbers in Table 2.2.

We shall not be reviewing here the detailed method of constructing a supersymmetric Lagrangian describing all possible interactions of the sparticles and

Names		spin 0	spin 1/2	$SU(3)_C$, $SU(2)_L$, $U(1)_Y$
squarks, quarks	Q	$(\widetilde{u}_L \;\; \widetilde{d}_L)$	$(u_L \;\; d_L)$	$(\mathbf{3}, \mathbf{2}, \frac{1}{3})$
	$\overline{u}$	$\widetilde{u}_R^*$	$u_R^\dagger$	$(\overline{\mathbf{3}}, \mathbf{1}, -\frac{4}{3})$
	$\overline{d}$	$\widetilde{d}_R^*$	$d_R^\dagger$	$(\overline{\mathbf{3}}, \mathbf{1}, \frac{2}{3})$
sleptons, leptons	L	$(\widetilde{\nu} \;\; \widetilde{e}_L)$	$(\nu \;\; e_L)$	$(\mathbf{1}, \mathbf{2}, -1)$
	$\overline{e}$	$\widetilde{e}_R^*$	$e_R^\dagger$	$(\mathbf{1}, \mathbf{1}, 2)$
Higgs, higgsinos	H_u	$(H_u^+ \;\; H_u^0)$	$(\widetilde{H}_u^+ \;\; \widetilde{H}_u^0)$	$(\mathbf{1}, \mathbf{2}, +1)$
	H_d	$(H_d^0 \;\; H_d^-)$	$(\widetilde{H}_d^0 \;\; \widetilde{H}_d^-)$	$(\mathbf{1}, \mathbf{2}, -1)$

Table 2.1.: Chiral supermultiplets in the Minimal Supersymmetric Standard Model. The spin-0 fields are complex scalars, and the spin-1/2 fields are left-handed two-component Weyl fermions [2].

particles of the MSSM. Instead, we refer the reader to excellent reviews [1, 2] on this subject for this. The most general non-gauge interactions of the chiral supermultiplets are determined by an analytic function of the complex scalar fields, known as the superpotential, W. Equivalently, the superpotential is often written in terms of the so-called chiral superfields, which contain all the bosonic, fermionic and auxiliary (non-dynamical, and therefore, physically irrelevant) components of a supermultiplet. The condition of supersymmetry invariance of the Lagrangian involving gauge and chiral superfields enforces the superpotential to be gauge invariant. The scalar potential involving generic scalar fields ϕ in a SUSY theory is completely determined by the other interactions (gauge and Yukawa) of the theory, and therefore, is very restrictive. This is an unique feature of supersymmetric models. It is given by

$$V(\phi, \phi^*) = |\frac{\partial W}{\partial \phi}|^2 + \frac{1}{2}\sum_a g_a^2(\phi^* T^a \phi)^2 \tag{2.1}$$

Note that, since $V(\phi, \phi^*)$ is a sum of squares, it is always non-negative, and therefore, bounded from below.

The MSSM superpotential is given by [2]

$$W_{MSSM} = {y^l}_{ij} L_i H_d \bar{E}_j + {y^d}_{ij} Q_i H_d \bar{D}_j + {y^u}_{ij} Q_i H_u \bar{U}_j + \mu H_u H_d \tag{2.2}$$

Names	spin 1/2	spin 1	$SU(3)_C$, $SU(2)_L$, $U(1)_Y$
gluino, gluon	$\widetilde{g}$	g	(**8**, **1** , 0)
winos, W bosons	$\widetilde{W}^{\pm}$ $\widetilde{W}^0$	$W^{\pm}$ W^0	(**1**, **3** , 0)
bino, B boson	$\widetilde{B}^0$	B^0	(**1**, **1** , 0)

Table 2.2.: Gauge supermultiplets in the Minimal Supersymmetric Standard Model [2].

where H_u and H_d are the two Higgs superfields, L and Q are the SU(2)-doublet lepton and quark superfields and E, U, and D are the singlet lepton, up-type quark, and down-type quark superfields, respectively. μ is the Higgsino mass parameter and y_{ij}'s are the strengths of the Yukawa interactions.

As we shall see in the next subsection, this is not the most general gauge invariant and renormalizable superpotential. The other possible terms in the superpotential violate either baryon (B) or lepton number (L) by one unit. They can be avoided by imposing an additional multiplicative discrete symmetry, known as R-parity, which is defined as $R_p = (-1)^{3B+L+2S}$, where S is the spin of the corresponding particle. This prevents, for example, terms which can lead to fast proton decay. However, the purpose is equally well-served if only *one* between B and L is conserved. It can be easily seen that all the sparticles are R-odd, while the SM particles are R-even. This leads to some very important consequences. First of all, in all the interaction vertices involving sparticles, there will be an even number of sparticles present. Thus, supersymmetric particles can only be produced in pairs in collider experiments, if R-parity conservation is assumed. Furthermore, the lightest SUSY particle, known as the LSP, will not be able to decay, thereby furnishing a viable dark matter candidate.

As mentioned before, since SUSY can at most be a broken symmetry in nature, we need to specify the soft SUSY breaking terms in the Lagrangian. Unless a specific mechanism for SUSY breaking is assumed, this leads to the introduction of a number of new unknown parameters in the theory, making supersymmetry phenomenology highly involved. In the MSSM, the most general soft SUSY breaking terms are given by [2, 6]

$$
\begin{aligned}
L_{\text{soft}} \;=\; & -\frac{1}{2}\left(M_1\tilde{B}\tilde{B} + M_2\tilde{W}\tilde{W} + M_3\tilde{g}\tilde{g} + c.c\right) \\
& - \left(\tilde{u}\mathbf{a_u}\tilde{Q}H_u - \tilde{d}\mathbf{a_d}\tilde{Q}H_d - \tilde{e}\mathbf{a_e}\tilde{L}H_d + c.c\right) \\
& - \tilde{Q}^\dagger \mathbf{m_Q^2}\tilde{Q} - \tilde{L}^\dagger \mathbf{m_L^2}\tilde{L} - \tilde{u}\mathbf{m_{\bar{u}}^2}\tilde{u}^\dagger - \tilde{d}\mathbf{m_{\bar{d}}^2}\tilde{d}^\dagger - \tilde{e}\mathbf{m_{\bar{e}}^2}\tilde{e}^\dagger \\
& - m_{H_u}^2 H_u^* H_u - m_{H_d}^2 H_d^* H_d - \left(bH_u H_d + c.c\right). \qquad (2.3)
\end{aligned}
$$

In writing eq. 2.3, we have suppressed all gauge indices in the fields. Here, M_1, M_2 and M_3 are the soft SUSY-breaking mass terms for the bino, wino and gluino respectively. Next we have the cubic scalar couplings, where each of $\mathbf{a_u}$, $\mathbf{a_d}$ and $\mathbf{a_e}$ are 3×3 matrices in family space. The five squark and slepton mass matrices $\mathbf{m_Q^2}$ etc. are also 3×3 complex matrices in the family space, which are however required to be hermitian. And finally we have the SUSY breaking terms for the Higgs potential in the last line of eq. 2.3.

After EWSB, in the Higgs sector we have five scalar mass eigenstates : two CP-even neutral scalars h^0 and H^0, one CP-odd neutral scalar A^0, and two charged scalars $H^\pm$. One crucial parameter in the Higgs sector is the ratio of the two Higgs VEV's, namely, $\tan\beta = v_u/v_d$. It can be shown that the lightest CP-even Higgs mass in MSSM has a tree-level upper bound of M_Z, while after including radiative corrections its mass can be lifted to around 135 GeV.

The higgsinos and electroweak gauginos also mix with each other after EWSB. The four mass eigenstates obtained by combining the two neutral higgsinos and two neutral gauginos are known as neutralinos $\tilde{\chi^0}_i$ ($i = 1, 2, 3, 4$). The charged higgsinos and winos mix to form two mass eigenstates with charge ± 1, known as charginos $\tilde{\chi^\pm}_i$ ($i = 1, 2$). The gluino, being a colour octet fermion, cannot mix with any other particle in the MSSM.

If the soft terms are chosen in the most general way, then the mass eigenstates of the MSSM squarks and sleptons should be obtained by diagonalizing the three 6×6 mass matrices for up- and down-type squarks and the charged sleptons, while the sneutrino mass matrix is a 3×3 one. But such general mixing can lead to potentially very large flavour changing and CP-violating effects, thereby placing severe constraints on the model [10]. In order to avoid these very large contributions, one generally assumes that the squark and slepton mass matrices are flavour-blind, each being proportional to a 3×3 identity matrix in the family space, for example, $\mathbf{m_Q^2} = m_Q^2\mathbf{1}$ etc. One further assumes that the possi-

ble mixing induced by $\mathbf{a_u}$, $\mathbf{a_d}$ and $\mathbf{a_e}$ are each proportional to the corresponding Yukawa coupling matrices. Since the Yukawa couplings for the first two generations are rather small, the only substantial mixing occurs among the third generation squarks and sleptons. Thus, for example, after EWSB, $\tilde{t}_L$ and $\tilde{t}_R$ can mix to give two mass eigenstates $\tilde{t}_1$ and $\tilde{t}_2$.

The phenomenology of SUSY models has been studied exhaustively in the literature, and various possible scenarios of SUSY breaking have been proposed. Usually, being within the MSSM field content, one does not find a successful mechanism to break SUSY spontaneously, without running into phenomenological inconsistencies. Therefore, the existence of a separate SUSY breaking sector is envisioned, known as the hidden sector, where SUSY is broken spontaneously by one of several possible mechanisms. This breaking is thereafter communicated to the visible MSSM sector. The case where gravitational interactions mediate the transfer of SUSY breaking from the hidden to the visible sector is known as gravity mediated SUSY breaking [11], which is one of the most widely studied mechanisms. There are other possible scenarios like gauge [12] and anomaly [13] mediated SUSY breaking , too.

As far as collider searches of R-parity conserving SUSY [14, 15] are concerned, they largely rely on the presence of large missing energies in the final state, coming from the undetected stable LSP. In addition, since strongly interacting SUSY particles, the squarks and gluinos, are dominantly produced in hadron colliders, in these environments, one generally also expects hard jets in the events coming from their decays. Thus, SUSY cascades originate in the initially pair produced sparticles and end with a pair of LSP's, together with jets, leptons etc. Leptonic signatures, with different possible lepton multiplicities, accompanied by jets and missing transverse energy are viable and widely used channels for SUSY searches at colliders.

2.1.3. R-parity violation

As mentioned in the previous subsection, if lepton and/or baryon number are allowed to be broken, the MSSM superpotential can be augmented by the following terms [16, 17]:

$$W_{\not R_p} = \lambda_{ijk} L_i L_j \bar{E}_k + \lambda'_{ijk} L_i Q_j \bar{D}_k + \lambda''_{ijk} \bar{U}_i \bar{D}_j \bar{D}_k + \epsilon_i L_i H_u. \tag{2.4}$$

where i, j, and k are flavour indices. Here the λ''_{ijk} term leads to baryon number (B) violating interactions while the other three terms lead to the violation of lepton number (L). Proton decay can be easily avoided if only *one* between B and L is conserved and R-parity violating (RPV) SUSY models are constructed with this in view. There are also upper bounds on individual R-parity violating operators, coming mainly from constraints in the flavour sector [16]. Since product couplings are often more constrained, one generally assumes the presence of one R-parity violating term at a time while studying phenomenological implications. Of these, the versions containing L-violating interactions, trilinear and/or bilinear, have the added motivation of offering explanations of neutrino masses and mixing [18,19]. It should be mentioned that one can obtain scenarios with only L-violating terms present by imposing a different type of discrete symmetry known as baryon triality, which is a Z_3 symmetry, defined by $Z_3^B = \exp(2\pi i[B-2Y]/3)$, where Y is the weak hypercharge [2].

The consequences of RPV interactions have been explored extensively in the literature [16, 17, 20]. In the presence of R-parity violating interactions, the collider searches for SUSY can be completely altered. There can be single sparticle production at colliders, in addition to the usual pair production processes. Furthermore, gauginos can be produced in association with SM fermions via t-channel sfermion exchange. Sparticle decays can also be modified by R-parity violating interactions. However, since the R-parity violating couplings are already constrained by many experiments, and also because of requirements coming from specific models (like neutrino mass generation by including L-violation), they are often required to be smaller than the gauge couplings. In that case, the heavier sparticles will all decay with the usual R-parity conserving modes down to the LSP, and then the LSP will no longer remain stable but decay through the new couplings. Thus one expects the multiplicity of final state particles to increase. In particular, when L-violation takes place, although the conventional large missing E_T signature of SUSY is degraded, the possibility of obtaining multilepton final states is enhanced [20]. Also, as will be shown in great detail in Chapter 5, we have demonstrated that in presence of these L-violating operators, rather striking same-sign three-and four-lepton final states, which are free from SM backgrounds, are expected with large rates at the LHC [21,22].

In presence of the λ-type couplings, if the neutralino is the lightest supersymmetric particle (LSP), it will decay to a lepton-antilepton pair (not necessarily

of the same flavour) and a neutrino. Thus, starting from the pair production of squarks/gluinos in the initial parton level $2 \to 2$ hard scattering, we can obtain two neutralinos at the end of the decay cascade, whose decay in turn can give rise to multilepton final states with large rates. The λ'-type interactions, on the other hand, cause a neutralino LSP to decay into a lepton and two quarks. The bilinear terms $\epsilon_i L_i H_u$ imply mixing between neutrinos and neutralinos as also between charged leptons and charginos [19]. Consequently, the lightest neutralino LSP can, for example, decay into a neutrino and the Z or a charged lepton and the W, the latter mode being of larger branching ratio.

It should be noted that if R-parity is violated, the LSP is no longer stable, and therefore it is no longer constrained to be neutral (which would otherwise be the case from cosmological considerations). Thus, one can have several possibilities for the LSP. However, in the constrained versions of supersymmetry, known as cMSSM or mSUGRA, whereby one assumes universal soft SUSY breaking terms near the GUT scale, one generally finds either the lightest neutralino or the lighter stau to be the LSP in most of the parameter space regions. In later chapters of this thesis, we shall consider some striking phenomenology of both the neutralino and stau LSP scenarios. Finally, we should mention that in the absence of R-parity, although the lightest neutralino is no longer a dark matter candidate, one can have alternative dark matter candidates such as the axino or the gravitino.

2.2. Minimal universal extra dimension

2.2.1. Introduction and a brief description of mUED

A rather exciting development in physics beyond the standard model in the last few years is the formulation of theories with compact spacelike extra dimensions, whose phenomenology can be tested at the TeV scale. The idea is based on concepts first introduced by Kaluza and Klein [23] in the 1920's. Extra-dimensional theories can be divided into two main classes. The first includes those where the standard model fields are confined to a (3 + 1) dimensional subspace (3-brane) of the full manifold. Models with the extra spacelike dimensions being both flat [24] or warped [25] fall in this category, although there have been numerous attempts to put some or all of the fields in the 'bulk' even within the ambits of these the-

ories. On the other hand, there is a class of models known as Universal Extra Dimension(s) (UED) [26], where all of the SM fields can access the additional dimensions.

In the minimal version of UED (mUED), there is only one extra dimension y compactified on a circle of radius R (S_1 symmetry). The need to introduce chiral fermions in the resulting four-dimensional effective theory prompts one to impose additional conditions on the extra dimension. This condition is known as 'orbifolding' where two diametrically opposite ends of the compact dimension are connected by an axis, about which there is a reflection symmetry. This Z_2 symmetry breaks the translational invariance along the fifth dimension (denoted by the co-ordinate y) and generates two fixed points at $y = 0$ and $y = \pi R$. From a four-dimensional viewpoint, every field will then have an infinite tower of Kaluza-Klein (KK) modes, the zero modes being identified as the corresponding SM states. The spectrum is essentially governed by R^{-1}, where R is the radius of the extra dimension.

UED scenarios can have a number of interesting phenomenological implications. These include a new mechanism of supersymmetry breaking [27], relaxation of the upper limit of the lightest supersymmetric neutral Higgs [28], addressing the issue of fermion mass hierarchy from a different perspective [29] and lowering the unification scale down to a few TeV's [30–32].

In the absence of the orbifold fixed points, the component of momentum along the extra dimension is conserved. From a four-dimensional perspective, this implies KK number conservation, where KK number is given by the position of an excited state in the tower. However, the presence of the two orbifold fixed points breaks the translational symmetry along the compact dimension, and KK number is consequently violated. In principle, one may have some additional interaction terms localised at these fixed points, causing mixing among different KK states. However, if these interactions are symmetric under the exchange of the fixed points (this is another Z_2 symmetry, not to be confused with the Z_2 of $y \leftrightarrow -y$), the conservation of KK number breaks down to the conservation of KK parity[1], given by $(-1)^n$, where n is the KK number. This not only implies that

[1]In principle, it is possible to have fixed point localized operators that are asymmetric in nature [26]. This could violate KK-parity, analogous to the violation of R-parity in supersymmetry. In absence of KK-parity, the phenomenology of UED will be drastically different and will be discussed in brief in the next subsection.

level-one KK-modes, the lightest among the new particles, are always produced in pairs, but also ensures that the KK modes do not affect electroweak processes at the tree level. The multiplicatively conserved nature of KK-parity implies that the lightest among the first excitations of the SM fields is stable, and a potential dark matter candidate [33].

The tree-level mass of a level-n KK particle is given by $m_n^2 = m_0^2 + n^2/R^2$, where m_0 is the mass associated with the corresponding SM field. Therefore, the tree level mUED spectrum is extremely degenerate and, to start with, the first excitation of any massless SM particle can be the lightest KK-odd particle (LKP). In practice, radiative corrections [34] play an important role in determining the actual spectrum. The correction term can be finite (bulk correction) or it may depend on Λ, the cut-off scale of the model (boundary correction). Bulk corrections arise due to the winding of the internal lines in a loop around the compactified direction [34], and are non-zero and finite only for the gauge boson KK-excitations. On the other hand, the boundary corrections are not finite, but are logarithmically divergent. They are just the counterterms of the total orbifold correction, with the finite parts being completely unknown. Assuming that the boundary kinetic terms vanish at the cut-off scale Λ, the corrections from the boundary terms, for a renormalization scale μ, are proportional to $L_0 \equiv \ln(\Lambda^2/\mu^2)$. The bulk and boundary corrections for level-n doublet quarks and leptons (Q_n and L_n), singlet quarks and leptons (q_n and e_n) and KK gauge bosons (g_n, W_n, Z_n and B_n) are given by,

- Bulk corrections:

$$\begin{aligned} \delta\,(m_{B_n}^2) &= -\frac{39\,\zeta(3)\,a_1}{2\,\pi^2\,R^2}\,, \\ \delta\,(m_{W_n}^2) &= -\frac{5\,\zeta(3)\,a_2}{2\,\pi^2\,R^2}\,, \\ \delta\,(m_{g_n}^2) &= -\frac{3\,\zeta(3)\,a_3}{2\,\pi^2\,R^2}\,, \end{aligned} \tag{2.5}$$

where, $\zeta(3) = \sum_{n=1}^{\infty} 1/n^3 \simeq 1.202$.

- Boundary corrections:

$$
\begin{aligned}
\bar{\delta}\, m_{Q_n} &= m_n \left(3\, a_3 + \frac{27}{16}\, a_2 + \frac{a_1}{16}\right) L_0\,, \quad \bar{\delta}\, m_{u_n} = m_n\, (3\, a_3 + a_1)\, L_0\,, \\
\bar{\delta}\, m_{d_n} &= m_n \left(3\, a_3 + \frac{a_1}{4}\right) L_0\,, \qquad \bar{\delta}\, m_{L_n} = m_n \left(\frac{27}{16}\, a_2 + \frac{9}{16}\, a_1\right) L_0\,, \\
\bar{\delta}\, m_{e_n} &= \frac{9\, a_1}{4}\, m_n\, L_0\,, \qquad \bar{\delta}\,(m^2_{B_n}) = -\frac{a_1}{6}\, m_n^2\, L_0 \\
\bar{\delta}\,(m^2_{W_n}) &= \frac{15\, a_2}{2}\, m_n^2\, L_0\,, \qquad \bar{\delta}\,(m^2_{g_n}) = \frac{23\, a_3}{2}\, m_n^2\, L_0\,, \\
\bar{\delta}\,(m^2_{H_n}) &= m_n^2 \left(\frac{3}{2}\, a_2 + \frac{3}{4}\, a_1 - \frac{\lambda_H}{16\pi^2}\right) L_0 + \overline{m}^2_H\,,
\end{aligned}
\tag{2.6}
$$

where $a_i \equiv g_i^2/16\,\pi^2$, $i = 1 \ldots 3$, g_i being the respective gauge coupling constants and $\overline{m}^2_H$ is the boundary term for the Higgs scalar, which has been chosen to be zero in our studies in Chapter 6.

These radiative corrections partially remove the degeneracy in the spectrum [34] and, over most of the parameter space, γ_1, the first excitation of the hypercharge gauge boson (B), is the LKP [2]. γ_1 can also produce the right amount of relic density and turns out to be a good dark matter candidate [33]. The mass of γ_1 is approximately R^{-1} and hence the overclosure of the universe puts an upper bound on $R^{-1} < 1400$ GeV. The lower limit on R^{-1} comes from the low energy observables and direct search of new particles at the Tevatron. Constraints from $g-2$ of the muon [35], flavour changing neutral currents [36–38], $Z \to b\bar{b}$ [39], the ρ parameter [26, 40], other electroweak precision tests [41], etc. imply that $R^{-1} \gtrsim 300$ GeV. The masses of KK particles are also dependent on Λ, the cut-off of UED as an effective theory, which is essentially a free parameter. One loop corrected $SU(3)$, $SU(2)$ and $U(1)$ gauge couplings show power law running in the mUED model and almost meet at the scale $\Lambda = 20R^{-1}$ [30]. Thus one often takes $\Lambda = 20R^{-1}$ as the cut-off of the model. If one does not demand such unification, one can extend the value of Λ to about $40R^{-1}$, above which the $U(1)$ coupling becomes nonperturbative.

After incorporating the radiative effects, the typical UED spectrum shows that the coloured KK states are on top of the spectrum. Among them, g_1, the $n = 1$ gluon, is the heaviest. It can decay to both $n = 1$ singlet (q_1) and doublet (Q_1) quarks with almost the same branching ratio, although there is a slight kinematic preference for the singlet channel. q_1 can decay only to γ_1 and an SM quark. On

[2] The KK Weinberg angle is small so that $B_1 \approx \gamma_1$ and $W_1^3 \approx Z_1$.

the other hand, a doublet quark Q_1 decays mostly to W_1 or Z_1. Hadronic decay modes of W_1 and Z_1 are closed kinematically, so that they decay to different $n = 1$ doublet leptons. Therefore Z_1 can decay only to $L_1 l$ or $\nu_1 \nu$. The KK leptons finally decay to γ_1 and SM leptons. Thus, the principal signals of such a scenario are n jets + m leptons + MET, where m can vary from 1 to 4.

2.2.2. KK-parity violation

Let us now briefly introduce KK-parity violation and its phenomenological consequences. As discussed in the previous subsection, operators localised at the orbifold fixed points give rise to mixing between different KK-states. In presence of such operators that are symmetric under exchange of the fixed points, even and odd KK-parity states mix separately, so that KK-parity is still a conserved quantity. However, it is possible to have fixed point operators which are asymmetric in nature, leading to the violation of KK-parity [26]. The phenomenology of KK-parity violation was studied in some detail in Ref. [42]. KK-parity violating couplings allow the LKP to decay into SM particles.

The asymmetry in the localised operators can be introduced by adding the following extra contribution to the operators localized at the point $y = 0$:

$$\mathcal{L}_f = \frac{\lambda}{\Lambda} \int \left[i\bar{\psi}\Gamma^\alpha D_\alpha \psi - i(D_\alpha \bar{\psi})\Gamma^\alpha \psi \right] \delta(y) dy, \tag{2.7}$$

where, $\psi(x^\mu, y)$ is the 5-dimensional fermion field, Γ^α are the gamma matrices and D_α are the covariant derivatives defined in (4+1) dimensions, λ is the strength of the KK-parity violating coupling, and Λ is the cut-off scale. The above operator has the following consequences:

- Equation 2.7 gives rise to KK-parity violating mixing between KK-even and odd states. Of them, the mixing between $n = 0$ and $n = 1$ states are most relevant from the point of view of LHC phenomenology. The admixture of $n \geq 2$ KK-states with the $n = 0$ state is suppressed by the higher masses of the former.
- Equation 2.7 leads to the coupling between two KK-fermions ($\psi^{(l)}$ and $\psi^{(m)}$) and a gauge boson ($A_\mu^{(n)}$): $ihg\bar{\psi}^{(l)}\gamma^\mu A_\mu^{(n)}\psi^{(m)}$, where h is a dimensionless coupling parametrised as $h = \lambda/(2\pi\Lambda R)$ and g is the gauge coupling. This coupling can be KK-parity violating, if $(-1)^{n+m+l} = -1$.

- In the KK-basis, interaction terms involving one $n = 0$ and two $n = 1$ particles are allowed by KK-parity. As an example consider the terms $ig\bar{\psi}^{(1)}_{KK}\gamma^{\mu}A^{(1)}_{\mu}\psi^{(0)}_{KK}$, $ig\bar{\psi}^{(1)}_{KK}\gamma^{\mu}A^{(0)}_{\mu}\psi^{(1)}_{KK}$ etc., where $\psi^{(n)}_{KK}$ is level-n fermion in the KK-basis. As a result of the mixing between $n = 0$ and 1 fermions , the above interactions give rise to KK-parity violating couplings between two $n = 0$ particles with one $n = 1$ particle in the mass eigenstate basis.

We have only considered the consequences of the fermionic kinetic terms localized at the point $y = 0$. However, in principle, one could also introduce kinetic terms for the 5-dimensional gauge bosons at $y = 0$. Such terms would lead to KK-parity violating decay of $n = 1$ gauge bosons into a pair of SM electroweak gauge bosons. For $W^{\pm}_1$ and Z_1-boson, the KK-parity conserving decays are overwhelmingly dominant. Therefore, the KK-parity violating decays of $W^{\pm}_1$ and Z_1-boson are phenomenologically insignificant. On the other hand, the LKP (γ_1), being completely B_1 dominated, can not have any coupling with the standard model ZZ or W^+W^- pairs. Therefore, from the point of view of collider phenomenology, the KK-parity violating kinetic terms for the 5-dimensional gauge bosons are not significant.

We have already noted that, as a consequence of KK-parity violation, the lightest $n = 1$ particle decays into two or more SM particles. Thus, γ_1 can decay into SM fermion-antifermion pairs. The KK-parity violating couplings of γ_1 with the SM fermions are given by

$$\mathcal{L}_{KKV} = \frac{eh}{\sqrt{2}\cos\theta_W}\bar{f}[Y_L\gamma_{\mu}(1-\gamma_5) - Y_R\gamma_{\mu}(1+\gamma_5)]\gamma^{\mu}_1 f, \tag{2.8}$$

where f is an SM fermion and Y_L and Y_R are the hypercharges of f_L and f_R respectively. For $\lambda \sim 1$ and $\Lambda R \sim 20$, the maximum value of the parameter h is $h_{max} \sim 0.01$. In our later analysis, we have taken h to be the same for all fermionic flavours. With this assumption, the decay branching fraction of γ_1 becomes independent of the value of h. We thus find a 53.3% branching fraction for $\gamma_1 \to q\bar{q}$ and 38.9 (7.8)% branching fraction for $\gamma_1 \to l\bar{l}$ $(\nu\bar{\nu})$. For small values of the parameter h, the decay branching fractions of other $n = 1$ particles are insensitive to KK-parity violation, since such effects are suppressed by the cut-off scale Λ, so that they cannot compete with the KK-parity conserving modes. Therefore, the only phenomenological difference between UED with KK-parity conserved and KK-parity violated is the decay of the LKP and its decay gives rise to additional jets and leptons in the final states of UED cascades. Thus the additional leptons

lead to rather clean signatures with the possibility of reconstructing the γ_1 as an invariant mass peak. On the whole, depending on whether either or both of the pair-produced γ_1's decay leptonically, the lepton multiplicity of the ensuing final states may vary between 0 and 8.

2.3. Little Higgs models

2.3.1. Introduction

Little Higgs models [43, 44] have been proposed a few years ago to explain electroweak symmetry breaking and, in particular, to solve the so-called little hierarchy problem [45]. We can view the Standard Model (SM) as an effective field theory (EFT) with a cutoff Λ and parametrize new physics in terms of higher-dimensional operators which are suppressed by inverse powers of Λ. Precision tests of the SM have not shown any significant deviations, which in turn translates into a cutoff of about $\Lambda \sim 5 - 10$ TeV which is more than an order of magnitude above the electroweak scale. Since radiative corrections to the Higgs mass are quadratically sensitive to the cutoff Λ, some amount of fine-tuning is needed to get a Higgs which is lighter than about 200 GeV as indicated by electroweak precision data.

Little Higgs models suggest a way of stabilizing the mass of the Higgs in the presence of a cut-off Λ of the above kind of magnitude. Here the Higgs particle is a pseudo-Goldstone boson of a global symmetry G which is spontaneously broken at a scale f to a subgroup H. This symmetry protects the Higgs mass from getting quadratic divergences at one loop. The electroweak symmetry is broken via the Coleman-Weinberg mechanism [46] and the Higgs mass is generated radiatively, which leads naturally to a light Higgs boson $m_H \sim (g^2/4\pi)f \approx 100$ GeV, if the scale $f \sim 1$ TeV. The little Higgs model can then be interpreted as an EFT up to a new cutoff scale of $\Lambda \sim 4\pi f \sim 10$ TeV.

Among the different versions of this approach, the littlest Higgs model [47] achieves the cancellation of quadratic divergences with a minimal number of new degrees of freedom. However, precision electroweak constraints imply that the mass scale of the new particles in such theories has to be of the order of $f \gtrsim 5$ TeV in most of the natural parameter space [48], thus necessitating fine-tuning once more. The problem is circumvented through the introduction of an additional

discrete symmetry, the so-called T-parity [49,50], whereby all particles in the spectrum are classified as T-even or T-odd. This allows one to have the Higgs mass protected from quadratic divergences, and at the same time see a spectrum of additional gauge bosons, scalars and fermions, in the mass range of a few hundred GeV, with the lightest T-odd particle (LTP), typically the heavy neutral partner of the photon, A_H, being stable. In particular, for the Littlest Higgs model with T-parity (LHT) [50–53] it was shown in Refs. [52, 54, 55], that a scale f as low as 500 GeV is compatible with electroweak precision data. Furthermore, if T-parity is exact, the LTP can also be a potential dark matter (DM) candidate [51, 54, 56].

The experimental signals at colliders of a scenario with exact T-parity have close resemblance with those of supersymmetry with conserved R-parity or universal extra dimensions with KK-parity. First of all, T-odd particles can only be produced in pairs. Furthermore, all T-odd particles cascade decay down to the LTP which then carries away substantial missing transverse momentum, accompanied by jets and/or leptons rendered hard through the release of energy in the decay of the heavy new particles.

The phenomenology of the LHT with exact T-parity at the Large Hadron Collider (LHC) has been studied quite extensively [57–60]. Efforts are also on to discriminate the LHT signals from those of other scenarios where large missing E_T is predicted [61]. Later on, it was pointed out in Ref. [62] that T-parity can be violated in the EFT by topological effects related to anomalies in the underlying theory (UV completion of the LHT), by the Wess-Zumino-Witten (WZW) [63] anomaly term. However, relatively few studies have taken place on the collider signals of the scenario with T-parity violation [64–66]. Although Ref. [66] gives a very comprehensive list of signals for several regions in the parameter space, definitely more detailed studies of this interesting possibility are required, in particular, since the WZW term is a direct window into the UV completion of the LHT.

2.3.2. The Littlest Higgs model with T-parity

In the LHT a global symmetry $SU(5)$ is spontaneously broken down to $SO(5)$ at a scale $f \sim 1$ TeV. An $[SU(2) \times U(1)]^2$ gauge symmetry is imposed, which is simultaneously broken to the diagonal subgroup $SU(2)_L \times U(1)_Y$, the latter being identified with the SM gauge group. This leads to four heavy gauge bosons

$W_H^{\pm}, Z_H$ and A_H with masses $\sim f$ in addition to the SM gauge fields. The SM Higgs doublet is part of an assortment of pseudo-Goldstone bosons which result from the spontaneous breaking of the global symmetry. This symmetry protects the Higgs mass from getting quadratic divergences at one loop, even in the presence of gauge and Yukawa interactions. The multiplet of Goldstone bosons contains a heavy $SU(2)$ triplet scalar Φ as well. In contrast to SUSY, the new states which cancel the quadratically divergent contributions to the Higgs mass due to the top quark, gauge boson and Higgs boson loops, respectively, are heavy fermions, additional gauge bosons and triplet Higgs states.

In order to comply with strong constraints from electroweak precision data on the Littlest Higgs model [48], one imposes T-parity [49] which maps the two pairs of gauge groups $SU(2)_i \times U(1)_i, i = 1, 2$ into each other, forcing the corresponding gauge couplings to be equal, with $g_1 = g_2$ and $g_1' = g_2'$. All SM particles, including the Higgs doublet, are even under T-parity, whereas the four additional heavy gauge bosons and the Higgs triplet are T-odd. The top quark has two heavy fermionic partners, T_+ (T-even) and T_- (T-odd). For consistency of the model, one has to introduce the additional heavy, T-odd vector-like fermions u_H^i, d_H^i, e_H^i and ν_H^i ($i = 1, 2, 3$) for each SM quark and lepton field. For further details on the LHT, we refer the reader to Refs. [50–53].

The masses of the heavy gauge bosons in the LHT are given by

$$M_{W_H} = M_{Z_H} = gf\left(1 - \frac{v^2}{8f^2}\right) \approx 0.65f, \qquad M_{A_H} = \frac{fg'}{\sqrt{5}}\left(1 - \frac{5v^2}{8f^2}\right) \approx 0.16f, \tag{2.9}$$

where corrections of $\mathcal{O}(v^2/f^2)$ are neglected in the approximate numerical values. Thus these particles have masses of several hundreds of GeV for $f \sim 1$ TeV, although A_H, the heavy partner of the photon, can be quite light, because of the small prefactor, and is usually assumed to be the LTP. The masses of the heavy, T-odd fermions are determined by general 3×3 mass matrices in the (mirror) flavour space, $m_{q_H, l_H}^{ij} \sim \kappa_{q,l}^{ij} f$ with $i, j = 1, 2, 3$. We simplify our analysis by assuming that $\kappa_q^{ij} = \kappa_q \delta^{ij}$. The parameter $\kappa_q \sim \mathcal{O}(1)$ thus determines the masses of the heavy quarks in the following way:

$$m_{u_H} = \sqrt{2}\kappa_q f\left(1 - \frac{v^2}{8f^2}\right), \qquad m_{d_H} = \sqrt{2}\kappa_q f, \tag{2.10}$$

thereby allowing the new heavy quarks to have masses ranging from several hundreds of GeV to a TeV, for $f \sim 1$ TeV. Similarly, the masses of the heavy leptons in

the spectrum are determined by a common parameter κ_l. Note that these heavy quarks and leptons cannot be decoupled from the model as there is an upper bound $\kappa \leq 4.8$ (for $f = 1$ TeV) obtained from 4-fermion operators [52]. We will come back to lower limits on the masses of the heavy quarks and therefore on κ_q in the context of the model with T-parity violation.

The mass of the triplet scalar Φ is related to the doublet Higgs mass by $m_\Phi = \sqrt{2} m_H f/v$. Two more dimensionless parameters λ_1 and λ_2 appear in the top quark sector; the top mass being given by $m_t = (\lambda_1/\sqrt{1+R^2})v$, where $R = \lambda_1/\lambda_2$. The masses of the two heavy partners of the top quark, T_+ and T_-, can be expressed as $m_{T_+} = \lambda_2\sqrt{1+R^2} f$ and $m_{T_-} = \lambda_2 f$. We use $m_t = 175$ GeV in our analysis and set $R = 1$.

2.3.3. T-parity violation

As mentioned before, it was first pointed out in Ref. [62] that T-parity can be violated in the EFT by topological effects related to anomalies in the underlying theory (UV completion of the LHT). This induces a Wess-Zumino-Witten (WZW) term [63] in the low-energy effective Lagrangian, similarly to the WZW term of odd intrinsic parity in the usual chiral Lagrangian for QCD. This term encodes the Adler-Bell-Jackiw chiral anomaly [67] within the EFT framework and describes, for instance, the decay $\pi^0 \to \gamma\gamma$. The structure of the WZW term is thereby uniquely determined by the symmetry breaking pattern $G \to H$ and the gauged subgroups, up to a multiplicative quantized constant. This constant is related to the representation of new fermions in the underlying theory, if we assume that it is strongly interacting and a fermion condensate forms which signals spontaneous symmetry breaking. Essentially, as in QCD, the prefactor of the WZW term is a function of the number of 'colors' in the underlying theory.

Of course, there is no such WZW term, if there are no chiral anomalies in the underlying theory, for instance, if the low-energy non-linear sigma model Lagrangian of the LHT derives from a linear sigma model with new heavy fundamental scalar fields which break the symmetry, see Ref. [68] for an explicit construction of such an UV completion with unbroken T-parity.

As mentioned above, T-parity violation in the LHT and thus the decay of the heavy photon A_H arises via the so-called Wess-Zumino-Witten term, which,

according to Ref. [62], can be written as follows:

$$\Gamma_{\mathrm{WZW}} = \frac{N}{48\pi^2}\left(\Gamma_0[\Sigma] + \Gamma[\Sigma, A_l, A_r]\right). \tag{2.11}$$

The functional $\Gamma_0[\Sigma]$ is the ungauged WZW term which depends only on the non-linear sigma model field Σ. It cannot be expressed as a four-dimensional integral over a local Lagrangian. Instead, a closed form can be written as an integral over a five-dimensional manifold with ordinary spacetime as its boundary [63]. The term $\Gamma[\Sigma, A_l, A_r]$ is the gauged part of the WZW term. This part can be written as an ordinary four-dimensional integral over a local Lagrangian. The explicit expressions for the functionals and the relation of the fields $A_{l,r}$ to the gauge fields in the LHT can be found in Ref. [62]. While these functionals are uniquely given by the symmetry breaking pattern $SU(5) \to SO(5)$ and the gauged subgroups in the LHT, the integer N in Eq. (2.11) depends on the UV completion of the LHT. In strongly coupled underlying theories it will be related to the representation of the fermions whose condensate acts as order parameter of the spontaneous symmetry breaking. In the simplest case, N will be the number of 'colours' in that UV completion, as is the case for the WZW term in ordinary QCD. The overall coefficient $N/48\pi^2$ encapsulates the effect of the chiral anomaly, which is a one-loop effect in the corresponding high-scale theory.

As noted in Ref. [62], the WZW term in Eq. (2.11) is not manifestly gauge invariant. Gauge invariance is violated by terms with three or four gauge bosons with an odd number of T-odd gauge bosons, e.g. by a term like $\epsilon_{\mu\nu\rho\sigma} V_H^\mu V^\nu \partial^\rho V^\sigma$, where V_H is a T-odd gauge boson and V denotes a SM gauge boson. Such anomalous terms need to be cancelled to have a consistent theory and some mechanisms to achieve this are discussed in Ref. [62]. After this cancellation, the leading T-odd interactions appear only at order $1/f^2$. For instance, we get a vertex with one T-odd gauge boson and two SM gauge bosons from $\epsilon_{\mu\nu\rho\sigma}(H^\dagger H/f^2) V_H^\mu V^\nu \partial^\rho V^\sigma$, after the Higgs doublet H gets a vacuum expectation value v.

To leading order in $1/f$, the part of the WZW term containing one neutral T-odd gauge boson is given, in unitary gauge, by

$$\begin{aligned}\Gamma_n = \frac{N g^2 g'}{48\pi^2 f^2}\int d^4x\,(v+h)^2\,\epsilon_{\mu\nu\rho\sigma}\times \\ \Big[-(6/5)A_H^\mu\left(c_w^{-2} Z^\nu \partial^\rho Z^\sigma + W^{+\nu} D_A^\rho W^{-\sigma} + W^{-\nu} D_A^\rho W^{+\sigma} + i(3g x_w + g' s_w) W^{+\nu} W^{-\rho} Z^\sigma\right) \\ + t_w^{-1} Z_H^\mu \left(2c_w^{-2} Z^\nu \partial^\rho Z^\sigma + W^{+\nu} D_A^\rho W^{-\sigma} + W^{-\nu} D_A^\rho W^{+\sigma} - 2i(2g c_w + g' s_w) W^{+\nu} W^{-\rho} Z^\sigma\right)\Big].\end{aligned} \tag{2.12}$$

Here h is the physical Higgs boson, $D_A^\mu W^{\pm\nu} = (\partial^\mu \mp ieA^\mu)W^{\pm\nu}$ and s_w, c_w and t_w denote the sine, cosine and tangent of the weak mixing angle, respectively. All T-violating vertices with up to four legs have been tabulated in Ref. [66] and implemented into a model file for CalcHEP 2.5 [69,70].

If A_H is heavy, the vertices in Eq. (2.12) lead to its decay into a pair of Z-bosons or into W^+W^- with a decay width of the order of eV [64]. On the other hand, if $M_{A_H} < 2M_W$, the heavy photon cannot decay into on-shell SM gauge bosons. It could still decay into (one or two) off-shell SM gauge bosons, but for low masses loop induced decays into SM fermions will dominate. In fact, as discussed in Ref. [66], the T-violating vertices can couple the A_H to two SM fermions via a triangle loop. But since the corresponding one-loop diagrams are logarithmically divergent, one needs to add counterterms to the effective Lagrangian of the form

$$\mathcal{L}_{\text{ct}} = \bar{f}\gamma_\mu \left(c_L^f P_L + c_R^f P_R\right) f A_H^\mu, \tag{2.13}$$

$$c_i^f = c_{i,\epsilon}^f \left(\frac{1}{\epsilon} + \log(\mu^2) + \mathcal{O}(1)\right), \tag{2.14}$$

where $P_{L,R} = (\mathbf{1} \mp \gamma_5)/2$. As shown in Ref. [66] the counterterms can also be written in a manifestly gauge invariant way. These counterterms are only some of the infinitely many terms which have to be included anyway at higher orders in the momentum and loop expansion in the EFT. This procedure to renormalize the EFT order by order is well known from chiral perturbation theory [71] and, as usually done there, dimensional regularization was used in Ref. [66] which preserves chiral and gauge invariance.

The coefficients $c_i^f(\mu)$ of the counterterms can be estimated by naive dimensional analysis [72] or naturalness arguments. Since the scale dependence of the loop diagrams is cancelled by the scale dependence of the counterterms $c_i^f(\mu)$, any change of order one in the renormalization scale should be compensated by a change of order one in $c_i^f(\mu)$. Therefore these coefficients are given, up to $\mathcal{O}(1)$ factors, by the coefficients of the leading $1/\epsilon$ divergence in dimensional regularization of the loop integrals. The coefficients $c_{i,\epsilon}^f$ are explicitly listed in Ref. [66] and we have included the vertices from Eq. (2.13) in the CalcHEP model file.

Note that the unknown constant N from Eq. (2.12) cancels out in the branching ratios of A_H. Actually, if we could measure the total decay width of A_H, we could even get information on N itself, in the same way as the decay $\pi^0 \to \gamma\gamma$

yields information about the number of colors in ordinary QCD, however, the width of $\mathcal{O}\,(\mathrm{eV})$ for A_H is too small to be measurable.

The prefactor of the WZW term, $N/48\pi^2$, is of the size of a one-loop effect, thus the coupling of A_H and other T-odd gauge bosons to SM fermions via a triangle-loop is effectively 2-loop suppressed. Therefore these T-violating couplings will not affect the production mechanism of T-odd particles and their cascade decays at colliders, or EW precision observables [66]. In particular, T-parity violation should still satisfy the EW data with a rather small scale f. It is only in decays of the A_H that the anomaly term acquires phenomenological importance. As we demonstrate in what follows, reconstruction of the A_H mass becomes possible through such decays, thus confirming the bosonic nature of the LTP.

The phenomenology at colliders of the LHT with T-parity violation changes completely [62, 64–66]. Assuming that A_H is the LTP, the T-violating terms will lead to its decay into SM particles either directly into two electroweak gauge bosons or via one-loop graphs into SM fermion pairs. The decay width will be very small, of the order of eV. Nevertheless, A_H will promptly decay inside the detector and one does therefore not expect events with large missing transverse energy. As we will see in Chapter 4, this allows one to reconstruct the masses of the new particles, in particular of A_H itself. On the other hand, since the T-violating couplings are very small, the production mechanism of T-odd particles is essentially unchanged from the case with exact T-parity and the T-odd particles will again cascade decay down to A_H. Of course, with T-parity violation, the unstable LTP will now no longer be a suitable DM candidate. The LEP bounds of order 100 GeV still apply to all T-odd particles except for the A_H. In addition, based on an analysis of recent Tevatron data from CDF Vista on multijet events [73], it has been argued in Ref. [66] that a bound of $m_{q_H} > 350$ GeV applies to the LHT with broken T-parity.

Bibliography

[1] For an introduction, see, for example, H. P. Nilles, Phys. Rept. **110**, 1 (1984); H. E. Haber and G. L. Kane, Phys. Rept. **117**, 75 (1985); J. Wess and J. Bagger, *Supersymmetry and Supergravity*, (Princeton Univ. Press, 1992); G. Kane (ed), *Perspectives on Supersymmetry*, (World Scientific, 1998); M. Drees, R. Godbole and P. Roy, *Theory and Phenomenology of Sparticles*, (World Scientific, 2004); H. Baer and X. Tata *Weak Scale Supersymmetry From Superfields to Scattering Events*, (Cambridge University Press, 2006).

[2] S. P. Martin, "A supersymmetry primer," arXiv:hep-ph/9709356.

[3] J. Wess and B. Zumino, Nucl. Phys. B **70**, 39 (1974). J. Wess and B. Zumino, Phys. Lett. B **49**, 52 (1974). J. Wess and B. Zumino, Nucl. Phys. B **78**, 1 (1974). J. Wess and B. Zumino, Phys. Lett. B **74**, 51 (1978).

[4] A. Salam and J. A. Strathdee, Phys. Lett. B **51**, 353 (1974). A. Salam and J. A. Strathdee, Nucl. Phys. B **76**, 477 (1974). A. Salam and J. A. Strathdee, Nucl. Phys. B **80**, 499 (1974). A. Salam and J. A. Strathdee, Nucl. Phys. B **87**, 85 (1975).

[5] P. Fayet, Phys. Lett. B **58**, 67 (1975). P. Fayet, Nucl. Phys. **B90**, 104 (1975). P. Fayet, Nuovo Cim. A **31**, 626 (1976). P. Fayet, Phys. Lett. B **64**, 159 (1976). P. Fayet and S. Ferrara, Phys. Rept. **32**, 249 (1977).

[6] L. Girardello and M.T. Grisaru Nucl. Phys. B **194**, 65 (1982); D.J.H. Chung et al., Phys. Rept. **407**, 1 (2005).

[7] S. Dimopoulos, S. Raby and F. Wilczek, Phys. Rev. D **24**, 1681 (1981); S. Dimopoulos, H. Georgi, Nucl. Phys. **B193**, 150 (1981).

[8] S. R. Coleman and J. Mandula, Phys. Rev. **159**, 1251 (1967);

[9] R. Haag, J. Lopuszanski, and M. Sohnius, Nucl. Phys. B **88**, 257 (1975).

[10] F. Gabbiani, E. Gabrielli, A. Masiero and L. Silvestrini, Nucl. Phys. B **477**, 321 (1996).

[11] A. H. Chamseddine, R. Arnowitt and P. Nath, Phys. Rev. Lett. **49**, 970 (1982); R. Barbieri, S. Ferrara and C. A. Savoy, Phys. Lett. B **119**, 343 (1982); L. J. Hall, J. Lykken and S. Weinberg, Phys. Rev. D **27**, 2359 (1983); P. Nath, R. Arnowitt and A. H. Chamseddine, Nucl. Phys. B **227**, 121 (1983); N. Ohta, Prog. Theor. Phys. **70**, 542 (1983).

[12] M. Dine, A. E. Nelson, Phys. Rev. D **48**, 1277 (1993) [hep-ph/9303230]; M. Dine, A.E. Nelson, Y. Shirman, Phys. Rev. D **51**, 1362 (1995) [hep-ph/9408384]; M. Dine, A.E. Nelson, Y. Nir, Y. Shirman, Phys. Rev. D **53**, 2658 (1996) [hep-ph/9507378].

[13] L. Randall and R. Sundrum, Nucl. Phys. B **557**, 79 (1999) [hep-th/9810155]; G.F. Giudice, M.A. Luty, H. Murayama and R. Rattazzi, JHEP **9812**, 027 (1998) [hep-ph/9810442].

[14] H. Baer, M. Drees and X. Tata, Phys. Rev. D **41**, 34143420 (1990); The LEP SUSY Working Group (LEPSUSYWG), `http://www.cern.ch/lepsusy`.

[15] H. Baer, C. Kao and X. Tata, Phys. Rev. D **48**, 51755180 (1993); M. Carena, R. Culbertson, H. Frisch, S. Eno and S. Mrenna, Rev. Mod. Phys. **71**, 937981 (1999); The Tevatron Run II studies on supersymmetry: S. Abel *et al.* [SUGRA Working Group Collaboration], [hep-ph/0003154]; S. Ambrosanio *et al.* [MSSM Working Group Collaboration], [hep-ph/0006162]; R. Culbertson *et al.* [SUSY Working Group Collaboration], [hep-ph/0008070].

[16] For a review see, for example, R. Barbier *et al.*, Phys. Rept. **420**, 1 (2005).

[17] V. D. Barger, G. F. Giudice and T. Han, Phys. Rev. D **40**, 2987 (1989).

[18] B. Mukhopadhyaya, arXiv:hep-ph/0301278, and references therein.

[19] S. Roy and B. Mukhopadhyaya, Phys. Rev. D **55**, 7020 (1997); B. Mukhopadhyaya, S. Roy and F. Vissani, Phys. Lett. B **443**, 191 (1998); M. Hirsch *et al.*, Phys. Rev. D **62**, 113008 (2000).

[20] H. Baer, C. Kao and X. Tata, Phys. Rev. D **51** (1995) 2180.

[21] B. Mukhopadhyaya, S. Mukhopadhyay, Phys. Rev. **D82**, 031501 (2010).

[22] S. Mukhopadhyay and B. Mukhopadhyaya, Phys. Rev. D **84**, 095001 (2011).

[23] T. Kaluza, Sitzungsber. Preuss. Akad. Wiss. Berlin (Math. Phys.) **1921**, 966 (1921); O. Klein, Z. Phys. **37**, 895 (1926).

[24] I. Antoniadis, Phys. Lett. B **246**, 377 (1990); N. Arkani-Hamed, S. Dimopoulous and G. Dvali, Phys. Lett. B **429**, 263 (1998); I. Antoniadis,

N. Arkani-Hamed, S. Dimopoulos and G. R. Dvali, Phys. Lett. B **436**, 257 (1998).

[25] L. Randall and R. Sundrum, Phys. Rev. Lett. **83**, 3370 (1999); *ibid* **83**, 4690 (1999).

[26] T. Appelquist, H. C. Cheng and B. A. Dobrescu, Phys. Rev. D **64** (2001) 035002; H. C. Cheng, K. T. Matchev and M. Schmaltz, Phys. Rev. D **66** (2002) 056006.

[27] I. Antoniadis, Phys. Lett. B **246** (1990) 377.

[28] G. Bhattacharyya, S. K. Majee and A. Raychaudhuri, Nucl. Phys. B **793** (2008) 114.

[29] N. Arkani-Hamed and M. Schmaltz, Phys. Rev. D **61** (2000) 033005.

[30] K. Dienes, E. Dudas, and T. Gherghetta; Nucl. Phys. B **537** (1999) 47.

[31] K. R. Dienes, E. Dudas and T. Gherghetta, Phys. Lett. B **436** (1998) 55; For a parallel analysis based on a minimal length scenario, see S. Hossenfelder, Phys. Rev. D **70** (2004) 105003.

[32] G. Bhattacharyya, A. Datta, S. K. Majee and A. Raychaudhuri, Nucl. Phys. B **760** (2007) 117.

[33] G. Servant and T. M. P. Tait, Nucl. Phys. B **650** (2003) 391.

[34] H. C. Cheng, K. T. Matchev and M. Schmaltz, Phys. Rev. D **66**, 036005 (2002).

[35] P. Nath and M. Yamaguchi, Phys. Rev. D **60** (1999) 116006.

[36] D. Chakraverty, K. Huitu and A. Kundu, Phys. Lett. B **558** (2003) 173.

[37] A.J. Buras, M. Spranger and A. Weiler, Nucl. Phys. B **660** (2003) 225; A.J. Buras, A. Poschenrieder, M. Spranger and A. Weiler, Nucl. Phys. B **678** (2004) 455.

[38] K. Agashe, N.G. Deshpande and G.H. Wu, Phys. Lett. B **514** (2001) 309.

[39] J.F. Oliver, J. Papavassiliou and A. Santamaria, Phys. Rev. D **67** (2003) 056002.

[40] T. Appelquist and H. U. Yee, Phys. Rev. D **67** (2003) 055002.

[41] T.G. Rizzo and J.D. Wells, Phys. Rev. D **61** (2000) 016007; A. Strumia, Phys. Lett. B **466** (1999) 107; C.D. Carone, Phys. Rev. D **61** (2000) 015008.

[42] B. Bhattacherjee, Phys. Rev. D **79** (2009) 016006.

[43] N. Arkani-Hamed, A. G. Cohen and H. Georgi, Phys. Lett. B **513**, 232 (2001);

N. Arkani-Hamed, A. G. Cohen, T. Gregoire and J. G. Wacker, JHEP **0208**, 020 (2002).

[44] For reviews, see M. Schmaltz and D. Tucker-Smith, Ann. Rev. Nucl. Part. Sci. **55**, 229 (2005); M. Perelstein, Prog. Part. Nucl. Phys. **58**, 247 (2007); M. C. Chen, Mod. Phys. Lett. A **21**, 621 (2006); E. Accomando *et al.*, hep-ph/0608079, Chapter 7.

[45] R. Barbieri and A. Strumia, hep-ph/0007265; Phys. Lett. B **462**, 144 (1999).

[46] S. R. Coleman and E. Weinberg, Phys. Rev. D **7**, 1888 (1973).

[47] N. Arkani-Hamed, A. G. Cohen, E. Katz and A. E. Nelson, JHEP **0207**, 034 (2002).

[48] C. Csaki *et al.*, Phys. Rev. D **67**, 115002 (2003); J. L. Hewett, F. J. Petriello and T. G. Rizzo, JHEP **0310**, 062 (2003); C. Csaki *et al.*, Phys. Rev. D **68**, 035009 (2003); M. Perelstein, M. E. Peskin and A. Pierce, Phys. Rev. D **69**, 075002 (2004); M. C. Chen and S. Dawson, Phys. Rev. D **70**, 015003 (2004); W. Kilian and J. Reuter, Phys. Rev. D **70**, 015004 (2004); G. Marandella, C. Schappacher and A. Strumia, Phys. Rev. D **72**, 035014 (2005).

[49] H. C. Cheng and I. Low, JHEP **0309**, 051 (2003); JHEP **0408**, 061 (2004).

[50] I. Low, JHEP **0410**, 067 (2004).

[51] J. Hubisz and P. Meade, Phys. Rev. D **71**, 035016 (2005).

[52] J. Hubisz, P. Meade, A. Noble and M. Perelstein, JHEP **0601**, 135 (2006).

[53] C. R. Chen, K. Tobe and C. P. Yuan, Phys. Lett. B **640**, 263 (2006).

[54] M. Asano, S. Matsumoto, N. Okada and Y. Okada, Phys. Rev. D **75**, 063506 (2007).

[55] R. S. Hundi, B. Mukhopadhyaya and A. Nyffeler, Phys. Lett. B **649**, 280 (2007).

[56] A. Birkedal, A. Noble, M. Perelstein and A. Spray, Phys. Rev. D **74**, 035002 (2006); C. S. Chen, K. Cheung and T. C. Yuan, Phys. Lett. B **644**, 158 (2007).

[57] A. Freitas and D. Wyler, JHEP **0611**, 061 (2006).

[58] A. Belyaev, C. R. Chen, K. Tobe and C. P. Yuan, Phys. Rev. D **74**, 115020 (2006). *A* CalcHEP *model file for the Littlest Higgs model with T-parity*, `http://hep.pa.msu.edu/LHT/`

[59] C. O. Dib, R. Rosenfeld and A. Zerwekh, JHEP **0605**, 074 (2006); L. Wang, W. Wang, J. M. Yang and H. Zhang, Phys. Rev. D **75**, 074006 (2007);

M. Carena, J. Hubisz, M. Perelstein and P. Verdier, Phys. Rev. D **75**, 091701 (2007); Q. H. Cao, C. S. Li and C. P. Yuan, Phys. Lett. B **668**, 24 (2008); S. Matsumoto, M. M. Nojiri and D. Nomura, Phys. Rev. D **75**, 055006 (2007); D. Choudhury and D. K. Ghosh, JHEP **0708**, 084 (2007); Q. H. Cao and C. R. Chen, Phys. Rev. D **76**, 075007 (2007); S. Matsumoto, T. Moroi and K. Tobe, Phys. Rev. D **78**, 055018 (2008).

[60] G. Cacciapaglia *et al.*, arXiv:0911.4630 [hep-ph]; G. Cacciapaglia, S. R. Choudhury, A. Deandrea and N. Gaur, arXiv:0911.4632 [hep-ph].

[61] P. Meade and M. Reece, Phys. Rev. D **74**, 015010 (2006); L. T. Wang and I. Yavin, JHEP **0704**, 032 (2007); C. S. Chen, K. Cheung and T. C. Yuan, Phys. Lett. B **644**, 158 (2007); M. M. Nojiri and M. Takeuchi, Phys. Rev. D **76**, 015009 (2007); C. Kilic, L. T. Wang and I. Yavin, JHEP **0705**, 052 (2007); L. Wang, W. Wang, J. M. Yang and H. Zhang, Phys. Rev. D **76**, 017702 (2007); A. Datta *et al.*, Phys. Lett. B **659**, 308 (2008); J. Hubisz, J. Lykken, M. Pierini and M. Spiropulu, Phys. Rev. D **78**, 075008 (2008). A. Belyaev *et al.*, Pramana **72**, 229 (2009) [arXiv:0806.2838 [hep-ph]]; B. Bhattacherjee, A. Kundu, S. K. Rai and S. Raychaudhuri, arXiv:0910.4082 [hep-ph].

[62] C. T. Hill and R. J. Hill, Phys. Rev. D **75**, 115009 (2007); Phys. Rev. D **76**, 115014 (2007).

[63] J. Wess and B. Zumino, Phys. Lett. B **37**, 95 (1971); E. Witten, Nucl. Phys. B **223**, 422 (1983).

[64] V. Barger, W. Y. Keung and Y. Gao, Phys. Lett. B **655**, 228 (2007).

[65] W. Y. Keung, I. Low and J. Shu, Phys. Rev. Lett. **101**, 091802 (2008).

[66] A. Freitas, P. Schwaller and D. Wyler, JHEP **0809**, 013 (2008).

[67] S. L. Adler, Phys. Rev. **177**, 2426 (1969); J. S. Bell and R. Jackiw, Nuovo Cim. A **60**, 47 (1969).

[68] C. Csaki, J. Heinonen, M. Perelstein and C. Spethmann, Phys. Rev. D **79**, 035014 (2009).

[69] A. Pukhov, arXiv:hep-ph/0412191.

[70] A. Freitas, P. Schwaller and D. Wyler, *A* CalcHEP *model file for the Littlest Higgs model with broken T-parity*,
`http://www.itp.uzh.ch/~pedro/lht/`

[71] S. Weinberg, Physica (Amsterdam) **96A**, 327 (1979); J. Gasser and

H. Leutwyler, Ann. Phys. (N.Y.) **158**, 142 (1984); J. Gasser and H. Leutwyler, Nucl. Phys. **B250**, 465 (1985).

[72] A. Manohar and H. Georgi, Nucl. Phys. B **234**, 189 (1984).

[73] Vista/Sleuth Global Search for New Physics in 2.0 fb^{-1} of $p\bar{p}$ Collisions at $\sqrt{s} = 1.96$ TeV,
http://www-cdf.fnal.gov/physics/exotic/r2a/20080228.vista_sleuth/publicPage.html

Chapter 3.

LHC : probing physics with hadron colliders

3.1. The Large Hadron Collider : An overview

The Large Hadron Collider (LHC) [1] is the highest energy man-made accelerator ever built. It's located at CERN, Geneva, where it spans the border between Switzerland and France about 100 meters underground. It is a proton-proton collider situated within a tunnel of circumference 27 kilometers. Its design energy is 7 TeV per proton, giving rise to 14 TeV energy in the centre of mass. Apart from protons, the LHC also collides lead ions for studying heavy ion physics, especially the formation of quark-gluon plasma. The highest energy hadron collider before the LHC was the Tevatron collider at Fermilab, Chicago, which made important advances in particle physics including the discovery of the top quark. Tevatron was a proton-antiproton collider with a centre of mass energy of 1.96 TeV.

Unlike in electron-positron colliders like LEP, at hadron colliders the effective energy scale that can be probed is not the centre of mass energy, but a fraction of that, since the constituent partons inside the proton (quarks and gluons), which participate in hard collisions producing heavier particles, carry only a part of the proton's energy. Therefore, the energy scale that can be probed at the LHC is of

the order of a TeV. In addition to centre of mass energy, another important factor in a collider experiment is the number of particles passing each other per unit time through unit transverse area at the interaction point, which is known as instantaneous luminosity. The design luminosity of the LHC is $10^{34}\ cm^{-2}\ s^{-1}$ which is generally expressed as $10\ nb^{-1}\ s^{-1}$. This instantaneous luminosity corresponds to an integrated luminosity of around $100\,\text{fb}^{-1}$ per year.

Due to certain technical problems, in the initial phase of its running, the LHC operated at a lower centre of mass energy of 7 TeV and by the end of 2011, has collected around $5\,\text{fb}^{-1}$ of data. During its 2012 run, the energy will be upgraded to 8 TeV with a target of accumulating around $15\,\text{fb}^{-1}$ of data by the end of this year.

Six primary experiments are underway at the LHC, each one being characterised by its unique particle detector. The two large experiments, ATLAS [2] and CMS [3], are general-purpose detectors designed to look for and study Higgs physics, electroweak and QCD physics (most importantly physics with heavier quarks like the top and bottom), and any new physics that may exist beyond the standard model. Having two independently designed detectors is vital for cross-confirmation of any new discoveries made. The ATLAS (A Toroidal LHC Apparatus) detector is the largest volume particle detector ever constructed. It is 46 m long, 25 m high and 25 m wide and weighs 7000 tonnes. The CMS (Compact Muon Solenoid) detector is built around a huge solenoid magnet. This takes the form of a cylindrical coil of superconducting cable that generates a magnetic field of 4 Tesla. Although it is smaller in size than ATLAS (21 m long, 15 m wide and 15 m high), it weighs much more, a staggering 12500 tonnes.

Apart from ATLAS and CMS, there are two medium-size experiments, ALICE and LHCb. The ALICE experiment is designed to study heavy-ion collisions, and the formation of quark-gluon plasma, while the LHCb experiment will study the physics of B-hadrons, trying to uncover any hint of new physics through precision studies. Two further experiments, TOTEM and LHCf, are much smaller in size. They are designed to focus on "forward particles" (protons or heavy ions). These are particles that just brush past each other as the beams collide, rather than meeting head-on.

The ATLAS, CMS, ALICE and LHCb detectors are installed in four huge underground caverns located around the ring of the LHC. The detectors used by the TOTEM experiment are positioned near the CMS detector, whereas those

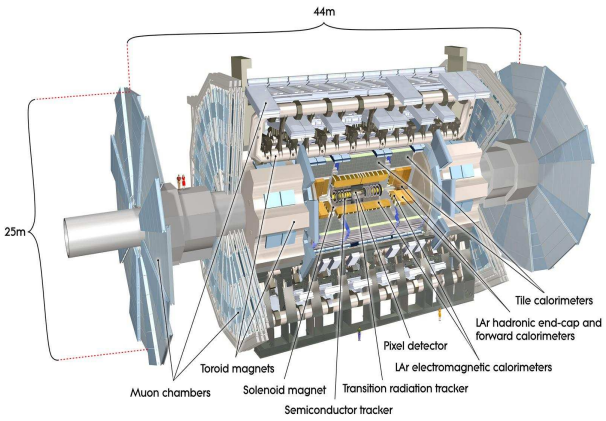

Figure 3.1.: A schematic view of the ATLAS detector.

used by LHCf are near the ATLAS detector.

3.2. Particle detection : important components of a detector

Since in this thesis we shall be concerned with studying the manifestations of new physics beyond the standard model at the LHC in the form of various events comprising of leptons, jets and missing transverse momentum, it will be useful to note down the various components of a general purpose detector like ATLAS and CMS, which are used to identify the particles and determine their momentum, energy, electric charge etc. We describe below these important components one by one [4] (also see Fig.3.1 for an illustrative picture of the ATLAS detector):

1. **Tracker:** The tracking chamber, placed at the innermost part of a cylindrical detector, is used to determine trajectories of charged particles and their electromagnetic energy loss. At ATLAS and CMS, the trackers can cover a pseudo-rapidity range of around $|\eta| < 2.5$. For measuring charge particle momenta, a high magnetic field is used (2 Tesla for ATLAS and 4 Tesla for CMS), the curvature of the trajectory being inversely proportional to the particle momentum. If B is the external magnetic field, and Q is the electric charge of a particle, then the curvature is proportional to (QB/p), where

p is the particle's momentum. As charged particles travel through matter they also lose energy, and this energy loss measurement as a function of distance traversed can also be used for particle identification. In particular, the dependence of the energy loss by excitation and ionization on a particle's charge and its speed is given by the Bethe-Bloch formula:

$$\frac{dE}{dx} \propto \left(\frac{Q}{\beta}\right)^2 \tag{3.1}$$

Using this formula, one can determine $\beta(= v/c)$, and therefore the mass of the particle, if the momentum is known from the curvature measurement. All these measurements are possible if the value of the electric charge Q is known from some other source, if not, then one might need some additional measurement like the time-of-flight, to determine the particle's identity completely.

2. **Electromagnetic Calorimeter:** Surrounding the tracking system is the electromagnetic calorimeter, which is used to measure the energy of electrons and photons. As is well-known, high-energy electrons and photons often lead to cascades of electromagnetic showers due to bremsstrahlung and pair production. The number of particles created increase exponentially with the depth of the medium. Since the incident energy to be measured by the electromagnetic calorimetry (ECAL) is proportional to the maximum number of particles created (N), the energy resolution is characterized by $1/\sqrt{N}$. The rapidity coverage of the ECAL can be around $|\eta_{e,\gamma}| < 3.0$ or slightly higher for ATLAS and CMS.
3. **Hadronic Calorimeter:** The hadronic calorimeter (HCAL) is used to measure the energies of hadrons, and functions similarly as the ECAL, using showers generated by high-energy hadrons. The rapidity coverage of the HCAL, which is located outside the ECAL component, is about $|\eta_{hadrons}| <$ 5.0, which is higher than that of ECAL.
4. **Muon Chamber:** Since very high energy muons have a longer lifetime than that of a muon at rest, they travel a long distance before decaying. Therefore, the muon chamber is located at the outermost layer of the detectors. They are used to measure the momenta of the muons very precisely.

3.3. Modelling detector resolution effects

The effects of finite resolution of a detector is taken into account by smearing the momenta and energies of the particles in a prescribed manner determined by the detector materials. Throughout this thesis, we have followed the prescriptions given for the ATLAS detector as a prototype [2, 5]. We have approximated the detector resolution effects by smearing the energies or transverse momenta with Gaussian functions. The different contributions to the resolution error have been added in quadrature. In the following, we note down the resolution parameters used in our work:

- **Electron energy (E) resolution:**

$$\frac{\sigma(E)}{E} = \frac{a}{\sqrt{E}} \oplus b \oplus \frac{c}{E}, \tag{3.2}$$

where

$$(a, b, c) = \begin{cases} (0.030\ \text{GeV}^{1/2},\ 0.005,\ 0.2\ \text{GeV}), & |\eta| < 1.5, \\ (0.055\ \text{GeV}^{1/2},\ 0.005,\ 0.6\ \text{GeV}), & 1.5 < |\eta| < 2.5. \end{cases} \tag{3.3}$$

- **Muon transverse momentum (p_T) resolution:**

$$\frac{\sigma(P_T)}{P_T} = \begin{cases} a, & p_T < 100\ \text{GeV}, \\ a + b\ \log \dfrac{p_T}{100\ \text{GeV}}, & p_T > 100\ \text{GeV}, \end{cases} \tag{3.4}$$

with

$$(a, b) = \begin{cases} (0.008,\ 0.037), & |\eta| < 1.5, \\ (0.020,\ 0.050), & 1.5 < |\eta| < 2.5. \end{cases} \tag{3.5}$$

- **Jet transverse energy (E_T) resolution:**

$$\frac{\sigma(E_T)}{E_T} = \frac{a}{\sqrt{E_T}}, \tag{3.6}$$

with $a = 0.5\ \text{GeV}^{1/2}$.

3.4. Important kinematic variables used at a hadron collider

The constituents of the colliding protons, the partons, carry a fraction of the original proton momenta. In particular, each parton-parton collision has a different centre of mass frame, which is boosted along the beam direction with respect to the proton-proton centre of mass frame (which is also the lab frame). Here we call the beam direction the longitudinal direction (or z-direction), and the other two orthogonal directions constitute the transverse plane. To describe the final states of a collision, it is thus convenient to use a co-ordinate system that transforms in a simple manner under longitudinal boosts [4]. Therefore, instead of using a spherical polar co-ordinate system to describe the momentum components of a particle (namely, p, the magnitude of the momentum, θ, the polar angle and ϕ, the azimuthal angle), we use the transverse momentum $p_T (= \sqrt{p_x^2 + p_y^2} = p \sin\theta)$, rapidity ($y$) and azimuthal angle ϕ. The rapidity of a particle is defined by:

$$y = \frac{1}{2} \ln \frac{E + p_z}{E - p_z} \tag{3.7}$$

Now, it can be easily seen that in a frame boosted with respect to the lab frame with a relative velocity β_0, the rapidity of the particle will be given by

$$y' = y - y_0 \tag{3.8}$$

where $y_0 = \frac{1}{2} \ln \frac{1+\beta_0}{1-\beta_0}$. Thus, a longitudinal boost is just a translation in y. Hence if we use the variables (p_T, y, ϕ) to describe a final state instead of (p_T, θ, ϕ), the boosted final state will look identical except for a shift in y, thus making it very convenient. As a corollary, the rapidity difference $\Delta y = y_2 - y_1 = y_2' - y_1'$ will be invariant in two frames.

To summarize, we therefore use a co-ordinate system, in which a particle's four-momentum is written in terms of (p_T, y, ϕ) with

$$p^\mu = (E_T \cosh y, p_T \cos\phi, p_T \sin\phi, E_T \sinh y) \tag{3.9}$$

where $E_T = \sqrt{p_T^2 + m^2}$.

For very highly energetic particles with $p_T \gg m$, $E_T \sim p_T$, and

$$y \to \frac{1}{2} \ln \frac{1 + \cos\theta}{1 - \cos\theta} \equiv \eta \tag{3.10}$$

η is known as the pseudo-rapidity, which is in one-to-one correspondence with the polar angle θ, with $-\infty < \eta < \infty$. But note that, a small excursion in η takes one to very forward angles, for example, $\eta = 5$ corresponds to $\theta = 0.77^{\circ}$.

Another particular variable which is useful for defining separation (in the pseudo-rapidity azimuthal angle plane) among objects like jets and leptons is defined as:

$$\Delta R = \sqrt{(\Delta\eta)^2 + (\Delta\phi)^2} \tag{3.11}$$

We shall make use of these variables throughout in our studies, and shall define other relevant kinematic variables in the specific contexts where they will be useful.

Bibliography

[1] The LHC Study Group, Large Hadron Collider, The Accelerator Project, CERN/AC/93-03 (LHC); The LHC Study Group, P. Lefevre and T. Pettersson (editors), The Large Hadron Collider, Conceptual Study, CERN/AC/95-05 (LHC); (http://lhc.web.cern.ch/lhc/).

[2] G. Aad *et al.* [The ATLAS Collaboration], arXiv:0901.0512 [hep-ex].

[3] G. L. Bayatian *et al.* [CMS Collaboration], J. Phys. G **34**, 995 (2007).

[4] For a review of collider physics, see, T. Han, arXiv: hep-ph/0508097.

[5] Private communication with Bruce Mellado.

Part II.

Low Missing Energy New Physics: Identification at the LHC

Chapter 4.

Low mass resonances in the littlest Higgs model with T-parity violation

4.1. Introduction

We introduced little Higgs models, and in particular, the littlest Higgs model with T-parity (LHT) in Chapter 2.3. There, we also saw that in the presence of the T-parity violating Wess-Zumino-Witten (WZW) anomaly term, the otherwise stable heavy photon A_H in the LHT decays to either Standard Model (SM) gauge boson pairs, or to SM fermions via loop diagrams. In this chapter, we make a detailed study of the collider signatures where the A_H can be reconstructed from invariant mass peaks in the opposite sign same flavour dilepton or the four-lepton channel [1]. This enables us to obtain information about the fundamental symmetry breaking scale f in the LHT and thereby the low-lying mass spectrum of the theory. In addition, indication of the presence of the WZW term gives us hints of the possible UV completion of the LHT via strong dynamics.

This chapter is organized as follows. In Section 4.2 we discuss the dilepton and four-lepton signal processes, starting with the parton-level production of

heavy T-odd quark pairs and the decay modes and branching ratios of A_H. We also argue why the A_H is different from the often considered Z' gauge boson or the first Kaluza-Klein excitation of the graviton and thus could have escaped detection, even with a low mass of the order of 100 GeV. Finally, we present our choice of benchmark points for several values for the heavy quark masses m_{q_H} and for several values for the mass of the heavy photon M_{A_H}. Section 4.3 gives details on our event generation for the signal and the background. We describe the main sources of backgrounds from the SM and from within the LHT. We then go on to present our event selection criteria for the dilepton and the four-lepton signal and the various cuts to reduce the backgrounds. In Sec. 4.4 we present our results, first for the dilepton signal and then for the four-lepton signature. In both cases, we give numbers for the expected signal and background cross-sections after the cuts for the LHC running at a center of mass energy of 10 TeV (14 TeV) and the number of signal and background events for an integrated luminosity of $200\,\text{pb}^{-1}$ ($30\,\text{fb}^{-1}$). We summarize and conclude in Section 4.5.

4.2. The dilepton and four-lepton signal processes

4.2.1. Parton level production of heavy T-odd quark pairs

As the cross-section for direct single or pair production of A_H is very tiny, this gauge boson can essentially only be produced via the decay of heavier T-odd particles. Hence, in principle, we should be considering the production of all such T-odd particle pairs and their subsequent decays. But owing to the substantial technical difficulties in simulating all such processes together, we restrict our attention to the production of heavy T-odd quarks in the initial parton level hard scattering. Needless to say, our cross-sections for the specific final states that we consider are then rather underestimated, and can be taken as lower bounds.

We consider the following processes for the production of T-odd quark pairs at the LHC:

$$pp \;\to\; q_H\bar{q}_H + X, \qquad \text{where } q_H = u_H, d_H, c_H, s_H, b_H, t_H, \tag{4.1}$$

$$\begin{aligned} pp \;\to\; & u_H u_H + X,\;\; \bar{u}_H\bar{u}_H + X,\;\; d_H d_H + X,\;\; \bar{d}_H\bar{d}_H + X, \\ & u_H d_H + X,\;\; \bar{u}_H\bar{d}_H + X,\;\; u_H\bar{d}_H + X, \end{aligned} \tag{4.2}$$

where t_H denotes the lighter T-odd partner of the top quark. Since, T_-, the heavier

T-odd partner of the top quark has a mass of 1013 GeV (for $f = 1$ TeV) and is thus heavier than t_H (for most of our choices for κ_q below), its cross-section is much smaller and we have neglected its pair production. Of course, for lower values of f, both $T_- \bar{T}_-$ and heavy T-odd gauge boson productions can have appreciable cross-section at the LHC.

In general, we expect the processes in Eq. (4.1) to be dominant because of the strong interaction production channels through gluon-gluon fusion and $q\bar{q}$-annihilation. But the electroweak processes from Eq. (4.2) also contribute significantly to the cross-section via t-channel T-odd gauge boson exchange, especially when the T-odd gauge bosons become relatively light, i.e. for low values of f. For instance, for $f = 1$ TeV and $\kappa_q = 0.5$, we find $m_{q_H} \sim 700$ GeV and the total production cross-section for a pair of heavy T-odd quarks is about 2.1 (0.7) pb for the LHC running at 14 (10) TeV. On the other hand, we can also obtain $m_{q_H} \sim 700$ GeV by choosing $f = 500$ GeV and $\kappa_q = 1$. In this later case the cross-section goes up to 5.8 (2.3) pb, where actually the electroweak processes from Eq. (4.2) are found to dominate. This fact has also been observed recently in Ref. [2]. We will come back to this point below. If the heavy T-odd quarks do not lie much above the lower bound of $m_{q_H} > 350$ GeV, we get a cross-section of 36 (13) pb for $m_{q_H} \sim 400$ GeV with $f = 1$ TeV. For details on the production of the heavy quarks and the relevant plots for the variation of these cross-sections with f or m_{q_H}, we refer the reader to the Refs. [3, 4]. We have checked that for individual processes, our results agree with them. Note, however, as f determines the mass of A_H, and in turn its decay modes, in order to study the effect of variation of quark masses with M_{A_H} fixed, in some cases we vary κ_q to adjust the masses of the heavy T-odd quarks.

The important fact is that the sum of the cross-sections of all T-odd quark pair production processes can be sizeable, in particular for not too large m_{q_H}. This will allow us to extract a clear signal after cuts are applied. Furthermore, since additional electroweak processes which can, for instance, produce pairs of T-odd gauge bosons $V_H V_H$, finally also lead to two A_H's, the given cross-sections, as mentioned before, are actually rather lower bounds.

The initially produced T-odd heavy quarks subsequently decay as $q_H \to W_H q', Z_H q, A_H q$ and then $W_H \to A_H W$, $\bar{q} q'_H$ and $Z_H \to A_H h$, $q\bar{q}_H$. At one point in such decay chains of a pair of q_H's, we are left with two A_H bosons, which will further decay as discussed in the next subsection. There will also be several hard

jets and leptons and some amount of missing E_T, if there are decays of $W^{\pm}$ and Z into neutrinos.

The initial parton level hard-scattering matrix elements and the relevant decay branching ratios for the signal in the LHT with T-parity violation are calculated with the help of CalcHEP (Version 2.5.1) [5]. We have used the CalcHEP model files for the LHT (with exact T-parity) from Ref. [4][1] and the one from Refs. [7,8] for the T-violating terms. We have used the leading order CTEQ6L [9] parton distribution functions with NLO running of α_s with $\alpha_s(M_Z) = 0.118$. The QCD factorization and renormalization scales were set equal to the sum of the masses of the particles which are produced in the initial parton level scattering process.

4.2.2. Decay modes of A_H

A comprehensive list of possible final states in the LHT with T-parity violation after the decay of the A_H's is given in Ref. [8]. Here we are interested in either dilepton or four-lepton signals from the decay of the two A_H's. The advantage of these leptonic decay channels of A_H is very apparent. As we will see, one can obtain clean signatures over the backgrounds with a minimal number of selection cuts and with luminosity building up, clear peaks in the invariant-mass distributions of dileptons or four leptons give us information about the A_H mass and thus on the symmetry breaking scale f. The decay branching fractions of A_H to either leptons (electron, muon) or to a pair of Z bosons (one of which might be off-shell) are given in Table 4.1. Note that the BR for the further decay $ZZ \to l^+l^-l'^+l'^-$, where $l, l' = \{e, \mu\}$, is only 4.5×10^{-3}, but the signal in this channel is very clean and the SM backgrounds, primarily from ZZ production, can be reduced efficiently as we will discuss below.

As already observed in Ref. [8], for lower masses ($M_{A_H} \lesssim 120$ GeV, $f \lesssim 800$ GeV) the decay of A_H is dominated by the loop-induced two-body modes into fermions, whereas for higher masses ($M_{A_H} > 2M_W$, $f > 1070$ GeV) the two-body modes to gauge boson pairs dominate. For intermediate masses, both the two-body and three-body modes compete (in the three-body mode we have one

[1] A new CalcHEP model file has been written by the authors of Ref. [2] which includes some missing factors of order v^2/f^2 in the couplings of T-odd fermions to the Z- and W-bosons, which were found in Ref. [6]. These changes in the Feynman rules will, however, not significantly affect our analysis, which focuses on the decays of the A_H boson.

f (GeV)	M_{A_H} (GeV)	$\mathrm{BR}(A_H \to e^+e^-) + \mathrm{BR}(A_H \to \mu^+\mu^-)$ (%)	$\mathrm{BR}(A_H \to ZZ^{(*)})$ (%)
500	66	7.59	~ 0
750	109	7.40	0.18
1000	150	3.42	11.03
1100	166	0.99	8.67
1500	230	0.02	22.45

Table 4.1.: Decay branching fractions of A_H to leptons ($l = e, \mu$) or $ZZ^{(*)}$ as a function of the scale f, i.e. the mass M_{A_H}.

on-shell $W^\pm$ or Z). The decay into two off-shell Z's for low f will have a very small branching-fraction, as the relative one-loop suppression is already compensated by the off-shellness of one vector boson.

As mentioned earlier, the decay rates of A_H into fermions (quarks, charged leptons, neutrinos) via one-loop triangle diagrams depend on the values of the finite terms in the counterterms from Eq. (2.13). To obtain the results given in Table 4.1 we followed Ref. [8] and used naive dimensional analysis to fix the $\mathcal{O}(1)$ constants from Eq. (2.14) to be exactly equal to one. These finite terms are determined by the UV completion of the LHT and could easily be different from one. In particular, one could imagine a situation, where the underlying theory couples differently to quarks and leptons. For instance, it could happen that all the couplings of the charged leptons could be bigger by a factor of two, which is well within the uncertainty of naive dimensional analysis. This would increase the partial decay width $\Gamma(A_H \to \text{all charged leptons})$ by a factor of four. The corresponding change of the branching ratio $\mathrm{BR}(A_H \to e^+e^-) + \mathrm{BR}(A_H \to \mu^+\mu^-)$, which is relevant for our study, depends on the total decay width and therefore on the mass of A_H or the scale f. It increases by about a factor of three for $M_{A_H} = M_Z$, i.e. for $f = 650$ GeV. Such a scenario would of course require less luminosity to get a certain number of dilepton events in our analysis below. On the other hand, if the underlying theory increases the couplings of A_H to only

the quarks by a factor of two compared to naive dimensional analysis, then the $\mathrm{BR}(A_H \to e^+e^-) + \mathrm{BR}(A_H \to \mu^+\mu^-)$ would be smaller (by a factor of about three for $M_{A_H} = M_Z$) and we would need more luminosity. While the precise numbers for these fermionic branching ratios therefore crucially depend on the unknown $\mathcal{O}(1)$ coefficients in the counterterms, the overall results of our analysis are not expected to change. In particular, the required luminosity is not expected to change by more than a factor of three, up or down.

As already noted in Ref. [8] as soon as the $WW^{(*)}$ and $ZZ^{(*)}$ decay channels for A_H open up for larger M_{A_H} or f, they quickly dominate over the fermionic modes. Therefore the overall picture and the value of f where this cross-over occurs, does not depend too sensitively on the precise values of the counterterms, as long as they vary only in a reasonably small window around the values as predicted by naive dimensional analysis.

4.2.3. Why is the A_H different from a usual Z' ?

Of course, the strategy to look for a resonance peak in the invariant mass distribution of dileptons is well known from the searches for a Z' gauge boson which appears in many models of New Physics, see for instance the recent reviews [10] and references therein.

Low energy weak neutral current experiments are affected by Z' exchange, which is mainly sensitive to its mass, and by $Z - Z'$ mixing. On the other hand, measurements at the Z-pole are very sensitive to $Z - Z'$ mixing, which lowers the mass of the Z relative to the SM prediction and also modifies the $Zf\bar{f}$ vertices. For e^+e^- colliders, like LEP2, a Z' much heavier than the center of mass energy would manifest itself through induced four-fermion interactions, which then interfere with virtual γ and Z contributions for leptonic and hadronic final states. The primary discovery mode at hadron colliders, like the Tevatron, is from the direct Drell-Yan production of a dilepton resonance.

The bounds on the Z' mass in a variety of popular models are usually obtained by assuming the Z' coupling to SM fermions to be of electroweak strength and family universal. Then for some models the strongest bounds come from electroweak precision tests yielding $M_{Z'} \gtrsim 1200 - 1400$ GeV at 95% confidence level. On the other hand, for a sequential Z' model, the LEP2 lower bound is even around 1800 GeV. For other models, the bounds from direct searches at the Teva-

tron are better than those derived from electroweak data, typically one obtains $M_{Z'} \gtrsim 800 - 1000$ GeV for these models [10].

Why does this fact not rule out a A_H with a mass around $50 - 250$ GeV which we will consider below ? The crucial point is that although a light A_H decays with a large BR into a pair of SM fermions, the actual coupling of A_H to two SM fermions is very small. Essentially, the coupling is of the size of a two-loop effect as discussed in Section 2.3.3. Thus the couplings are very different from the most commonly considered Z' models with couplings of electroweak strength for which the above limits apply. Therefore the direct production cross-section of such a low-mass A_H in e^+e^- colliders like LEP2 or at the Tevatron is tiny, of the order of 10^{-6} pb [8]. Also the four-fermion operators induced by Z' at low energies have only a small coupling and will not affect low-energy weak observables. Furthermore, the coupling of A_H to WW or ZZ which is directly induced by the WZW term, see Eq. (2.12), is very small and thus the production cross-section for A_H radiated off some W or Z boson is again very small. Therefore the A_H cannot be produced directly, but only via the decay of heavier T-odd particles, which themselves have not yet been observed.

As far as the decay $A_H \to ZZ$ is concerned, again the small coupling of A_H to SM fermions leads to a tiny s-channel production cross-section at LEP2 or the Tevatron. This is in contrast to the case of models with warped extra dimensions, like Randall-Sundrum (RS) [11], where the first Kaluza-Klein excitation of the graviton, G_1, can have a sizeable coupling to SM fermions and also often decays into ZZ with a branching ratio of typically 5%. From the absence of any deviation from the SM signal in $e^+e^- \to ZZ$ at LEP2 it was concluded in Ref. [12] that $M_{G_1} > 700$ GeV. Recently, CDF [13] has searched for a new heavy particle decaying to $ZZ \to eeee$ in the mass range of $500 - 1000$ GeV. In $1.1\,\text{fb}^{-1}$ of integrated luminosity, no event was observed after all the selection cuts, with an expected background of 0.028 ± 0.014 events. Within the RS-model, this translates into $\sigma(p\bar{p} \to G_1) \times \text{BR}(G_1 \to ZZ) < 4\,\text{pb}$ at 95% C.L. for $M_{G_1} \sim 500$ GeV. Since the mass region below 400 GeV was used to control the background from hadrons faking electrons, a potential signal from a lighter resonance, like the A_H with a mass around $150 - 250$ GeV, could not be observed. In any case, no signal is expected, since for a A_H of mass 230 GeV, produced in cascade decays of T-odd quarks with mass 400 GeV, $\sigma(p\bar{p} \to A_H) \times \text{BR}(A_H \to ZZ) = 0.03\,\text{pb}$. This is well below the above bound. A light A_H with a mass well below 1 TeV, giving

a simultaneous signal in the dilepton and four-lepton channels (via ZZ), also sets the LHT with T-parity violation apart from R-parity violating SUSY models with an additional Z' which can decay into four leptons via a slepton/sneutrino pair, as proposed in Ref. [14].

4.2.4. Choice of benchmark points

As discussed above, the production cross-section of heavy T-odd quark pairs decreases with increasing mass m_{q_H}, up to the discussed enhancement of the electroweak processes from Eq. (4.2) for low f. We therefore will choose benchmark points (BP's) with $m_{q_H} \sim 400, 700, 1000$ GeV to see this effect. The point with the lightest mass is close to the bound $m_{q_H} > 350$ GeV found in Ref. [8] from recent Tevatron data.

The intermediate mass region 120 GeV $< m_{A_H} <$ 165 GeV (800 GeV $< f <$ 1100 GeV) will be the most difficult to analyze, since neither the BR of A_H into dileptons nor into four leptons (via ZZ) dominates as can be seen from Table 4.1. Therefore we first take a benchmark point from this region and choose $f = 1$ TeV which corresponds to $M_{A_H} = 150$ GeV. Later, we will also take $f = 500$ GeV, where the dilepton mode dominates and $f = 1500$ GeV, where the dilepton mode is negligible and the decay into ZZ and thus into four leptons is important.

The first two BP's with $f = 1$ TeV are chosen in order to illustrate the effect of low and heavy quark masses both at the production level and at the level of kinematical variables. We take for the first BP-1 $m_{q_H} = 400$ GeV ($\kappa_q = 0.285$) and for the second BP-2 $m_{q_H} = 700$ GeV ($\kappa_q = 0.5$), see Table 4.2.

As we will see below, BP-1 with a rather low m_{q_H} leads to a clean dilepton signal over the backgrounds with rather modest luminosity. Therefore such a scenario should be testable during the early run of the LHC with 10 TeV center of mass energy, even in the difficult intermediate mass region for M_{A_H}. We expect the analysis to be easier for either lighter M_{A_H} (lower f) or heavier M_{A_H} (higher f), where one of the dilepton or four-lepton signals will clearly dominate.

For the further BP's, we therefore restrict ourselves to the heavier quark masses $m_{q_H} \sim 700, 1000$ GeV. For $m_{q_H} \sim 700$ GeV, we show the possible reconstruction of the A_H mass in the invariant mass distributions of dileptons for a point with very low values of $f = 500$ GeV ($M_{A_H} = 66$ GeV) (BP-3) and of four leptons for a point with a higher value of $f = 1500$ GeV ($M_{A_H} = 230$ GeV)

(BP-4), see Table 4.2. As the T-odd quarks become heavier, their production cross-section goes down. It then becomes increasingly difficult to obtain a reasonable number of signal events over the background. In such a scenario, in order to check the reach of the LHC, we choose the last two benchmark points such that $m_{q_H} \sim 1000$ GeV. For reasons discussed above, here also we consider two different values of f, $f = 1000$ GeV ($M_{A_H} = 150$ GeV) (BP-5) and $f = 1500$ GeV ($M_{A_H} = 230$ GeV) (BP-6).

Benchmark Point	m_{d_H} (GeV)	m_{u_H} (GeV)	M_{A_H} (GeV)	f (GeV)	κ_q	$\sqrt{s} = 10$ TeV $\sigma_{q_H q_H}$ (fb)	$\sqrt{s} = 14$ TeV $\sigma_{q_H q_H}$ (fb)
BP-1	403	400	150	1000	0.285	12764.6	35989.0
BP-2	707	702	150	1000	0.5	660.8	2061.0
BP-3	707	686	66	500	1.0	2298.1	5750.4
BP-4	742	740	230	1500	0.35	373.0	1283.1
BP-5	1025	1018	150	1000	0.725	119.9	421.0
BP-6	1008	1004	230	1500	0.475	66.3	261.0

Table 4.2.: The different benchmark points (BP's) for our study. These choices are made in view of the different scenarios that can arise in terms of production cross-sections, decay branching fractions and kinematic distributions. We also present the heavy quark pair production cross-section $\sigma_{q_H q_H}$ for the sum of all parton-level processes from Eqs. (4.1) and (4.2) at the LHC with center of mass energies of 10 TeV and 14 TeV.

In Table 4.2 we have also listed the total production cross-section for the sum of all parton-level processes from the strong-interaction processes from Eq. (4.1) and the electroweak processes from Eq. (4.2) at the LHC with center of mass energies of 10 TeV and 14 TeV. For BP-2, the strong interaction processes dominate and yield about 1.47 pb, while the electroweak processes give only a contribution of 0.60 pb at 14 TeV, i.e. about 29%. On the other hand, for BP-3 with low

$f = 500$ GeV and therefore rather light A_H, Z_H (exchanged in the t-channel), the electroweak processes contribute 3.75 pb at a center of mass energy of 14 TeV, i.e. 65% of the total, compared to 2.0 pb from strong interaction processes. The biggest individual parton-level cross-section is $\sigma(pp \to u_H d_H + X) = 2.39\,\text{pb}$. This has to be compared with the QCD process $\sigma(pp \to u_H \bar{u}_H + X) = 0.44\,\text{pb}$ from $q\bar{q}$-annihilation and gluon-fusion, the latter contributing about one third. The relative smallness of the QCD processes can be understood from the small value of $\alpha_s(\mu_R = 2m_{q_H} = 1.4\text{ TeV}) = 0.084$ and the size of the various parton density functions for $\mu_F = 2m_{q_H} = 1.4$ TeV around $x \sim m_{q_H}/7\text{ TeV} = 0.1$.

4.3. Event generation: backgrounds and signal event selection

As noted earlier, the initial parton level hard-scattering matrix elements in the LHT with T-parity violation were calculated and the events generated with the help of CalcHEP. These events, along with the relevant masses, quantum numbers and two-body and three-body decay branching fractions were passed on to PYTHIA (Version 6.421) [15] with the help of the SUSY Les Houches Accord (SLHA) (v1.13) SUSY/BSM spectrum interface [16] for their subsequent decays, showering, and hadronization. Initial and final state radiations from QED and QCD and multiple interactions were also taken into account in PYTHIA. The SM backgrounds, except for $Z^{(*)}/\gamma^*$ (Drell-Yan process), were simulated with ALPGEN [17] and then subsequently the unweighted event samples are passed onto PYTHIA for their showering and hadronization. The matching of matrix-element hard partons and shower-generated jets is performed using the MLM prescription [17]. This jet-parton matching allows us to generate inclusive samples of arbitrary jet multiplicity without any over-counting. Owing to the very large cross-section for the Drell-Yan process, it was not possible to generate statistically significant samples of events with additional hard jets using ALPGEN. Instead, the Drell-Yan background has been simulated with PYTHIA. As we will explain below, after appropriate cuts, the Drell-Yan background is reduced to a negligible level. We have again used the leading order CTEQ6L parton distribution functions (for PYTHIA we use the Les Houches Accord Parton Density Function (LHAPDF) interface [18]). The QCD factorization and renormalization scales are in general kept fixed at the sum of the masses of the particles which

are produced in the initial parton level scattering process. For the production of $Z^{(*)}/\gamma^*$, we have chosen the scale to be M_Z. If we would decrease the QCD scales by a factor of two, the cross-section can increase by about 30%.

4.3.1. Background from SM processes and within the LHT

The main SM backgrounds for the dilepton channel come from the Drell-Yan process via $Z^{(*)}/\gamma^*$ and the abundantly produced top quark pairs, whereas for the four-lepton channel, ZZ is the dominant source of background.[2] For the dilepton channel we have also considered the backgrounds coming from ZZ, ZW, WW and tW. We have included additional multiple hard jets in the simulations as follows:

- $t\bar{t} + n$ jets, $0 \leq n \leq 4$
- $ZZ + n$ jets, $0 \leq n \leq 3$
- $ZW + n$ jets, $0 \leq n \leq 3$
- $WW + n$ jets, $0 \leq n \leq 3$
- $tW + n$ jets, $0 \leq n \leq 1$

For the other possible dilepton and four-lepton backgrounds, we have checked that their cross-sections are small compared to the above ones, for instance, for $t\bar{t}Z$, where $Z \to l^+l^-$, the cross-section is around 40 fb at $\sqrt{s} = 14$ TeV.[3] After putting a large effective mass cut as described below, these backgrounds are not expected to be significant. Additional leptons coming from the photons radiated by charged particles, or from the decay of pions, are generally expected to be removed by the basic isolation cuts described later.

For the strongly produced process $t\bar{t}$ + jets, which has a long tail in the effective mass distribution, we have multiplied the leading order cross-sections from ALPGEN by appropriate K-factors wherever they are available in the literature. For $t\bar{t}$ + 0 jet the K-factor used is 2.2 from next-to-leading order (NLO) and next-to-leading-log resummed (NLL) corrections according to the analysis in

[2] Although $t\bar{t}$ events can also give rise to four-lepton events, such backgrounds are relatively easily reduced with the requirement that among the four leptons, there are at least two opposite sign same flavour ones, whose invariant mass is around the Z boson mass, followed by the effective mass cut, as shown in our subsequent analysis.

[3] In case of a jet faking a lepton, W+ jets can also give rise to dilepton events. Although we do not consider the possibility of such fakes, we expect the large M_{eff} cut to reduce this background significantly.

Ref. [19]. For $t\bar{t}+1$ jet we have used a K-factor of 1.29 according to the NLO calculation in Ref. [20], whereas for $t\bar{t}+2$ jets we used 1.28 as inferred from the recent NLO calculation in Ref. [21].[4]

In addition, two-and four-lepton final states can occur from processes within the LHT model itself. The heavy T-odd gauge bosons, W_H and Z_H, produced in various cascades, can lead to hard isolated leptons. Leptons from b-quarks and τ's in LHT cascades can also fake our signals *prima facie*. For small κ_l, T-odd leptons l_H will also give rise to leptons in the final state. Since we have taken $\kappa_l = 1$, the latter decay does not occur for the chosen benchmark points. On the whole, substantial as several of the aforementioned backgrounds may be, they do not in general affect the invariant mass peaks from A_H decays.

4.3.2. Event selection criteria

In our analysis we demand for the *dilepton signal* that we have exactly one pair of opposite sign same flavour (OSSF) leptons from the decay $A_H \to l^+l^-$, with $l = \{e, \mu\}$. For the *four-lepton signal* from the decay $A_H \to ZZ^{(*)} \to l^+l^-l'^+l'^-$, where $l, l' = \{e, \mu\}$, we demand that there should be four leptons, among which at least one OSSF lepton pair should have an invariant mass peaked around M_Z (i.e., $M_Z - 20$ GeV $\leq M_{ll} \leq M_Z + 20$ GeV). The last criterion is used because in the scenarios that we consider, at least one Z-boson is on-shell.

The following basic selection cuts (denoted by Cut-1 below) were applied for both the signal and the background [23, 24]:

Lepton selection:

- $p_T > 10$ GeV and $|\eta_\ell| < 2.5$, where p_T is the transverse momentum and η_ℓ is the pseudorapidity of the lepton (electron or muon).
- **Lepton-lepton separation:** $\Delta R_{\ell\ell} \geq 0.2$, where $\Delta R = \sqrt{(\Delta\eta)^2 + (\Delta\phi)^2}$ is the separation in the pseudorapidity–azimuthal angle plane.
- **Lepton-jet separation:** $\Delta R_{\ell j} \geq 0.4$ for all jets with $E_T > 20$ GeV.
- The total energy deposit from all *hadronic activity* within a cone of $\Delta R \leq 0.2$ around the lepton axis should be ≤ 10 GeV.

[4] Note that this K-factor has been obtained with a minimum p_T of 50 GeV for the jets whereas we will employ a cut of only 20 GeV. Based on the observation in Ref. [22], that in many cases the K-factor diminishes for processes with more hard jets, the actual K-factor for $t\bar{t}+2$ jets might be lower than 1.28.

Jet selection:

- Jets are formed with the help of PYCELL [5], the inbuilt cluster routine in PYTHIA. The minimum E_T of a jet is taken to be 20 GeV, and we also require $|\eta_j| < 2.5$.

We have approximated the detector resolution effects by smearing the energies (transverse momenta) with Gaussian functions following the prescriptions described in detail in Chapter 3.3.

An important cut will be imposed on the effective mass variable, defined to be the scalar sum of the transverse momenta of the isolated leptons and jets and the missing transverse energy,

$$M_{eff} = \sum p_T^{jets} + \sum p_T^{leptons} + \not{E}_T, \tag{4.3}$$

where the missing transverse energy is given by

$$\not{E}_T = \sqrt{\left(\sum p_x\right)^2 + \left(\sum p_y\right)^2}. \tag{4.4}$$

Here the sum goes over all the isolated leptons, the jets, as well as the 'unclustered' energy deposits. The energies of the 'unclustered' components, however, have not been smeared in this analysis.

In Fig. 4.1 we plot the distribution of the effective mass after the basic cuts (Cut-1) for dilepton events for the benchmark points BP-1 ($m_{q_H} \sim 400$ GeV), BP-2 ($m_{q_H} \sim 700$ GeV), BP-5 ($m_{q_H} \sim 1000$ GeV) and the SM background, dominantly from Drell-Yan and $t\bar{t}$ + jets. Recall that we have included appropriate K-factors for the latter process. The SM backgrounds are huge; however, the distributions peak around $2m_{q_H}$ for the signal and between M_Z and $2m_t$ for the SM background. It is clear that the production of heavy particles in the initial hard-scattering will lead to a high M_{eff} in most cases. Therefore, imposing the *effective mass cut:*

$$M_{eff} \geq 1 \text{ TeV} \qquad \text{(Cut-2)}, \tag{4.5}$$

will reduce the SM background substantially, although the distribution from SM processes with additional hard jets has a long tail towards larger values of M_{eff}. Note that the log-plot makes the differences between the curves look smaller than they actually are. Although this fixed cut also reduces the signal for the lighter

[5] Since we primarily focus on leptonic signals, our results should not be sensitive to the choice of various jet algorithms.

$m_{q_H} \sim 400$ GeV from BP-1 by about half, the corresponding larger production cross-section makes up for this loss. In a more realistic analysis one would of course try to optimize the choice of the cut on M_{eff}, depending on the expected signal.

In addition to the effective mass cut from Eq. (4.5), we will also use the fact that we expect a peak in the invariant mass distribution of dileptons (M_{ll}) or four leptons (M_{4l}) near the mass of A_H. In our analysis, we will therefore impose the condition that the invariant mass should be in a *window around* M_{A_H}

$$M_{A_H} - 20 \text{ GeV} \leq M_{ll,4l} \leq M_{A_H} + 20 \text{ GeV} \qquad \text{(Cut-3)}. \tag{4.6}$$

As we will see, this condition will in particular help to reduce the background from leptons within the LHT model. Of course, in a realistic experimental analysis, where the mass of A_H is unknown, one would scan the whole range of invariant masses and impose such a window around some seed-mass M_{A_H}, thereby looking for an excess of the signal over the SM and LHT model backgrounds, which are almost flat except near the Z-mass. Moreover, this excess should stand out in this window, as compared to the adjoining bins.

Unfortunately, the need to implement such a cut in our analysis will not allow us to detect a heavy photon A_H with a mass very close to M_Z, since in that case the cut cannot free the peak from contamination by Z-production within the SM and in LHT cascades. In principle, by looking at the relative size of the branching fractions into charged leptons, including τ, and hadrons (jets), one might still be able to distinguish the A_H from the Z-boson. However, if we look at a heavy photon with $M_{A_H} = 92$ GeV, we get $R_{A_H} \equiv \text{BR}(A_H \to \text{quarks})/\text{BR}(A_H \to \text{all charged leptons}) = 6.27$, which is not much different from the corresponding ratio for the Z-boson, $R_Z = 6.92$. So the signature of A_H in this situation might be difficult to distinguish at the LHC.

4.4. Results

4.4.1. Dilepton signal

LHC with $\sqrt{s} = 10$ TeV

In Table 4.3 we list, for the opposite sign same flavour (OSSF) dilepton signal ($l = e, \mu$), the cross-sections of the dominant SM background processes after the

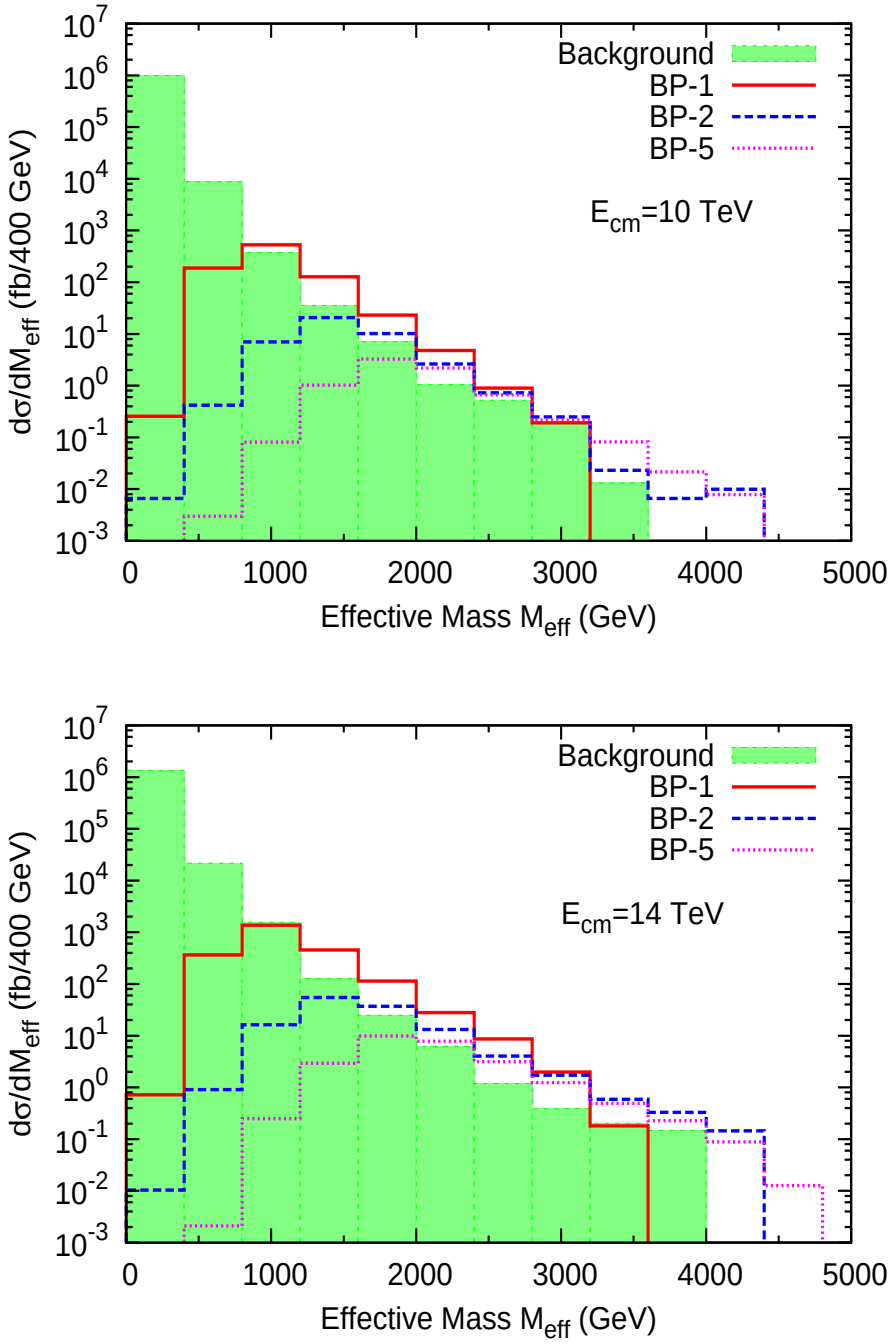

Figure 4.1.: Effective mass distribution of dilepton events after the basic cuts (Cut-1) for BP-1 ($m_{q_H} \sim 400$ GeV), BP-2 ($m_{q_H} \sim 700$ GeV), BP-5 ($m_{q_H} \sim 1000$ GeV) and the SM background, mostly Drell-Yan and $t\bar{t}$ + jets, at $\sqrt{s} = 10$ TeV (top panel) and $\sqrt{s} = 14$ TeV (bottom panel).

basic cuts (Cut-1) and the effective mass cut $M_{eff} > 1$ TeV (Cut-2) for the LHC running at $\sqrt{s} = 10$ TeV. We can see that the effective mass cut reduces all the SM dilepton backgrounds significantly, in particular from the Drell-Yan process via Z/γ^*, which is the overwhelming background after the basic cuts. After the cut on M_{eff}, $t\bar{t}$ + jets is the largest background due to the long tail in the effective mass distribution, see Fig. 4.1.[6]

Background	Cut-1 (fb)	Cut-2 (fb)
Z/γ^*	1247174	~ 0.00
$t\bar{t}$ + jets	6278	84.03
ZZ + jets	546	5.76
WW + jets	946	9.58
ZW + jets	624	13.39
tW + jets	719	8.37
Total	1256287	121.13

Table 4.3.: Dominant opposite sign same flavour dilepton ($l = e, \mu$) SM background cross-sections for $\sqrt{s} = 10$ TeV after the basic cuts (Cut-1) and after the cut $M_{eff} \geq 1$ TeV (Cut-2).

In our simulation of the Drell-Yan process with PYTHIA, out of 10^6 Monte-Carlo (MC) events, we did not see any dilepton event with $M_{eff} > 1$ TeV . Actually, in the simulation for the LHC running at 14 TeV, where the cross-section is higher and where we expect more events with larger M_{eff}, we did not get a

[6] We should note that in the simulation with ALPGEN a substantial number of events in $t\bar{t} + 4$ jets and $VV + 3$ jets ($V = W, Z$) pass the M_{eff} cut. We can therefore not exclude the possibility that the inclusion of more hard jets might increase the total background cross-section after Cut-2 by some amount. Such a simulation is beyond the scope of our present study. At least part of the effects of these hard jets is taken into account by the PYTHIA showering and MLM matching of the ALPGEN samples with the highest jet multiplicity.

single event with $M_{eff} > 1$ TeV out of 10^7 simulated Drell-Yan events. A larger MC sample would be needed to put a definite number on the cross-section after Cut-2. If we simply assume an upper bound of one event after Cut-2, which is probably much bigger than the correct number, this leads to an upper bound on the dilepton cross-section from Z/γ^* after Cut-2 of about 45 fb, i.e. quite sizeable compared to $t\bar{t}$. In the following we assume that we can neglect the SM background from Z/γ^* after the effective mass cut. In any case, after the Cut-3, i.e. that the dilepton invariant mass should be in a narrow window around M_{A_H}, see Eq. (4.6), a further reduction of the cross-section and number of dilepton events from Z/γ^* will occur anyway.

In Fig. 4.2 we plot the invariant mass distributions of OSSF dileptons for all the benchmark points and the corresponding SM background after the basic cuts (Cut-1) and the M_{eff} cut (Cut-2). For BP-1, BP-2, BP-3 and BP-5, a peak emerges at the mass of A_H, in particular very clearly for BP-1 and BP-3. BP-1 has a large parton-level T-odd quark pair production cross-section because of the relatively small $m_{q_H} \sim 400$ GeV, compared to $m_{q_H} \sim 700$ GeV for BP-2. BP-3 has also $m_{q_H} \sim 700$ GeV, but a small value of $f = 500$ GeV. Therefore the T-odd quark production cross-section is strongly enhanced by electroweak contributions, as discussed earlier, see Table 4.2. Furthermore, the leptonic branching ratio for the light $M_{A_H} = 66$ GeV is also large, see Table 4.1, leading to more dilepton events. Note, however, that the 'signal' after Cut-2 also includes dileptons from within the LHT coming for instance from the decay via the Z-boson, leading to an enhancement in the peak at M_Z for BP-1 and BP-2 in Fig. 4.2. Since for BP-3 with $f = 500$ GeV the branching ratio $A_H \to l^+l^-$ is higher than for BP-1 and BP-2, the Z-peak is much smaller compared to the A_H-peak.

The total integrated luminosity at the LHC running at 10 TeV will probably be around $200\,\text{pb}^{-1}$. For this integrated luminosity, there will be 73 dilepton 'signal' events for BP-1 and 33 events for BP-3, compared to a SM background of 24 events. Note, however, that there will be only 8 dilepton events for BP-2 and 1.5 events for BP-5.

As mentioned in Section 2.3.3, the total decay width of A_H is only of the order of eV and therefore radiative corrections and detector effects will determine the observed width of the resonance peak in reality.

For BP-4 and BP-6 with $f = 1500$ GeV, the decay branching ratio $A_H \to l^+l^-$ is negligible compared to $A_H \to ZZ^{(*)}$, see Table 4.1, and therefore the four-

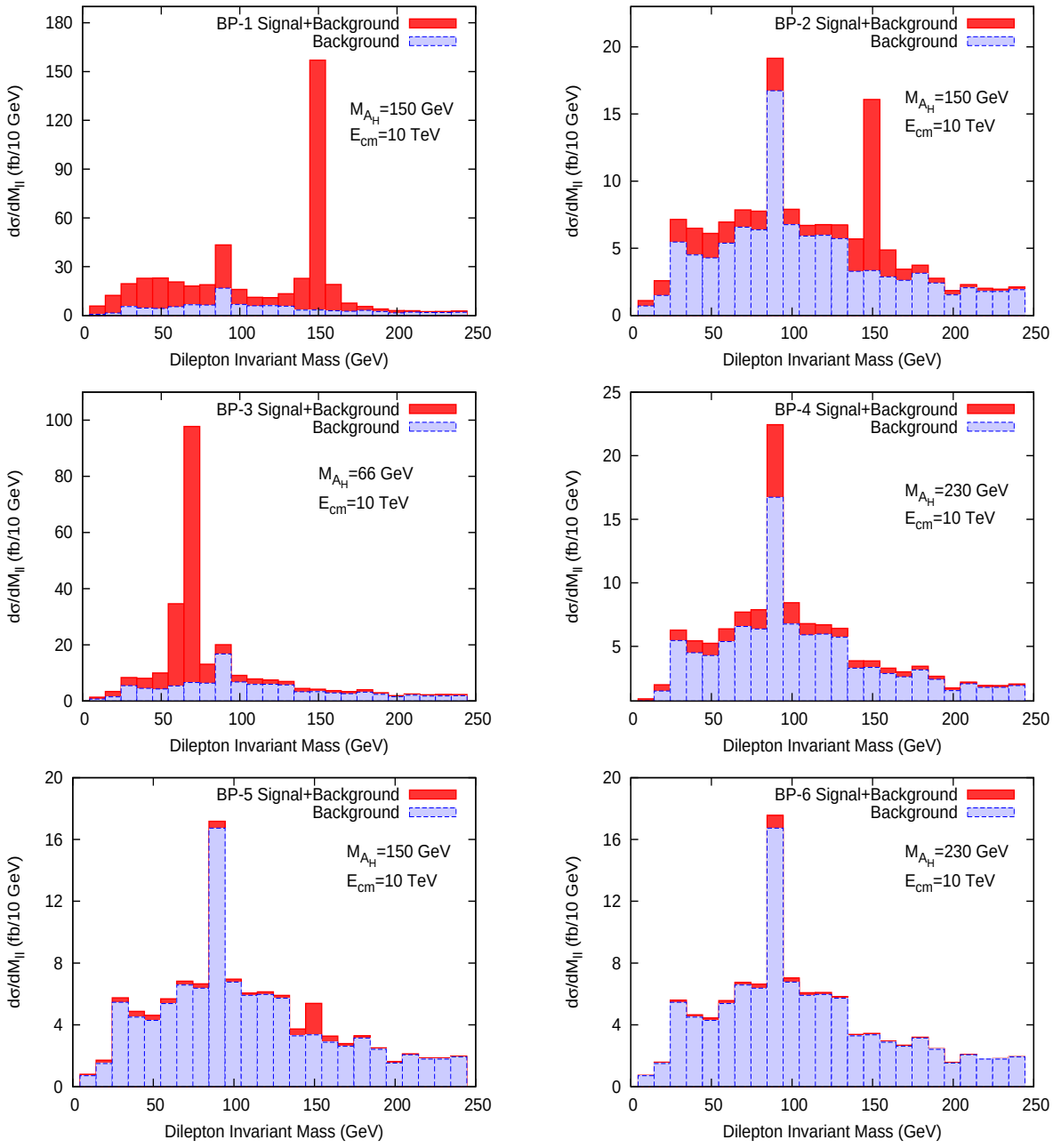

Figure 4.2.: Invariant mass distribution of OSSF dilepton pairs ($l = e, \mu$) for $\sqrt{s} =$ 10 TeV after the basic cuts (Cut-1) and the effective mass cut $M_{eff} \geq$ 1 TeV (Cut-2) for all the benchmark points, with the corresponding SM background. Note that the 'signal' also includes dileptons within the LHT not coming from A_H, but, for instance through the decay of the Z-boson. This is in particular the case for BP-4 and BP-6 where we do not expect any dileptons from A_H. For an integrated luminosity of 200 pb^{-1} there are 73 signal events for BP-1 and 33 events for BP-3, but only 8 signal events for BP-2 and 1.5 events for BP-5, compared to 24 events from the SM background. See Table 4.4 for more details.

lepton signal will be the relevant signature for discovery. Nevertheless, we get some dilepton events, in particular for BP-4, but the dilepton invariant mass distribution peaks at the Z-boson mass and not at M_{A_H}.

In order to reduce the SM background further, and also to eliminate the background from dileptons within the LHT which do not come from the decay $A_H \to l^+l^-$, we impose the additional constraint that the invariant mass of the dileptons should be in a window of ± 20 GeV around M_{A_H} (Cut-3), see Eq. (4.6). In Table 4.4 we give the cross-sections for OSSF dilepton events after the basic cuts (Cut-1) and after Cut-2 and Cut-3 for all the benchmark points for the LHC running at $\sqrt{s} = 10$ TeV. The total cross-section for the SM background after Cut-2 and Cut-3 is also given. We also list in Table 4.4 the number of signal and background events after Cut-2 and after Cut-3 for an integrated luminosity of $200\,\text{pb}^{-1}$.

	Cut-1 [S] (fb)	Cut-2 [S] (fb)	Cut-2 [BG] (fb)	S_2	B_2	Cut-3 [S] (fb)	Cut-3 [BG] (fb)	S_3	B_3
BP-1	871.5	367.0	121.1	73.4	24.2	196.7	12.4	39.3	2.5
BP-2	41.9	39.8	121.1	8.0	24.2	18.2	12.4	3.6	2.5
BP-3	175.2	168.1	121.1	33.6	24.2	132.9	23.3	26.6	4.7
BP-4	21.9	21.3	121.1	4.3	24.2	0.5	7.2	0.1	1.4
BP-5	7.6	7.6	121.1	1.5	24.2	3.1	12.4	0.6	2.5
BP-6	3.5	3.5	121.1	0.1	24.2	0.1	7.2	0.02	1.4

Table 4.4.: OSSF dilepton signal (S) from all T-odd quark-pair production processes and total SM background (BG) cross-sections at the LHC with $\sqrt{s} = 10$ TeV after the different cuts described in the text. The number of signal and background events after Cut-2 with an integrated luminosity of $200\,\text{pb}^{-1}$ are also given as S_2 and B_2, respectively. The corresponding numbers after Cut-3 are denoted by S_3 and B_3.

We can see from Table 4.4 that with an integrated luminosity of $200\,\text{pb}^{-1}$, only BP-1 and BP-3 yield a clear signal over the SM background after Cut-2. The Cut-3 then reduces the SM background and the dilepton background from within the LHT model almost completely, with $S_3/B_3 = 15.7$ for BP-1 and $S_3/B_3 = 5.7$ for BP-3 with more that 10 signal events for both benchmark points. Although the high $M_{eff} \geq 1$ TeV cut (Cut-2) reduces the signal for BP-1 with a low mass $m_{q_H} = 400$ GeV by about a factor two, the larger production cross-section compensates for that. Therefore, at least for BP-1 and BP-3, one expects a clear dilepton signal from the decay of the A_H in the LHT with T-parity violation at the early stage of the LHC run with low center of mass energy and modest luminosity. With the predicted number of signal events after Cut-3, it will presumably also be possible to reconstruct the mass of A_H and determine the symmetry breaking scale f.

If we demand that we have at least 10 signal events, BP-2 yields not enough events with an integrated luminosity of $200\,\text{pb}^{-1}$, in particular after Cut-3. Furthermore, with this luminosity there will be almost no dilepton events for BP-5, already after Cut-2, because of the small production cross-section for $m_{q_H} \sim 1$ TeV. Also the branching ratio of A_H into dileptons is small for this benchmark point, since $f = 1$ TeV.

Note that the BP-4 with $M_{A_H} = 230$ GeV yields about half the dilepton events of BP-2 for the same mass $m_{q_H} \sim 700$ GeV of the heavy T-odd quarks. However, these dileptons for BP-4 are not coming from the decay $A_H \to l^+l^-$, but from other sources, mostly the Z-boson, as mentioned above. In Table 4.4 this is visible after imposing the Cut-3 which almost completely removes all dilepton events for BP-4, whereas about half the dilepton events survive for BP-2. For BP-6 there are essentially no dilepton events for $200\,\text{pb}^{-1}$. As for BP-4, we expect for this benchmark point, which has $f = 1500$ GeV and $M_{A_H} = 230$ GeV, the four-lepton mode to be relevant for discovery.

We should caution the reader about the numbers given in Table 4.4 for the SM background cross-sections and the number of BG events after Cut-2 and in particular after Cut-3. The total number of MC events in the OSSF channel we simulated (including all possible processes) is 350987 after Cut-1. After the cut on M_{eff} (Cut-2), we have 4296 events in our MC sample and after Cut-3 there remain 644 MC events in the window of ± 20 GeV around the A_H mass (for the case $M_{A_H} = 66$ GeV). Therefore, there is an intrinsic uncertainty of about 4% on the numbers for B_3 given in the Table 4.4. A much larger MC simulation to pin down

these numbers more precisely is beyond the scope of the present work. Note, however, that we have enough simulated events for the signal. For instance, for BP-2, we have 12041 MC events after Cut-2 and 5501 MC events after Cut-3.

LHC with $\sqrt{s} = 14$ TeV

In Table 4.5 we list, for the opposite sign same flavour (OSSF) dilepton signal ($l = e, \mu$), the cross-sections of the dominant SM background processes after the basic cuts (Cut-1) and the effective mass cut $M_{eff} > 1$ TeV (Cut-2) for the LHC running at $\sqrt{s} = 14$ TeV. As for 10 TeV, we can see that the effective mass cut reduces all the SM dilepton backgrounds significantly, in particular from the Drell-Yan process via Z/γ^* which is the main background after the basic cuts. Again, after the cut on M_{eff}, $t\bar{t}$ is the largest background due to the long tail in the effective mass distribution, see Fig. 4.1. As noted in the previous subsection, in our simulation of the Drell-Yan process with PYTHIA, we did not see any dilepton event with $M_{eff} > 1$ TeV out of 10^7 MC events. There were 30048 OSSF dilepton MC events which passed the basics cuts. If we would simply assume an upper bound of one event after the Cut-2, which might be way off the correct number, this would lead to an upper bound on the dilepton cross-section from Z/γ^* after Cut-2 of about 57 fb, i.e. again quite sizeable compared to $t\bar{t}$. In the following we assume again that we can neglect the SM background from Z/γ^* after Cut-2.

In Fig. 4.3 we plot the invariant mass distributions of OSSF dileptons for all the benchmark points and the corresponding SM background after the basic cuts (Cut-1) and the cut on M_{eff} (Cut-2). Again for BP-1, BP-2, BP-3 and BP-5, a peak emerges at the mass of A_H, in particular very clearly for BP-1, BP-2 and BP-3. With an integrated luminosity of 30 fb^{-1}, there are 36088 signal events for BP-1, 3723 events for BP-2 and 2135 events for BP-3, compared to 14208 SM background events. Again, for BP-1 and BP-2 we have a non-negligible amount of dilepton background from within the LHT, in particular from the decays via the Z-boson, as can be clearly seen in the Fig. 4.3.

As mentioned before, for BP-4 and BP-6 with $f = 1500$ GeV, the decay branching ratio $A_H \to l^+l^-$ is negligible compared to $A_H \to ZZ^{(*)}$, see Table 4.1, and therefore the four-lepton signal will be the relevant signature for discovery. Nevertheless, we get many dilepton events even for these two benchmark points, but there is a peak at the Z-boson mass and not at M_{A_H}.

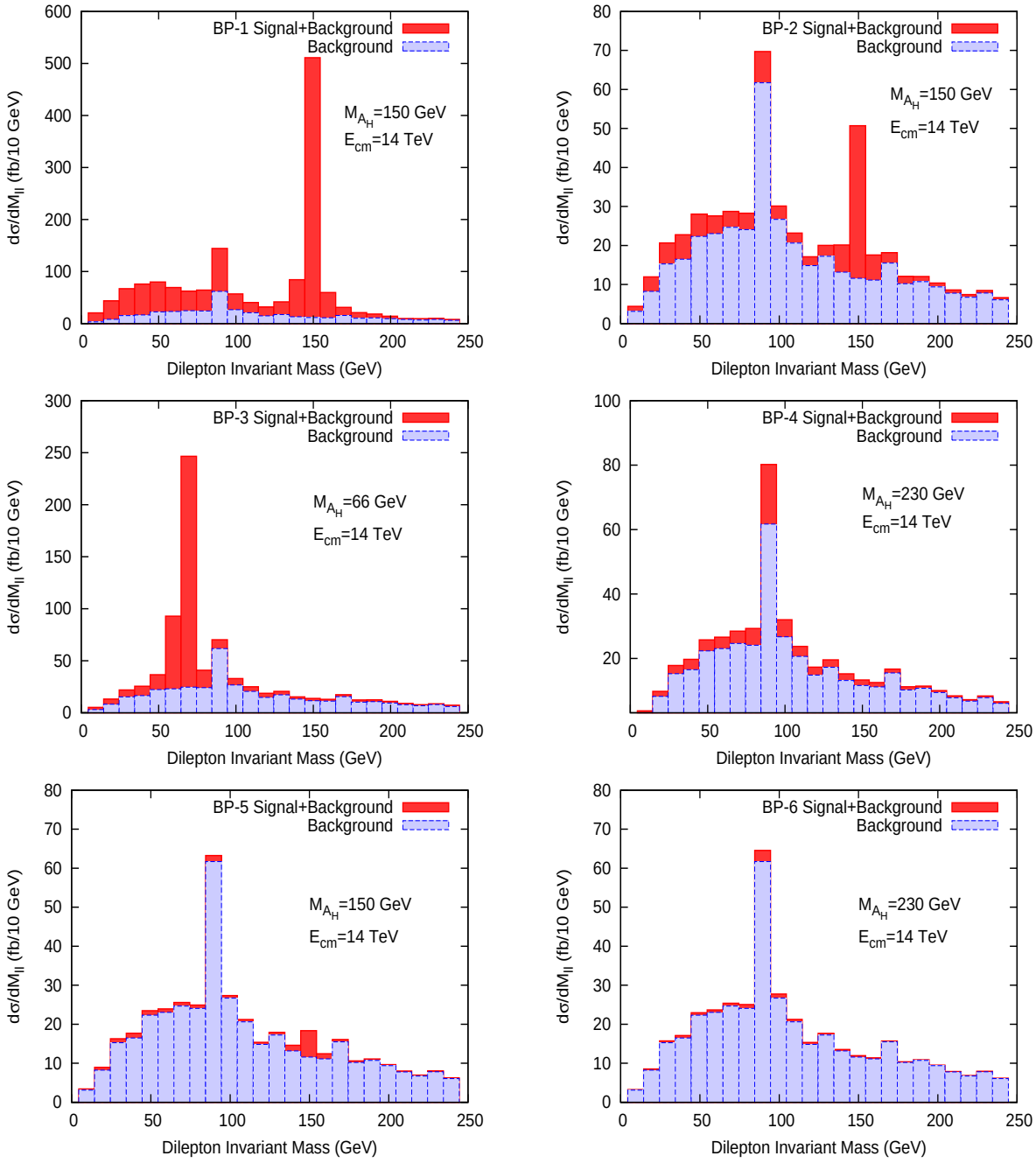

Figure 4.3.: Same as Fig. 4.2 for $\sqrt{s} = 14$ TeV.

Background	Cut-1 (fb)	Cut-2 (fb)
Z/γ^*	1711746	~ 0.00
$t\bar{t}$ + jets	13854	344.33
ZZ + jets	827	13.82
WW + jets	1385	30.17
ZW + jets	951	43.40
tW + jets	1604	41.89
Total	1730366	473.61

Table 4.5.: Same as Table 4.3 for $\sqrt{s} = 14$ TeV.

In order to reduce the SM background further, but also to eliminate the background from dileptons within the LHT which do not come from the decay $A_H \to l^+l^-$, we impose again the additional constraint that the invariant mass of the dileptons should be in a window around M_{A_H} (Cut-3), see Eq. (4.6). In Table 4.6 we give the cross-sections for OSSF dilepton events after the basic cuts (Cut-1) and after Cut-2 and Cut-3 for all the benchmark points for the LHC running at $\sqrt{s} = 14$ TeV. The total cross-section for the SM background after Cut-2 and Cut-3 is also given. We also list in Table 4.6 the number of signal and background events after Cut-2 and after Cut-3 for an integrated luminosity of $30\,\text{fb}^{-1}$.

The qualitative features of the benchmark points for the LHC running at $\sqrt{s} = 14$ TeV are very similar to the case of $\sqrt{s} = 10$ TeV, but now we have higher event rates. First of all, after the Cut-2, all the signal and background cross-sections are about a factor of three bigger, see Tables 4.4 and 4.6. Furthermore, we assume that we have now much more integrated luminosity, $30\,\text{fb}^{-1}$ compared to $200\,\text{pb}^{-1}$ earlier. The Cut-2 again removes about half of the signal events for BP-1. For all benchmark points, we now get more than 10 signal events even after Cut-3 and also the number of background events is much larger than 100. It makes

therefore sense to consider the signal significance by looking at $S/\sqrt{B}$ which is also given in Table 4.6 for the number of events after Cut-3.

	Cut-1 [S] (fb)	Cut-2 [S] (fb)	Cut-2 [BG] (fb)	S_2	B_2	Cut-3 [S] (fb)	Cut-3 [BG] (fb)	S_3	B_3	$S_3/\sqrt{B_3}$
BP-1	2341.8	1202.9	473.6	36088	14208	642.9	50.3	19286	1508	496.6
BP-2	129.1	124.1	473.6	3723	14208	55.5	50.3	1665	1508	42.9
BP-3	428.9	413.3	473.6	12398	14208	322.9	95.8	9686	2873	180.7
BP-4	72.7	71.2	473.6	2135	14208	1.9	27.0	56	809	2.0
BP-5	26.1	26.0	473.6	781	14208	10.3	50.3	308	1508	7.9
BP-6	13.4	13.4	473.6	401	14208	0.4	27.0	11	809	0.4

Table 4.6.: Same as Table 4.4 for $\sqrt{s} = 14$ TeV and an integrated luminosity of $30\,\text{fb}^{-1}$.

Looking at the significance, we can now better see the importance of imposing the Cut-3, i.e. the dilepton invariant mass should be in a window of ± 20 GeV around M_{A_H}. For instance, BP-4 has 2135 dilepton events for $30\,\text{fb}^{-1}$, but they are not coming from the decay $A_H \to l^+l^-$ as mentioned earlier, but instead from Z-decays. After Cut-2 we get a large apparent statistical significance of $S_2/\sqrt{B_2} = 17.9$ (note that $\sqrt{B_2} = 119.2$), but the huge reduction in the number of events after Cut-3, from 2135 down to 56 events, tells us that these dileptons are not coming from the decay of A_H, instead they come from an almost flat background. Of course, this can be clearly seen by looking at the plot of the dilepton invariant mass distribution in Fig. 4.3. On the other hand, the Cut-3 removes only about one third of the signal events for BP-3 and about half the events for BP-1, BP-2 and BP-5. This indicates the presence of a peak around M_{A_H} for these benchmark points, see Fig. 4.3. But note that for BP-4 even after Cut-3, we still have $S_3/\sqrt{B_3} = 2.0$, but, of course, there will be no peak in the dilepton distribution around A_H. Even for BP-6 we get after Cut-2 a signal of $S_2/\sqrt{B_2} = 3.4$, but

again they are not from the dilepton decay of the A_H, as can be seen after Cut-3 is applied where we get $S_3/\sqrt{B_3} = 0.4$.

We have seen in the previous Section 4.4.1 for the LHC running at $\sqrt{s} = 10$ TeV and with $200\,\text{pb}^{-1}$ integrated luminosity that we had a clear dilepton signal over the SM background for BP-1 and BP-3.

It is obvious from the last column in Table 4.6 that with a center of mass energy of 14 TeV and an integrated luminosity of $30\,\text{fb}^{-1}$, we can now also cover BP-2 and BP-5. That means it will be possible at these benchmark points to reconstruct the peak of A_H in the dilepton invariant mass distribution and to determine the mass M_{A_H} and the scale f. In particular with an integrated luminosity of $11.9\,\text{fb}^{-1}$, it will be possible to get 5σ statistical significance for BP-5 after Cut-3. As a reminder, BP-5 has a rather heavy T-odd quark mass of $m_{q_H} \sim 1$ TeV. Furthermore we have chosen the difficult intermediate region with $f = 1$ TeV, where the dilepton mode is not dominant. For lower f, the discovery will be even easier for the same m_{q_H} or, conversely, for lower f, we get a larger reach in m_{q_H}, if we demand a 5σ signal with $30\,\text{fb}^{-1}$.

Again we should caution the reader about the numbers given in Table 4.6 for the SM background cross-sections and the number of BG events after Cut-2 and in particular after Cut-3, because of the limited statistics in the Monte-Carlo simulation. The total number of MC events in the OSSF channel we simulated (including all possible processes) is 139429 after Cut-1. After the cut on M_{eff} (Cut-2), we have 4170 events in our MC sample and after Cut-3 there remain 730 MC events in the window of ± 20 GeV around the A_H mass (for the case $M_{A_H} = 66$ GeV). Therefore, there is an intrinsic uncertainty of about 4% on the numbers for B_3 given in the Table 4.6 and correspondingly about 2% uncertainty on the significance $S_3/\sqrt{B_3}$. In particular, the required luminosity for a 5σ statistical significance for BP-5 should be taken with a grain of salt. A much larger MC simulation to pin down these numbers more precisely is again beyond the scope of the present work. Note, however, that we have enough simulated events for the signal. For instance, for BP-5, we have 12365 MC events after Cut-2 and 4880 MC events after Cut-3.

4.4.2. Four-lepton signal

LHC with $\sqrt{s} = 10$ TeV

The biggest SM background for the four-lepton signal, as defined in Section 4.3.1, arises from the production of ZZ + jets and the subsequent fully leptonic decays.[7] For the LHC running at $\sqrt{s} = 10$ TeV, the corresponding cross-section after the basic cuts (Cut-1) is 13.78 fb. It is drastically reduced to 0.14 fb by the cut on the effective mass $M_{eff} \geq 1$ TeV (Cut-2). The second largest SM background is from $t\bar{t}$ + jets, but after the basic cuts and the requirement that at least two OSSF leptons among the total four have an invariant mass in a window of ± 20 GeV around M_Z, it is only 0.53 fb and it is completely removed by the effective mass cut.

In Table 4.7 we list for all the benchmark points, except BP-3, the cross-sections for the four-lepton signal for the LHC running at a center of mass energy of 10 TeV, successively after the basic cuts (Cut-1), Cut-2 on the effective mass and Cut-3, i.e. the condition that the four-lepton invariant mass should be in a window of ± 20 GeV around the mass of A_H, see Eq. (4.6). The total SM background after Cut-2 and Cut-3 is also given. Note that for BP-3 with $f = 500$ GeV, the BR of A_H into $ZZ^{(*)}$ is essentially zero, see Table 4.1, and therefore we have not included that benchmark point in the table.

Unfortunately, although the four-lepton signal cross-sections are larger than the SM background after Cut-2 for all the benchmark points considered in the table, there will be always less than 10 signal events for an integrated luminosity of $200\,\text{pb}^{-1}$. Therefore we will not be able to see a clear A_H mass peak in the early stages of the LHC run.

LHC with $\sqrt{s} = 14$ TeV

The biggest SM background for the four-lepton signal comes again from ZZ + jets production. For the LHC running at $\sqrt{s} = 14$ TeV, the corresponding cross-section after the basic cuts (Cut-1) is 18.79 fb. It is drastically reduced to 0.40 fb by the cut on the effective mass $M_{eff} \geq 1$ TeV. The second largest SM background is from $t\bar{t}$ + jets. After the basic cuts and the requirement that at least two OSSF leptons among the total four have an invariant mass around M_Z, it is 0.26 fb, but

[7] For details on a method to normalize the production rate of ZZ from data see Ref. [25].

	Cut-1 S (fb)	Cut-2 S (fb)	Cut-2 BG (fb)	Cut-3 S (fb)	Cut-3 BG (fb)
BP-1	21.70	6.45	0.14	1.53	0.003
BP-2	1.21	1.07	0.14	0.19	0.003
BP-4	1.34	1.26	0.14	0.33	0.010
BP-5	0.23	0.23	0.14	0.02	0.003
BP-6	0.18	0.18	0.14	0.04	0.010

Table 4.7.: Four-lepton signal cross-sections (S) for $\sqrt{s} = 10$ TeV after the basic cuts (Cut-1), after Cut-2 and after Cut-3. For BP-3 there is no signal. The total SM background (BG) cross-section (mostly from ZZ) after Cut-2 and Cut-3 is also given. Note that we always demand that among the four leptons, there is always at least one OSSF lepton pair with its invariant mass being around ± 20 GeV of M_Z.

it is again completely removed by the effective mass cut.

In Fig. 4.4 we show the four-lepton invariant mass distributions for all the benchmark points, except BP-3, and the corresponding SM background for the LHC running at $\sqrt{s} = 14$ TeV after the basics cuts (Cut-1) and the cut of M_{eff} (Cut-2).

As can be seen from Fig. 4.4, after the effective mass cut (Cut-2) the signal is larger than the SM background, except for BP-5 and BP-6. But for all benchmark points a clear peak emerges at the mass of A_H. Note that we do not observe any four-lepton events with an invariant mass of less than 100 GeV, which reflects the fact that we demand at least one OSSF lepton pair to have an invariant mass around M_Z.

In Table 4.8 we list for all the benchmark points, except BP-3, the cross-sections for the four-lepton signal for the LHC running at a center of mass energy of 14 TeV after the basic cuts (Cut-1), after Cut-2 on the effective mass and after

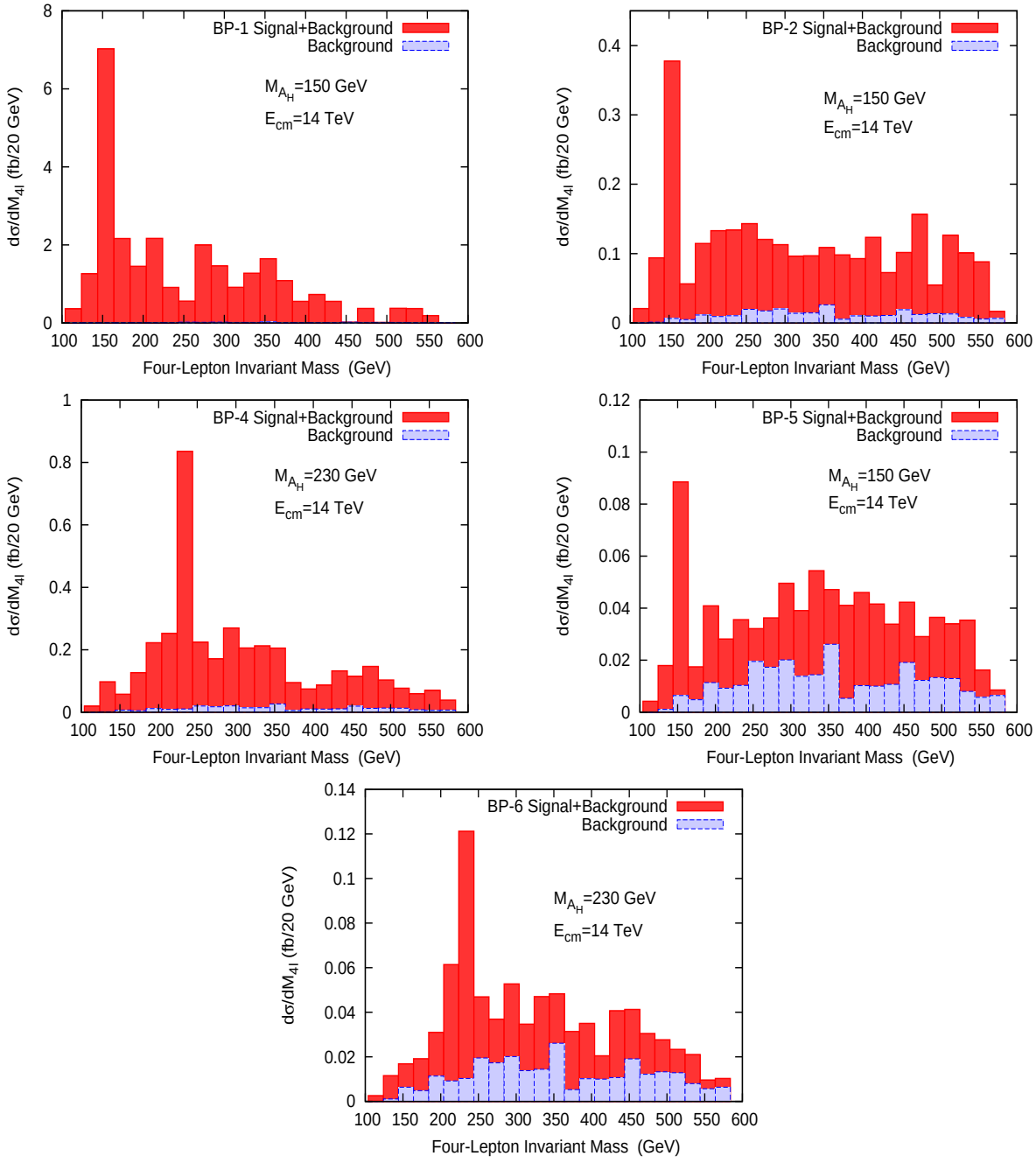

Figure 4.4.: Four-lepton invariant mass distribution for all the benchmark points, except BP-3, where we do not expect any signal, after the basic cuts (Cut-1) and after the cut on $M_{eff} \geq 1$ TeV (Cut-2) for $\sqrt{s} = 14$ TeV.

Cut-3. The total SM background after Cut-2 and Cut-3 is also given. In addition, we give the number of events for an integrated luminosity of $30\,\text{fb}^{-1}$ after Cut-2 and after Cut-3.

	Cut-1 [S] (fb)	Cut-2 [S] (fb)	Cut-2 [BG] (fb)	S_2	B_2	Cut-3 [S] (fb)	Cut-3 [BG] (fb)	S_3	B_3
BP-1	58.85	28.80	0.40	864.0	12	9.18	0.01	275.4	0.3
BP-2	3.12	2.89	0.40	86.7	12	0.47	0.01	14.1	0.3
BP-4	4.25	4.02	0.40	120.6	12	1.12	0.03	33.6	0.9
BP-5	0.79	0.79	0.40	23.7	12	0.10	0.01	3.0	0.3
BP-6	0.67	0.66	0.40	19.8	12	0.17	0.03	5.1	0.9

Table 4.8.: Same as Table 4.7 for $\sqrt{s} = 14$ TeV. The number of signal and background events after Cut-2 with an integrated luminosity of $30\,\text{fb}^{-1}$ are also given as S_2 and B_2, respectively. The corresponding numbers after Cut-3 are denoted by S_3 and B_3.

We can see from the table that Cut-2, as for the dilepton signal, removes about half of the four-lepton events for BP-1, but this is compensated by the large parton-level cross section for $m_{q_H} \sim 400$ GeV. The Cut-3 reduces the signal by a factor of six for BP-2, by a factor of four for BP-4 and by a factor of three for BP-1.

It is obvious that with essentially no background, we have a very clear signal and many events after Cut-3 for BP-1 and BP-4 with $30\,\text{fb}^{-1}$ of integrated luminosity. This should allow the reconstruction of the peak of the A_H boson and the determination of the mass M_{A_H}. For BP-2 we have about 14 events after Cut-3, therefore the reconstruction of the peak might not be so precise.

Recall that from the dilepton signature, we had a significant signal over the background for BP-1 and BP-3 at $\sqrt{s} = 10$ TeV and with $200\,\text{pb}^{-1}$ of integrated luminosity. In addition, at $\sqrt{s} = 14$ TeV and with $30\,\text{fb}^{-1}$, we could also cover BP-2 and BP-5. Now, with four-lepton events, we get a very clear signal after

Cut-3 for BP-4 (34 events compared to about 1 background event) and, for an integrated luminosity of about $59\,\text{fb}^{-1}$, we would get at least 10 signal events even for BP-6, with around 2 background events. Both of these benchmark points have $f = 1500$ GeV and the branching fraction $A_H \to ZZ$ is 22.5% and thus it is enhanced compared to BP-1 and BP-2, where for $f = 1000$ GeV it is only about 11%, see Table 4.1. This allows us to use the four-lepton signal for discovery for BP-4 and, maybe, BP-6.

Of course, it would be a convincing cross-check on the LHT model with T-parity violation, if one could see the A_H peak in the dilepton and in the four-lepton channel at the same mass. At least for BP-1 and BP-2 this will be possible with the LHC running at 14 TeV and with $30\,\text{fb}^{-1}$. For BP-5, we would need $100\,\text{fb}^{-1}$ to get 10 four-lepton signal events after Cut-3. Note that other New Physics models which have such a Z'-type boson like the A_H might lead to a different pattern in the invariant mass distributions or the relative number of events in the dilepton and four-lepton channels might be very different from the ones in the LHT.

As suggested in Ref. [26], looking at the angular distributions of the two lepton pairs coming from ZZ-decays, one might be able to determine whether the decay $A_H \to ZZ$ is really described by a vertex which originates from the WZW-term. At least for BP-1 with 275 four-lepton events after Cut-3, such an analysis seems to be feasible.

4.5. Summary and Conclusions

In this chapter, we have analyzed dilepton and four-lepton events at the LHC originating from the decay of the heavy photon A_H in the Littlest Higgs model with T-parity violation. These decays of A_H, assumed to be the lightest T-odd particle, are induced by T-violating couplings from the Wess-Zumino-Witten anomaly term. For larger masses $M_{A_H} > 150$ GeV, A_H predominantly decays into $WW^{(*)}$ and $ZZ^{(*)}$. On the other hand, for smaller masses, loop-induced decays into SM fermions are possible.

Due to the tiny coupling of A_H to SM particles, its direct production at e^+e^- or hadron colliders only has a cross-section of the order of 10^{-6} pb. On the other hand, the production of the other T-odd particles is not affected by the presence of the WZW term. Therefore, these particles are still pair-produced and cascade de-

cay down to A_H by the T-conserving interactions in the LHT and finally the two A_H's decay promptly in the detector. Therefore, summing all production processes of heavy T-odd quark pairs leads to a sizeable cross-section at the LHC, of the order of several pb, and this corresponds to a lower bound on the production cross-section of A_H pairs.

We have studied the dilepton and four-lepton signals for six benchmark points, see Table 4.2, which have different values for the heavy quark mass $m_{q_H} \sim 400, 700, 1000$ GeV and different values for the mass of the heavy photon $M_{A_H} = 66, 150, 230$ GeV ($f = 500, 1000, 1500$ GeV). The values of the heavy quark mass essentially determine the parton-level pair-production cross-section via strong interaction processes, although the effects of electroweak contributions from t-channel exchanges of A_H and Z_H can be very important and even dominate for low values of f, i.e. light A_H and Z_H. On the other hand, the mass of A_H determines the expected signal because of the different branching ratios into leptons or ZZ, see Table 4.1 . For low and intermediate masses of A_H, the dilepton decays are sizeable, whereas for $M_{A_H} = 230$ GeV the decay into ZZ and then into four-leptons is relevant.

We have studied the case of the LHC running at a center of mass energy of $\sqrt{s} = 10$ TeV with a modest integrated luminosity of $200\,\text{pb}^{-1}$ and the case of $\sqrt{s} = 14$ TeV with an integrated luminosity of $30\,\text{fb}^{-1}$.

In order to reduce the SM background from Z/γ^* and $t\bar{t}$ + jets for the dilepton signal and from ZZ + jets for the four-lepton signal, we have imposed a large cut on the effective mass of the events of $M_{eff} > 1$ TeV, since in general M_{eff} approximately peaks at the sum of the masses of the initially produced particles. Essentially, this cut removes a considerable fraction of the SM backgrounds, except for processes with multiple additional hard jets, which have a long tail in the effective mass distribution (see Figure 4.1). On the other hand, there are many sources of leptons in the decay cascades leading to A_H and in general we also get many events with leptons which do not originate from the decay of A_H. We have reduced the corresponding background from within the LHT by imposing the condition that the invariant mass of dileptons or four leptons should lie in a window of ± 20 GeV around M_{A_H}.

For the *dilepton signal*, the main conclusion is that for regions of the parameter space where either the T-odd quarks are relatively light, $m_{q_H} \sim 400$ GeV (BP-1 with $f = 1000$ GeV) or the scale f is rather low, $f = 500$ GeV (BP-3

with $m_{q_H} \sim 700$ GeV), we get after all the cuts a clear signal above the background for the early run of the LHC with center of mass energy of 10 TeV and integrated luminosity of $200\,\text{pb}^{-1}$. More details can be found in Table 4.4. For the LHC with $\sqrt{s} = 14$ TeV and $30\,\text{fb}^{-1}$ luminosity, also BP-2 ($m_{q_H} \sim 700$ GeV, $M_{A_H} = 150$ GeV) and BP-5 ($m_{q_H} \sim 1000$ GeV, $M_{A_H} = 150$ GeV) yield a significant signal with $S/\sqrt{B} = 42.9$ for the former and $S/\sqrt{B} = 7.9$ for the latter benchmark point, see Table 4.6 for details.

The *four-lepton channel* is very clean and the signal cross-sections are larger than the SM backgrounds after all the cuts, with the exception of BP-3 with small $f = 500$ GeV, where we do not expect a four-lepton signal. Unfortunately, for the LHC running at 10 TeV and with $200\,\text{pb}^{-1}$ of integrated luminosity, we always get less than 10 signal events. For $\sqrt{s} = 14$ TeV and $30\,\text{fb}^{-1}$, the background is again negligible (< 0.9 events) and we can easily cover again BP-1 and BP-2. In addition, we now also get a clear signal for BP-4 ($m_{q_H} \sim 700$ GeV, $M_{A_H} = 230$ GeV). We would need $59\,\text{fb}^{-1}$ to get 10 signal events for BP-6 ($m_{q_H} \sim 1000$ GeV, $M_{A_H} = 230$ GeV). Note that these BP's with large $f = 1500$ GeV can only be covered in the four-lepton channel. Details can be found in Table 4.8.

Therefore, with the LHC running at 14 TeV and an integrated luminosity of $30\,\text{fb}^{-1}$, we can cover with the dilepton and / or the four-lepton signal a large part of the typical parameter space of the LHT with values of f up to 1500 GeV and with T-odd quark masses up to about 1000 GeV. In general, a clear peak emerges at M_{A_H}, if one plots the invariant mass distributions for dileptons, see Fig. 4.2 for the LHC running at 10 TeV, and Fig. 4.3 for $\sqrt{s} = 14$ TeV. The four-lepton invariant mass distribution for the LHC at 14 TeV is shown in Fig. 4.4. For all the studied benchmark points we have enough signal events after all the cuts, therefore it should be easy to reconstruct the mass peak of A_H, maybe with the exception of BP-6.

Note that the reconstruction of the peak and the measurement of M_{A_H} directly determines the symmetry breaking scale f in the LHT, which is one of the fundamental parameters of any Little Higgs model. Together with the M_{eff} distribution which peaks around $2m_{q_H}$, this would then allow a rough determination of the parameter κ_q as well.

Of course, it would also be an important cross-check on the LHT model with T-parity violation, if we could see the A_H peak in both the dilepton and the four-lepton channel at the same mass. This, including the ratio of events in

the two channels, distinguishes the case of A_H in the LHT from other models of New Physics, like most Z' models. At least for benchmark points with intermediate values of $f = 1000$ GeV, which yield both enough dilepton and four-lepton events, this could be achieved. For BP-1 and BP-2 this will be possible for the LHC running at 14 TeV and with $30\,\text{fb}^{-1}$. For BP-5 we would need $100\,\text{fb}^{-1}$ to get 10 four-lepton events (with essentially very low background).

Note about 10 TeV **LHC.** After the results of this chapter were first submitted as a manuscript, the LHC schedule was revised, targeting a run at 7 TeV with about 5 fb^{-1} luminosity, followed by a direct upgrade to 14 TeV. Since the 14 TeV run maximizes our reach in the parameter space, we have presented the results corresponding to this energy in detail. However, we have retained the results for 10 TeV, which can give us an indication about the reach at 7 and 8 TeV runs also, in which the qualitative features remain similar.

Bibliography

[1] S. Mukhopadhyay, B. Mukhopadhyaya and A. Nyffeler, JHEP **1005**, 001 (2010).

[2] G. Cacciapaglia *et al.*, arXiv:0911.4630 [hep-ph]; G. Cacciapaglia, S. R. Choudhury, A. Deandrea and N. Gaur, arXiv:0911.4632 [hep-ph].

[3] A. Freitas and D. Wyler, JHEP **0611**, 061 (2006).

[4] A. Belyaev, C. R. Chen, K. Tobe and C. P. Yuan, Phys. Rev. D **74**, 115020 (2006). *A* CalcHEP *model file for the Littlest Higgs model with T-parity*, `http://hep.pa.msu.edu/LHT/`

[5] A. Pukhov, arXiv:hep-ph/0412191.

[6] T. Goto, Y. Okada and Y. Yamamoto, Phys. Lett. B **670**, 378 (2009); F. del Aguila, J. I. Illana and M. D. Jenkins, JHEP **0901**, 080 (2009); M. Blanke *et al.*, arXiv:0906.5454 [hep-ph].

[7] A. Freitas, P. Schwaller and D. Wyler, *A* CalcHEP *model file for the Littlest Higgs model with broken T-parity*, `http://www.itp.uzh.ch/~pedro/lht/`

[8] A. Freitas, P. Schwaller and D. Wyler, JHEP **0809**, 013 (2008).

[9] H. L. Lai *et al.*, Phys. Rev. D **51**, 4763 (1995); J. Pumplin *et al.*, JHEP **0207**, 012 (2002); D. Stump *et al.*, JHEP **0310**, 046 (2003).

[10] P. Langacker, Rev. Mod. Phys. **81**, 1199 (2009); E. Salvioni, A. Strumia, G. Villadoro and F. Zwirner, arXiv:0911.1450 [hep-ph]; P. Langacker, arXiv:0911.4294 [hep-ph].

[11] L. Randall and R. Sundrum, Phys. Rev. Lett. **83**, 3370 (1999); Phys. Rev. Lett. **83**, 4690 (1999).

[12] P. Achard *et al.* [L3 Collaboration], Phys. Lett. B **572**, 133 (2003).

[13] T. Aaltonen *et al.* [CDF Collaboration], Phys. Rev. D **78**, 012008 (2008).

[14] H. S. Lee, Phys. Lett. B **674**, 87 (2009).

[15] T. Sjöstrand, S. Mrenna and P. Skands, JHEP **0605**, 026 (2006).

[16] J. Alwall *et al.*, arXiv:0712.3311 [hep-ph]; P. Skands *et al.*, JHEP **0407**, 036 (2004).

[17] M. L. Mangano *et al.*, JHEP **0307**, 001 (2003).

[18] M. R. Whalley, D. Bourilkov and R. C. Group, arXiv:hep-ph/0508110.
`http://projects.hepforge.org/lhapdf/`

[19] M. Cacciari *et al.*, JHEP **0809**, 127 (2008).

[20] S. Dittmaier, P. Uwer and S. Weinzierl, Phys. Rev. Lett. **98**, 262002 (2007); Eur. Phys. J. C **59**, 625 (2009).

[21] G. Bevilacqua, M. Czakon, C. G. Papadopoulos and M. Worek, arXiv:1002.4009 [hep-ph].

[22] J. Huston, arXiv:1001.2581 [hep-ph].

[23] G. Aad *et al.* [The ATLAS Collaboration], arXiv:0901.0512 [hep-ex]; G. L. Bayatian *et al.* [CMS Collaboration], J. Phys. G **34**, 995 (2007).

[24] Private communication with Bruce Mellado.

[25] J. M. Campbell *et al.*, Phys. Rev. D **80**, 054023 (2009).

[26] W. Y. Keung, I. Low and J. Shu, Phys. Rev. Lett. **101**, 091802 (2008).

Chapter 5.

Same-sign trileptons and four-leptons at the LHC

5.1. Introduction

Finding physics beyond the standard electroweak theory is an important goal of the LHC. However, most proposed signals are beset with backgrounds from processes driven by the standard model (SM) itself, and the reduction of backgrounds requires a Herculean effort. This was clearly seen in the previous chapter, where we observed that the opposite-sign dilepton backgrounds were huge, and even though we were looking for quite a distinctive peak in the invariant mass distribution of the leptons, it required a series of strong selection cuts to isolate the signal over and above the backgrounds. Therefore, it is always useful to identify signals which are distinctive of specific new scenarios on the one hand, and are less background-prone on the other. Final states containing a multitude of leptons undoubtedly satisfy the second criterion. In fact, this is why we tried to reconstruct the A_H in the previous chapter in the leptonic channels, and not in hadronic ones, even though those modes have a much larger branching fraction.

In order to address the criterion of finding distinctive signals for specific new physics scenarios, it is often necessary to probe additional features of the leptons. One such feature is the sign(s) of the leptonic charge(s). It is well-established now that same-sign dilepton (SSD) carries a rather distinct signature of supersymmetry (SUSY) [1], and other new physics scenarios [2], once we carefully apply the event selection criteria to suppress the top-antitop background.

A curiosity that immediately arises is whether same-sign leptons of higher multiplicity can tell us something more. Although this idea of same-sign trileptons (SS3ℓ) was floated originally in the context of top quark signals [3], its efficacy in new physics search was unexplored until very recently. This is somewhat unfortunate, because the standard model (SM) backgrounds for them are extremely small. Some studies in the context of heavy neutrino signals were reported, though with rather limited scope [4]. As we shall describe in detail in this chapter, in two recent studies [5, 6], we pointed out that SS3ℓ as well as its four-lepton extension (SS4ℓ) has considerable potential in unearthing scenarios where Z_2-type discrete symmetries are broken in a limited manner. In particular, we show that various R-parity violating SUSY scenarios [7] (with R = $(-1)^{(3B+L+2S)}$, B, L and S being baryon number, lepton number and spin, respectively) predict large signal rates for SS3ℓ and moderate rates for even SS4ℓ, with hardly any backgrounds. The SS3ℓ signal is substantial over a range of the parameter space in the 7 TeV LHC run, while the predictions for both SS3ℓ and SS4ℓ are copious for 14 TeV. This suggestion has since been utilized in a number of subsequent studies in the literature [8].

Let us begin by pointing out the current relevance of studies in this direction. First of all, the LHC searches for new physics, particularly SUSY, at the initial stage, are concentrating on signals with large missing transverse energy. So far the results have been negative. If they continue to be so, some possibilities to consider will be (a) SUSY without R-parity, (b) a highly compressed SUSY spectrum, and (c) SUSY with stable visible particles. While the signatures of each of the above scenarios have been proposed and investigated in the literature, the SS3ℓ and SS4ℓ signals are exclusively indicative of SUSY with R-parity broken via lepton number violation. Since such signals can arise with large rates even during the early run, they are worth studying seriously, even from the sheer event counting point of view.

As we have discussed in Chapter 2.1.3, L-violating SUSY has considerable

appeal, because mechanisms of neutrino mass generation are suggested there. It is also being increasingly realised nowadays that one may end up with a dark matter candidate such as the axino or the gravitino in spite of R-parity violation. Some search limits for R-parity violating SUSY exist in the literature, based on multilepton ($\geq 3\ell$) signals. However, SS3ℓ is a rather more unequivocal indication of R-parity violation, since it is very difficult to produce three leptons of the same sign unless the seed of lepton number violation is there. Moreover, as will be discussed later in this chapter, enhanced rates for such signals are very unlikely to be found in R-parity conserving versions of SUSY, even in a purely phenomenological scan of its parameter space. The background is also vanishingly small, in contrast with the other channels advocated so far. With this in view, we shall also demonstrate regions in the SUSY parameter space (taking minimal supergravity (mSUGRA) as an example) where one can have five signal events, with zero background events expected, for some given integrated luminosity.

The enhanced signal rates are first studied within the framework of an mSUGRA scenario. It is, however, important to go beyond the most simple of 'top-down' models and investigate SUSY signals at the LHC in a phenomenological, 'bottom-up' approach. Therefore, we have also considered this alternative approach and looked at the SUSY parameter space in a relatively unbiased manner, although some simplification has been inevitable in order to keep the number of free parameters manageable. This allows us to point out features of the SUSY spectrum, for which same-sign multileptons are most likely to be observed.

We have opened another new direction in the studies presented in this chapter. There are a number of ways in which R-parity can be violated via L, since one can have the so-called λ-type, $\lambda^{'}$-type and the L-violating bilinear terms in the superpotential. Besides, the lightest neutralino need not be the lightest SUSY particle (LSP) when R-parity is violated, the stau-LSP scenario being the next most common possibility. We contend here that the SS3ℓ and SS4ℓ signal rates, in conjunction with their mixed-sign counterparts of the same multiplicity, display certain mutual relations which distinguish among at least some of the candidate scenarios. These relations can be used to extract dynamical information about the underlying SUSY theory, namely, the Majorana character of the decaying lightest neutralino and the nature of L-violating couplings. We define suitable variables and relationships between them which can be verified experimentally and which are largely independent of the SUSY production cross-sections and

the cascade decay branching fractions. These theoretical predictions are then validated by Monte Carlo simulations including detector and background effects. Consequently, one may use these signals to find out in a generic way the distinction among the λ-type, $\lambda^{'}$-type or bilinear couplings. Although our discussion is largely based on scenarios with a neutralino LSP, alternative scenarios, for example, with stau LSP, can be brought within its scope, as has been briefly indicated in this chapter.

It should be noted that same-sign multileptons in general, and SS3ℓ in particular, can be seen in some other non-standard scenarios as well. In most cases, however, the rates are considerably smaller than what one would expect for R-parity violating cases with new particles of similar masses. The first example of this is minimal SUSY standard model (MSSM) where R-parity is conserved; our scan of its parameter space, with the usual constraints satisfied, reveals rather low event rates for SS3ℓ. One has predictions of some interest for Little Higgs theories where T-parity is broken by the Wess-Zumino-Witten anomaly terms [9–11]. However, we shall see that the rates are much smaller than those for R-parity violating SUSY with a spectrum of similar masses [5]. In addition, models with heavy charged leptons and Majorana neutrinos [4] and triply charged heavy leptons [12] can also lead to an SS3ℓ signature.

This chapter has been organized as follows. Section 5.2 is devoted to the standard model contributions to same-sign and mixed-sign multilepton channels, and we suggest event selection criteria that suppress such contributions as potential backgrounds to the new physics signals. In Section 5.3, we review the different cases of R-parity violating SUSY, and show the event rates for different benchmark points for mSUGRA, for both the 14 and 7 TeV runs. Section 5.4 contains a study where the parameters are varied in a more phenomenological manner, and regions where R-parity violating SUSY shows up in the SS3ℓ channel are pointed out. We also explain in the same section why the SS3ℓ and SS4ℓ signals are not expected to occur with appreciable rates when R-parity is conserved, even in a generic MSSM model. Subsequently, in two short sections we discuss same-sign four-lepton signatures (Section 5.5) and the possibility of obtaining SS3ℓ in LHT with T-parity violation (Section 5.6). In Section 5.7 , we show in detail how we can extract information on the Majorana character of the lightest neutralino and the dynamics of R-parity violation from SS3ℓ and SS4ℓ signals. We summarise and conclude in Section 5.8.

5.2. Standard model backgrounds

We start by taking a look at the SM contributions to the SS3ℓ signal. The main sources here are (i) $t\bar{t}$, (ii) $t\bar{t}W$, (iii) $t\bar{t}b\bar{b}$ and (iv) $t\bar{t}t\bar{t}$ production. Of the various processes, $t\bar{t}$ production, copious as it is, generates SS3ℓ if a lepton comes from a charm quark produced from a b which in turn results from top-decay. This causes a significant degradation of momentum of at least the softest lepton, and judicious lepton isolation and hardness cuts suppress it. The other channels, too, suffer from either perturbative suppression at the initial production level or low branching ratios in the cascades. We summarise the SM backgrounds to SS3ℓ in Table 5.1.

We select events with three and only three leptons in the signal (for SS3ℓ), all of which have to be of the same-sign. In addition, we have primarily selected leptons with $p_T \geq 10$ GeV, $|\eta| \leq 2.5$, where p_T and η are respectively the transverse momentum and pseudorapidity of the lepton. We further demand a lepton-lepton separation $\Delta R_{ll} \geq 0.2$, where $(\Delta R)^2 = (\Delta\eta)^2 + (\Delta\phi)^2$ quantifies the separation in the pseudorapidity-azimuthal angle plane. We also demand a lepton-jet separation $\Delta R_{lj} \geq 0.4$ for all jets with $E_T \geq 20$ GeV. Also, a relative isolation criterion to restrict the hadronic activity around a lepton has been used, i.e., we demand $\sum p_T$ (hadron) $/\, p_T$ (lepton)≤ 0.2, where the sum is over all hadrons within a cone of $\Delta R \leq 0.2$ around the lepton. A missing-E_T ($\not{E}_T$) cut of 30 GeV is also included, in order to reduce the probability of jets faking leptons [4]. Subsequently, stronger p_T-cuts (as mentioned in the caption of Table 5.1) are applied, in order to ensure minimum hardness for even the softest of the three leptons [13]. This, together with the demand on lepton isolation, strongly suppresses the b(and c)-induced leptons, and makes the SM contributions quite small, as shown in Table 5.1. The events for the above-mentioned SM background processes contributing to SS3ℓ were generated with the code ALPGEN [14], and showering, decays and hadronisation were done using PYTHIA 6.421 [15]. Throughout this study, we have used the CTEQ6L1 [16] parton distribution functions. The effect of $B^0 - \bar{B}^0$ mixing on lepton signs has been taken into account within PYTHIA. We have approximated the detector resolution effects by smearing the energies (transverse momenta) of the leptons and jets with Gaussian functions [17], as described in Chapter 3.3.

Needless to say, the SM backgrounds to the SS4ℓ channel will be even

Process	$\sigma_{SS3\ell}$ (fb)	$\sigma_{SS3\ell}$ (fb)
	[Cut-1]	[+ Cut-2]
$t\bar{t}W$	2.80×10^{-2}	2.44×10^{-3}
$t\bar{t}b\bar{b}$	4.45×10^{-3}	$< 1.11 \times 10^{-3}$
$t\bar{t}t\bar{t}$	8.40×10^{-4}	6.45×10^{-5}
Total	3.33×10^{-2}	2.50×10^{-3}

Table 5.1.: Dominant same-sign trilepton SM background cross-sections ($\sigma_{SS3\ell}$) for $\sqrt{s} = 14$ TeV after the basic isolation cuts (Cut-1) and after demanding that $p_T^{l_1} > 30$ GeV, $p_T^{l_2} > 30$ GeV, $p_T^{l_3} > 20$ GeV and $\not{E}_T > 30$ GeV, which are collectively referred to as Cut-2. Here l_1, l_2 and l_3 are the three leptons ordered according to their p_T's. Note that the $t\bar{t}$ contribution falls drastically after Cut-1 itself.

smaller than SS3ℓ, and can be safely neglected. As we shall see later in section 5.7, we can construct certain observables which depend only on the Majorana nature of the LSP and the L-violating coupling involved and not upon other parameters determining the cascade decays. In addition to the SS3ℓ and SS4ℓ cross-sections, these variables shall also depend upon the total trilepton (3ℓ) and four-lepton (4ℓ) cross-sections in a given scenario, with specific kinematic criteria. Thus we need to evaluate and include the SM backgrounds in the 3ℓ and 4ℓ channels, and subject them to the same set of cuts irrespective of the sign of leptons. Therefore, while a Z-veto (removing events containing same flavour, opposite-sign leptons with invariant mass around the Z-boson mass) is often used to reduce the SM backgrounds in the sign-inclusive 3ℓ and 4ℓ channels, we cannot use such a veto here. Also, we use kinematic variables that only depend upon the lepton p_T's and the $\not{E}_T$ in an event. We find it useful to select events in terms of the variables m_{eff}^{ℓ} and m_{eff}, defined as follows:

$$m_{eff}^{\ell} = \sum p_T^{leptons} \tag{5.1}$$

$$m_{eff} = \sum p_T^{leptons} + \not{E}_T, \tag{5.2}$$

where the missing transverse energy is given by

$$\not{E}_T = \sqrt{\left(\sum p_x\right)^2 + \left(\sum p_y\right)^2}. \tag{5.3}$$

Here the sum goes over all the isolated leptons, the jets, as well as the 'unclustered' energy deposits.

Cut	$W^{\pm}(Z_0/\gamma^{\star})$	$t\bar{t}$	$t\bar{t}(Z_0/\gamma^{\star})$	$t\bar{t}W^{\pm}$	Total
Basic cuts (Cut-1+Cut-2)	34.50	9.88	2.82	0.73	47.93
$m^{\ell}_{eff} > 100$ GeV	33.53	8.23	2.80	0.71	45.27
$m^{\ell}_{eff} > 200$ GeV	5.01	0.00	1.43	0.33	6.77
$m_{eff} > 150$ GeV	32.06	8.23	2.80	0.72	43.81
$m_{eff} > 250$ GeV	6.18	1.65	1.81	0.48	10.12

Table 5.2.: SM contributions to the trilepton channel at 14 TeV LHC. The m^{ℓ}_{eff} or m_{eff} cut is applied one at a time. All the cross-sections are in femtobarns.

The SM contributions coming from the sign-inclusive 3ℓ and the 4ℓ channels are shown in Tables 5.2 and 5.3 respectively. The predictions for the 14 TeV run only are presented here; although the predictions for 7 TeV, too, are very small, we do not expect enough statistics for performing our suggested analysis there. We show the cross-sections after different cuts on the m^{ℓ}_{eff} and m_{eff} variables. In the 3ℓ channel the major backgrounds are $W^{\pm}(Z_0/\gamma^{\star})$, $t\bar{t}$, $t\bar{t}(Z_0/\gamma^{\star})$ and $t\bar{t}W^{\pm}$. Here, the $W^{\pm}(Z_0/\gamma^{\star})$ and $t\bar{t}(Z_0/\gamma^{\star})$ processes include the effect of Z, γ^{*} and their interference. In the 4ℓ channel, the dominant SM contributions come from $(Z_0/\gamma^{\star})(Z_0/\gamma^{\star})$, $t\bar{t}$ and $t\bar{t}(Z_0/\gamma^{\star})$. The processes $W^{\pm}(Z_0/\gamma^{\star})$ and $t\bar{t}(Z_0/\gamma^{\star})$ were simulated using MadGraph 5 [18] and PYTHIA, $t\bar{t}W^{\pm}$ using ALPGEN and PYTHIA and $t\bar{t}$ and $(Z_0/\gamma^{\star})(Z_0/\gamma^{\star})$ using PYTHIA alone. For the $t\bar{t}$ process we have multiplied the leading order cross-section from PYTHIA by a K-factor of 2.2 according to the analysis in Ref. [19]. We have taken showering, hadronisation and multiple interaction effects into account in all of our simulations.

Cut	$(Z_0/\gamma^\star)(Z_0/\gamma^\star)$	$t\bar{t}(Z_0/\gamma^\star)$	Total
Basic cuts (Cut-1+Cut-2)	9.33	0.46	9.79
$m^\ell_{eff} > 100$ GeV	9.25	0.46	9.71
$m^\ell_{eff} > 200$ GeV	3.71	0.32	4.03
$m_{eff} > 150$ GeV	7.87	0.45	8.32
$m_{eff} > 250$ GeV	1.67	0.36	2.03

Table 5.3.: SM contributions to the four-lepton channel at 14 TeV LHC. The m^ℓ_{eff} or m_{eff} cut is applied one at a time. The $t\bar{t}$ contribution is zero after the basic lepton selection and isolation cuts. All the cross-sections are in femtobarns.

5.3. SS3ℓ in L-violating SUSY

5.3.1. A brief review of the L-violating scenarios considered

In this section, we shall very briefly describe how SS3ℓ can arise in different scenarios of lepton-number (L) violating supersymmetry.

As discussed in Chapter 2.1.3, the superpotential in R-parity violating SUSY can contain the following $\Delta L = 1$ terms, over and above those present in the MSSM:

$$W_{\not L} = \lambda_{ijk} L_i L_j \bar{E}_k + \lambda'_{ijk} L_i Q_j \bar{D}_k + \epsilon_i L_i H_u$$

***Case 1*:** With the λ-type terms, we consider two possibilities, namely, having (a) the lightest neutralino ($\tilde{\chi_1}^0$) and (b) the lighter stau ($\tilde{\tau}_1$) as the lightest SUSY particle (LSP). In (a), SS3ℓ can arise if $\tilde{\chi_1}^0$ decays into a neutrino, a tau (τ) and a lepton of either of the first two families. When the τ decays hadronically, the two leptons from two $\tilde{\chi_1}^0$'s produced at the end of SUSY cascades are of identical sign in 50% cases. An additional lepton of the same sign, produced in the decays of a chargino ($\tilde{\chi_1}^\pm$) in the cascade, leads to SS3ℓ. If there is just one λ-type coupling (we have used λ_{123} for illustration), there is no further branching fraction sup-

pression in LSP decay, and one only pays the price of $\tilde{\chi_1}^{\pm}$-decay into a lepton of the same sign. In (b), two same-sign $\tilde{\tau_1}$'s can be produced from two $\tilde{\chi_1}^0$'s, due to its Majorana character. Each of these $\tilde{\tau_1}$'s goes into a lepton and a neutrino; these two leptons, together with one of identical sign from the cascade, lead to SS3ℓ signals.

***Case 2*:** With λ'-type interactions, a $\tilde{\chi_1}^0$-LSP decays into two quarks and one charged lepton or neutrino. If the LSP is not much heavier than the top quark, and if the effect of the difference between up and down couplings of the neutralino can be neglected, we obtain SSD's from a pair of $\tilde{\chi_1}^0$'s roughly in 12.5% of the cases. If another lepton of the same sign arises from a $\tilde{\chi_1}^{\pm}$, SS3ℓ is an immediate consequence. Therefore, the overall rate of SS3ℓ can be substantial in this case as well. Here, (and also partially in case 1(b)), the large boost of the $\tilde{\chi_1}^0$ can lead to collimated jets and leptons, making the latter susceptible to isolation cuts.

Although most of the analysis we have presented for such couplings is based on a $\tilde{\chi_1}^0$-LSP scenario, we shall see later that one with $\tilde{\tau_1}$-LSP, too, has potential for SS3ℓ events.

***Case 3*:** With bilinear R-parity breaking terms ($\sim \epsilon_i$), the most spectacular consequence is the mixing between neutralinos and neutrinos as well as between charginos and charged leptons. Consequently, over a substantial region of the parameter space, a $\tilde{\chi_1}^0$ LSP in this scenario decays into $W\mu$ or $W\tau$ in 80% cases altogether, so long as the R-parity breaking parameters are in conformity with maximal mixing in the $\nu_\mu - \nu_\tau$ sector [20]. From the decay of the two $\tilde{\chi_1}^0$'s, one can obtain SSD's either from these μ's, or from the leptonic decay of the W's or the τ's. An additional lepton from the SUSY cascade results in SS3ℓ again. Adding up all the above possibilities, the rates can become substantial.

Again, in addition to a $\tilde{\chi_1}^0$-LSP, a $\tilde{\tau_1}$-LSP also can lead to the signals under consideration. We shall briefly mention such possibilities later in our discussion.

5.3.2. SS3ℓ signal rates in mSUGRA for 14 TeV LHC

In Table 5.4 the predictions of SS3ℓ cross-section for all the aforementioned cases, corresponding to some representative points for each, are presented, for $\sqrt{s} =$ 14 TeV LHC. We have used CTEQ6L1 [16] parton distribution functions, with the renormalisation and factorisation scales kept at the PYTHIA default [15]. The value of each trilinear coupling (λ, λ') used for illustration is 0.001. For case 3, The

values of the ϵ-parameters are chosen consistently with the neutrino data; essentially, they are tuned to sneutrino vacuum expectation values of the order of 100 keV, in a basis where the bilinear terms are rotated away from the superpotential. The values of ϵ_i are also of this order in the absence of any additional symmetry. The exact values of ϵ_i that correspond to points $3(1)$ and $3(2)$ in Table 5.4 depend also on other parameters of the model, such as the L-violating soft terms in the scalar potential [21]. However, the range of values of these parameters is of little consequence to the neutralino decay branching ratios. Therefore, with appropriate values of these soft terms, $\epsilon_3 \approx 100$ keV, $\epsilon_1 = \epsilon_2 = 0$ is consistent with all our results.

The cross-sections were calculated with the help of PYTHIA, where all possible SUSY production processes were taken into account. We show values of SUSY parameters at the electroweak scale (in this case it has been fixed at $\sqrt{m_{\tilde{t}_1} m_{\tilde{t}_2}}$, where $\tilde{t}_1$ and $\tilde{t}_2$ are the two mass eigenstates of the top squarks respectively), though they have been generated, for the sake of economy, in a minimal supergravity (mSUGRA) scenario. Since the values of the L-violating couplings are very small, they do not affect the renormalisation group running of mass parameters from high to low scale [22]. We have therefore generated the spectrum using SuSpect 2.41 [23] and interfaced it with SDECAY [24] by using the programme SUSY-HIT [25] (for calculating the decay branching fractions of the sparticles) and finally have interfaced the spectrum and the decay branching fractions to PYTHIA. Also, we have neglected the role of R-violating interactions in all stages of cascades excepting when the LSP is decaying.

In Table 5.4, we show the SS3ℓ cross-sections for two different gluino masses in each case, one around 600 -800 GeV, and the other in the range of 1 TeV. We also have chosen different values of $\tan\beta$ (the ratio of the vacuum expectation values of the two Higgs doublets), and made allowance for different splittings and hierarchies between the ${\tilde{\chi_1}}^{\pm}$ and slepton masses. We use fixed values for the other mSUGRA parameters, namely, the universal soft SUSY-breaking trilinear scalar interaction $A_0 = 0$ and the Higgsino mass parameter $\mu > 0$. For each mass range, λ_{123} leads to the highest rates of the SS3ℓ signal, as in this case the possibility of obtaining an isolated charged lepton from the LSP decay is higher than in the two other cases. Also, if the ${\tilde{\chi_1}}^{\pm}$'s are heavier than the first two family sleptons (and sneutrinos), the rates go up, owing to the increase in leptonic branching fraction of the ${\tilde{\chi_1}}^{\pm}$. Overall, the SS3ℓ rates are substantial for all the cases; even moder-

ate luminosities can yield signals for gluino masses upto a TeV or so. In order to demonstrate the discovery reach of the LHC in this channel, we also show in Figure 5.1, the boundary contours of regions in the $M_0 - M_{1/2}$ plane (M_0 and $M_{1/2}$ being respectively the universal scalar and gaugino mass at high scale), where at least 5 signal events can be obtained (with zero background events expected) with a given integrated luminosity. This scan was performed for a sample case (case 1) with fixed values for the other mSUGRA parameters ($\tan\beta = 10, A_0 = 0, \mu > 0$). Similar discovery reaches are expected for the other cases also.

Note that there is a sharp fall observed in each curve of Figure 5.1. As we increase M_0 for a given $M_{1/2}$, the first two family sleptons eventually become heavier than the chargino, thereby reducing the branching fraction of $\tilde{\chi_1}^{\pm} \to l^{\pm}\nu\tilde{\chi_1}^0$. This leads to a drop in the SS3ℓ cross-section, giving rise to the faster fall in the curves.

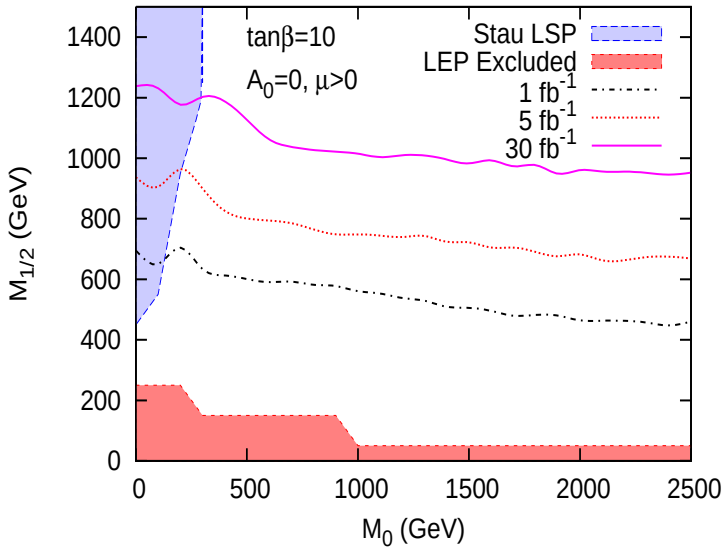

Figure 5.1.: 5-events LHC reach with SS3ℓ in the $M_0 - M_{1/2}$ plane for R-parity violating mSUGRA, at $\sqrt{s} = 14$ TeV, with $\lambda_{123} = 0.001$, after all selection cuts.

Case	$\tan\beta$	$m_{\tilde{g}}$ (GeV)	$m_{\chi_1^{\pm}}$ (GeV)	$m_{\chi_1^0}$ (GeV)	$m_{\tilde{\tau}_1}$ (GeV)	$m_{\tilde{e}_L}$ (GeV)	RPV Coupling	$\sigma^1_{SS3\ell}$ (fb)	$\sigma^2_{SS3\ell}$ (fb)
1a(1)	15	661	200	108*	115	204	λ_{123}	465.22	195.97
1a(2)	40	610	183	99*	139	265	λ_{123}	811.20	301.36
1a(3)	5	1009	331	176*	191	309	λ_{123}	81.54	55.31
1a(4)	40	1016	337	178*	246	418	λ_{123}	55.52	31.83
1b(1)	10	770	241	129	118*	222	λ_{123}	416.62	296.26
1b(2)	40	608	182	98	94*	236	λ_{123}	100.27	61.62
1b(3)	5	1008	330	176	171*	297	λ_{123}	53.00	42.74
1b(4)	40	1009	336	178	109*	328	λ_{123}	20.05	13.41
2(1)	15	661	200	108*	115	204	λ'_{112}	59.96	20.97
2(2)	40	610	183	99*	139	265	λ'_{112}	136.35	38.21
2(3)	5	1009	331	176*	191	309	λ'_{112}	21.76	12.26
2(4)	40	1016	337	178*	246	418	λ'_{112}	15.27	8.21
3(1)	5	1009	331	176*	191	309	ϵ_i	36.50	22.23
3(2)	40	1016	337	178*	246	418	ϵ_i	23.28	12.52

Table 5.4.: SS3ℓ cross-sections after Cut-1 ($\sigma^1_{SS3\ell}$) and Cut-2 ($\sigma^2_{SS3\ell}$) at $\sqrt{s} = 14$ TeV for the various cases discussed in the text (e.g., 1a(1) corresponds to the first example in case 1a). The LSP in a given point is indicated by a * against its mass. The low-scale MSSM parameters were generated in an mSUGRA framework. The λ and λ' couplings are set at 0.001, and the ϵ_i are within the limits set by neutrino data (see discussion in the text).

5.3.3. Results for 7 TeV LHC

In Table 5.5 we show the SS3ℓ cross-sections after all cuts for the 7 TeV LHC run. At 7 TeV, the total SM cross-section for SS3ℓ comes down to 7.01×10^{-4} fb. Since

the LHC experiments have already collected around $5\,\text{fb}^{-1}$ of data in the 7 TeV run, we present results for the mSUGRA points which can be accessed with this data. In particular, with this luminosity, we find that benchmark points with the squark-gluino masses in the TeV range can also be accessed in the SS3ℓ channel. These benchmark points include cases with $\tilde{\chi_1}^0$ LSP and λ-type couplings (points 1a(3) and 1a(4)) and also $\tilde{\tau}_1$ LSP with λ-type couplings (point 1b(3)). For $\tilde{\chi_1}^0$ LSP with λ'-type couplings, the SUSY sparticle mass-reach is somewhat smaller, and we can access masses slightly higher than 650 GeV during the 7 TeV run (point 2(1) in Table 5.5), if we insist on seeing 10 signal events without backgrounds with $5\,\text{fb}^{-1}$ of integrated luminosity. For 3 signal events with ≤ 1 background event, however, the reach is considerably higher. Thus, on the whole, the 7 TeV run has extremely encouraging prospects for more than one R-parity violating scenarios, from the viewpoint of total event rates.

Case	$\sigma_{SS3\ell}$ (fb)
1a(1)	19.82
1a(2)	29.45
1a(3)	4.29
1a(4)	2.01
1b(1)	30.74
1b(2)	6.46
1b(3)	3.35
2(1)	2.07
2(2)	4.03

Table 5.5.: SS3ℓ cross-sections after all selection cuts ($\sigma_{SS3\ell}$) at $\sqrt{s} = 7$ TeV for the different cases defined in Table 5.4.

5.3.4. Other possibilities in L-violating SUSY

We now discuss some other possible cases in L-violating SUSY where one can also get SS3ℓ events. In case of a $\tilde{\tau}_1$ LSP with λ'_{ijk}-type couplings, the $\tilde{\tau}_1$ will directly decay to two quarks if the index i takes the value 3. For the other two cases where i takes the value 1 or 2, $\tilde{\tau}_1$ cannot decay via two-body L-violating modes. In this case, it will go through a 4-body decay via an intermediate off-shell chargino or neutralino. In mSUGRA type of models, the lighter stau is mostly composed of the right-chiral field, in which case it will couple primarily to the bino component of the neutralino. Also, the lighter chargino there is mostly heavier than the lightest neutralino, and therefore the propagator suppression is more for off-shell chargino. Thus, the mode through off-shell neutralino will dominate. Thus, we shall find the dominant decay pattern for a $\tilde{\tau}_1$ to be $\tilde{\tau}_1 \to \tau \tilde{\chi_1}^{0(*)} \to \tau l^{\pm} q q'$. SS3$\ell$ events arise then in a very similar fashion as in the case of a $\tilde{\chi_1}^0$ LSP with λ'-type couplings.

Since the intermediate neutralino in $\tilde{\tau_1}^{\pm}$-decay is a Majorana particle, we shall not have equal rates for the $\tau^{\pm} l^+ q q'$ and the $\tau^{\pm} l^- \bar{q} \bar{q}'$ final states. Also, the production of the $\tilde{\tau}_1$ in the decay of each neutralino has also an accompanying tau, which is another source of leptons. Consequently, with two taus decaying together with two staus, there is a favourable combinatoric factor for SS3ℓ, which partially offsets the suppression due to branching ratios. The exact numerical evaluation of the relevant branching fractions and the resulting event rates is a detailed exercise by itself. In any case, we expect substantial cross-sections in the SS3ℓ channel, with the usual reduction of events in the presence of λ' -type couplings compared to the presence of λ-type couplings.

In presence of bi-linear L-violating couplings, a $\tilde{\tau}_1$ which is the LSP can mix with a charged Higgs, thereby leading to the decay mode $\tilde{\tau}_1 \to \tau \nu_\tau$, since the charged Higgs will couple more to the tau lepton than to electrons or muons. Thus, starting from a pair of neutralinos which can be produced in cascades, one can obtain two same-sign tau leptons, whose further leptonic decays can give rise to two leptons of the same sign. The third lepton of the same sign can come in the usual way from $\tilde{\chi_1}^{\pm}$ decay giving rise to SS3ℓ. Evidently, the rates in this case are expected to be rather small for various branching fraction suppressions. A detailed study of SS3ℓ in the $\tilde{\tau}_1$-LSP scenario for both of the above cases will be reported in a forthcoming publication [26].

5.4. SS3ℓ in phenomenological MSSM (pMSSM)

5.4.1. pMSSM with L-violation

Next we discuss the case of phenomenological MSSM, which includes many more possibilities than mSUGRA, as far as the mass spectra are concerned. In particular, the three gaugino mass parameters at the weak scale then need not be in the approximate ratio $M_1 : M_2 : M_3 = 1 : 2 : 6$. Thus the lighter chargino may not be about twice as massive as the lightest neutralino, a fact that can affect electroweak phenomenology considerably. Since one of the leptons in the SS3ℓ signal comes from the cascade decay of the chargino (via on or off-shell W's and sleptons) $\tilde{\chi_1}^{\pm} \to \tilde{\chi_1}^0 l^{\pm} \nu$, we need to look into other hierarchies between M_1 and M_2.

If $M_1 \simeq M_2$, $\tilde{\chi_1}^{\pm}$, $\tilde{\chi}_2^0$ and $\tilde{\chi_1}^0$ are all very close in mass, and therefore the lepton coming from chargino decay is rather soft in the $\tilde{\chi_1}^{\pm}$ rest frame. But, if the $\tilde{\chi_1}^{\pm}$ is resulting from the decay of the gluino or squarks, which could be much heavier, it can have a large boost, giving rise to high p_T leptons which will pass the required cuts.

Another interesting situation arises if $M_1 > M_2$. Here, the $\tilde{\chi_1}^0$ and the $\tilde{\chi_1}^{\pm}$ are mostly composed of wino components. This is what happens, for example, in the case of anomaly mediated SUSY breaking. The degeneracy in their masses is even more severe in this case, and some fine-tuning is necessary to make their mass difference of the order of pion mass. Here, one can have an additional channel in the cascade, from which a third lepton can arise. The second lightest neutralino can decay to a charged lepton, a neutrino and the $\tilde{\chi_1}^{\pm}$. The lepton produced in this way can have sufficient p_T to be detectable. The $\tilde{\chi_1}^{\pm}$, on the other hand, goes to the $\tilde{\chi_1}^0$ and an extremely soft pion (or lepton + neutrino), and the $\tilde{\chi_1}^0$ pair can be the source of same-sign dileptons, which, when of the same-sign as that of the initial lepton, leads to SS3ℓ. We also look into the case of $M_1 < M_2$ in pMSSM but with a wider mass separation than expected in mSUGRA, namely, $M_2 = 3M_1$. Here the rates of SS3ℓ are somewhat enhanced. Finally, we look into a kind of non-universality between the low-energy selectron (or smuon) and stau soft masses. This can lead to a scenario where all the sleptons except stau are lighter than $\tilde{\chi_1}^{\pm}$ and the BF of $\tilde{\chi_1}^{\pm}$ to leptons is around 95%. Needless to say, this enhances the SS3ℓ rates.

In order to be conservative, we fix the squark soft masses and M_3 at 1 TeV. We have already shown in the previous subsections that the strongly interacting sparticle mass scale of around 600 GeV is easily accessible at the LHC in the SS3ℓ channel during the 7 TeV run. The benchmark points chosen here are just to emphasize that the SS3ℓ signal can probe a generic MSSM model upto considerable higher masses of strongly interacting superparticles even during the early run. In addition, the situation of relatively closely spaced low-lying charginos/neutralinos, including those with an inverted hierarchy compared to mSUGRA, also turn up with substantial event rates. We present the most important parameters in the pMSSM benchmark points in Table 5.6 and the SS3ℓ cross-sections at these points in Table 5.7. As mentioned above, we have fixed the squark soft masses and M_3 at 1 TeV while A_t, A_b, A_τ and the μ parameter have been fixed at -500, -500, -250 and 975 GeV respectively. The cross-sections have been calculated for both the 7 TeV and the 14 TeV runs at the LHC, and we also give the required luminosities for a five-event discovery, with no events expected from the backgrounds. The overall usefulness of SS3ℓ in probing low-MET SUSY scenarios is thus brought out quite emphatically by the results presented by us. To this is added the rather striking prospect of extracting dynamic information (like the presence of Majorana gauginos and the exact nature of L-violating couplings) from the SS3ℓ and SS4ℓ channels, as will be explained in detail in section 5.7.

BP	M_1 (GeV)	M_2 (GeV)	$M_{\tilde{\chi_1}^0}$ (GeV)	$M_{\tilde{\chi_1}^\pm}$ (GeV)	$M_{\tilde{e}_L}$ (GeV)	$M_{\tilde{\tau}_1}$ (GeV)
1	150	150	146.54	154.80	254.13	180.91
2	160	150	154.08	154.80	254.13	217.69
3	100	300	97.69	395.30	254.10	180.68
4	125	250	121.65	254.35	156.76	217.52

Table 5.6.: Values of M_1, M_2 and some other relevant parameters for the SS3ℓ channel in the pMSSM benchmark points. The squark and gluino masses are fixed at ~ 1 TeV.

BP	$\sigma_{7\text{ TeV}}$ (fb)	$\mathcal{L}_{7\text{ TeV}}$ (fb^{-1})	$\sigma_{14\text{ TeV}}$ (fb)	$\mathcal{L}_{14\text{ TeV}}$ (fb^{-1})
1	0.91	5.49	4.60	1.09
2	0.41	12.20	1.62	3.09
3	2.81	1.78	20.67	0.24
4	8.78	0.57	42.93	0.12

Table 5.7.: SS3ℓ cross-sections in the different pMSSM benchmark points at 7 TeV and 14 TeV LHC. We also show the luminosities required to obtain 5 signal events at the two centre of mass energies.

5.4.2. pMSSM with conserved R-parity

If lepton number is conserved in the MSSM, then it is extremely difficult to find a scenario where one can obtain a same-sign trilepton signal (We specifically design the cuts to suppress leptons coming from b-decays, since otherwise they can boost the standard model backgrounds as well.) In fact, we do not find any such scenario in the simple mSUGRA picture. If one considers a purely phenomenological MSSM , one can of course generate a wide variety of mass spectra. We find one particular such spectrum where one can obtain SS3ℓ, but at a negligibly low rate because of branching fraction suppressions which are difficult to avoid. Thus, as far as we could analyze the MSSM processes with conserved R-parity, it is not possible to generate SS3ℓ with significant cross-section. Therefore, it seems, within a supersymmetric framework, a reasonably large cross-section of SS3ℓ is a clear indication of L-violation.

To convince the reader of this, let us outline a scenario in MSSM, where, in principle, it is possible to obtain an SS3ℓ signal, albeit with a small rate. Consider a situation where the sbottom is lighter than the stop. In this case, let us look at stop pair production ($\tilde{t_1}\tilde{t_1}^*$), followed by the decay $\tilde{t_1} \to \tilde{b_1}W^+$ (and a charge-conjugate decay process for $\tilde{t_1}^*$). The produced $\tilde{b_1}$ can then decay to $t\tilde{\chi_1}^-$, although with a very low branching fraction. The top quark, of course, then decays to bW^+. Thus starting from the initial $\tilde{t_1}\tilde{t_1}^*$ we can obtain a final state

$(W^+\tilde{\chi_1}^- bW^+)(W^-\tilde{\chi_1}^+ \bar{b}W^-)$. We can re-write this final state as $(b\bar{b})$ $(W^+W^+\tilde{\chi_1}^+)$ $(W^-W^-\tilde{\chi_1}^-)$. Now, it can be clearly seen that if a set of three same-charge $W^\pm$'s and $\tilde{\chi_1}^\pm$'s decay leptonically and the other set decays hadronically, we have a same-sign trilepton signal. In order to demonstrate the branching fraction suppression of this SS3ℓ final state, let us consider a typical pMSSM spectrum with $M_{\tilde{t_1}} = 522$ GeV and $M_{\tilde{b_1}} = 482$ GeV. We keep the first two generation squark masses at ~ 5 TeV in order to separate out the third generation squark production, which is the only relevant process for the SS3ℓ channel. The gluino mass is $\sim$ 1050 GeV, while the chargino and neutralino masses are at 264 GeV and 120 GeV respectively. With these parameters the SS3ℓ cross-section after all the cuts turns out to be 2.72×10^{-2} fb at the 14 TeV LHC, which is evidently very small.

5.5. Same-sign four-lepton (SS4ℓ) signal

In all the cases discussed in Section 5.3, owing to the Majorana nature of the gluino, it is possible to produce two $\tilde{\chi_1}^\pm$'s of the same sign in an event. Thus, in addition to SS3ℓ, one can also have four leptons with identical charge, coming from these two $\tilde{\chi_1}^\pm$'s and two LSP's. Such an SS4ℓ signal has negligible backgrounds within the SM, particularly when strong isolation and lepton p_T cuts are used to suppress the rate of leptons coming from heavy flavour decays. Though a further branching fraction suppression will reduce this signal as compared to SS3ℓ, we note in Table 5.8 (in case 1 for illustration) that the event rates can still be quite sizeable at the LHC, during the 14 TeV run, within an integrated luminosity of 5 fb^{-1}.

5.6. SS3ℓ in the littlest Higgs model

As discussed in the introduction, we would like to point out that the SS3ℓ signal is also possible in other scenarios of new physics. An example is the Littlest Higgs model [9] with T-parity (LHT) violated via the Wess-Zumino-Witten anomaly term [10], which was discussed in detail in Chapter 2.3. In this case, the heavy photon (A_H) (which in most models is the lightest T-odd particle) may decay into a W^+W^- pair. Pair-produced heavy quarks (q_H) can thus lead to four W's, two of which can decay leptonically to give same sign lepton pairs. The

Case	$\sigma^1_{SS4\ell}$ (fb)	$\sigma^2_{SS4\ell}$ (fb)
1a(1)	15.74	4.52
1a(2)	33.23	9.97
1a(3)	4.75	2.70
1a(4)	3.31	1.49
1b(1)	24.70	15.11
1b(3)	2.77	2.08

Table 5.8.: SS4ℓ cross-sections after Cut-1 ($\sigma^1_{SS4\ell}$) and after Cut-2 ($\sigma^2_{SS4\ell}$) at $\sqrt{s} = 14$ TeV for cases as defined in Table 5.4. For SS4ℓ Cut-2 refers to demanding lepton $p_T > 20$ GeV for all the four leptons and a $\not{E}_T > 30$ GeV. The RPV coupling in all the above cases is $\lambda_{123} = 0.001$.

third additional lepton can easily come from the cascade via the decay of the heavy partner of the W boson (W_H). Thus we find that in the region of LHT parameter space where $M_{A_H} > 2M_W$ and $M_{q_H} > M_{W_H}$ one can have a SS3ℓ signal. This, in fact, is a large region in the two-dimensional (f, κ_q) parameter space determining the heavy quark and gauge boson masses in LHT. In addition, if the T-odd leptons (l_H) are lighter than W_H, the SS3ℓ rates will be further enhanced. This is achievable within this framework for appropriate values of κ_l. As an example, we have generated events for the parameter choices $f = 1150$ GeV, $\kappa_q = 0.5$ and $\kappa_l = 0.25$, which correspond to $M_{q_H} = 809$ GeV, $M_{A_H} = 174$ GeV, $M_{W_H} = 747$ GeV and $M_{l_H} = 407$ GeV (the subscript H denotes T-odd partners of SM particles), with CalcHEP 2.5 [11, 27] and interfaced them with PYTHIA. We obtain an SS3ℓ cross-section of 3.34 fb at $\sqrt{s} = 14$ TeV, after Cut-2 as defined before.

5.7. Observable patterns in L-violating LSP decays

We have now reasons to feel reasonably confident that substantial SS3ℓ (or SS4ℓ) rates are unlikely to be seen in R-parity conserving SUSY, and that R-parity (read lepton number) violation will be strongly suggested by them. More pointedly, L-violation by odd units and the existence of more than one Majorana fermions in the scenario work together towards the enhancement of such signals.

The total rate of SS3ℓ in a particular L-violating scenario depends not only on the L-violating coupling and the LSP involved, it is also dictated by SUSY production cross-section and other parameters determining the cascade decay patterns. We shall now show that *it is possible to extract the information on the different L-violating couplings, through which a Majorana neutralino LSP decays, once we make use of the SS3ℓ and SS4ℓ final states.*

With this in view, we construct certain variables which involve not only the SS3ℓ and SS4ℓ rates in a given scenario, but also on the total rates in the 3ℓ and 4ℓ channels. In a generic MSSM scenario with a particular L-violating coupling, it is possible to make definite predictions involving these variables based on simple probability arguments and neutralino branching fraction information in different combinations of charged lepton final states. We then verify these predictions using Monte Carlo simulations, where we also show the effect of selection and isolation cuts, as well as the effect of adding the SM backgrounds in the 3ℓ and 4ℓ channels. Although we have demonstrated the results using some mSUGRA benchmark points for simplicity, the conclusions are generic to phenomenological scenarios.

5.7.1. Neutralino LSP with λ-type couplings

A neutralino LSP in presence of λ_{ijk}-type couplings contributes to same-sign trileptons only if one of the indices in $\{ijk\}$ is 3. As λ_{ijk} is anti-symmetric in i and j, there are nine independent couplings of λ-type. Out of these nine couplings, seven have 3 as one index, and only two do not have the index 3 anywhere. Now consider the generic decay mode of the ${\tilde{\chi_1}}^0$ where ${\tilde{\chi_1}}^0 \to \tau^{\pm} l^{\mp} \nu \, (l = e, \mu)$. The produced $\tau^{\pm}$ will decay leptonically in $\sim 35\%$ of the time, and hadronically in rest of the cases. Now consider the ratio of the number of same-sign trilepton (SS3ℓ) events to the total number of trilepton events (which includes both same-sign

trileptons (SS3ℓ) and mixed-sign trileptons (MS3ℓ)). This ratio can be calculated independent of the other SUSY parameters as follows. In the above case, in a trilepton event, we know that at most one of the leptons is coming from the cascade as the pair of neutralinos produced at the end of the decay chains will always give rise to at least 2 leptons. As mentioned before, the produced $\tau^{\pm}$'s decay to a semi-leptonic final state in $\sim 35\%$ of the cases, and to hadronic final states in 65% cases. Therefore, as the two $\tilde{\chi_1}^0$ decays will produce two leptons when both the $\tau^{\pm}$'s decay hadronically, the fraction of cases a pair of $\tilde{\chi_1}^0$'s goes to 2 leptons and jets and neutrinos is $(0.65)^2 = 0.4225$. Similarly, a pair of neutralinos can go to 3 leptons in a fraction $(2 \times 0.65 \times 0.35) = 0.455$ of all cases (i.e., when one $\tau^{\pm}$ decays leptonically and the other one decays hadronically). In rest of the cases they decay to a four-lepton final state (when both the $\tau^{\pm}$'s decay leptonically) which we are not considering in this case. Thus out of all possible trilepton events, in $\simeq 42\%$ cases one lepton comes from the cascade and in $\sim 46\%$ cases no lepton comes from the cascade. We can summarise the situation in Table 5.9.

No. of leptons (Cascade)	No. of leptons (LSP Decay)	Fraction of cases	SS3ℓ Fraction	MS3ℓ Fraction
1	2	0.42	0.25	0.75
0	3	0.46	0	1

Table 5.9.: Fraction of trilepton events with different origins for the leptons, and the fractions of SS3ℓ and MS3ℓ events among them (see explanation in text).

In Table 5.9, the first two columns represent the number of leptons coming from the two different sources that we distinguish, namely, from the cascade and from the decay of the two $\tilde{\chi_1}^0$ LSP's. As explained above, there are only two such possibilities in a trilepton event. Those two possibilities are described in the two rows of the table. The third column describes the fraction of cases in which each of these possibilities occur. We have explained the numbers in this column above. Finally, the last two columns represent the fraction of SS3ℓ and MS3ℓ events in each of the possible ways of obtaining a trilepton event, as explained below.

From Table 5.9, we see that in the first case where two of the leptons come

from the LSP-pair decay, and one from the cascade, the probability of getting an l^+l^+ pair from the LSP's is 0.25, and same for obtaining an l^-l^- pair (this stems from the fact that the $\tilde{\chi_1}^0$ is Majorana). Now, in a trilepton event, let P_1 be the probability of the single lepton coming from the cascades being of positive charge, and P_2 for it to be of negative charge. Then, the probability of obtaining an SS3ℓ event is $0.25 \times P_1 + 0.25 \times P_2 = 0.25$ as $P_1 + P_2 = 1$. Therefore, the probability of obtaining an MS3ℓ event is $1 - 0.25 = 0.75$. In the second case, where all three of the leptons are coming from the LSP decay, all the trilepton events are of MS3ℓ-type. Note that, we are demanding only three leptons in the final state, therefore any event with additional leptons (four or more) are vetoed out. Let us now define the ratio

$$x = \frac{\sigma_{SS3\ell}}{\sigma_{SS3\ell} + \sigma_{MS3\ell}} \tag{5.4}$$

From Table 5.9, we see that we can easily calculate this ratio as follows

$$x = \frac{\sigma_{total} \times 0.42 \times 0.25}{\sigma_{total} \times [(0.42 \times 0.25) + (0.42 \times 0.75 + 0.46)]} \simeq 0.12, \tag{5.5}$$

where σ_{total} is the total SUSY production cross-section which cancels out among the numerator and the denominator. As we have explained above, the trilepton events are a fraction of all possible SUSY events and SS3ℓ and MS3ℓ events are subsets of all 3ℓ events. This value of the ratio $x \simeq 0.12$ is therefore a prediction stemming from the L-violating decay mode of the neutralino under study and also the Majorana character of the neutralino. Whatever be the values of the other SUSY parameters, as long as we have a $\tilde{\chi_1}^0$ LSP decaying via a λ_{123} type of coupling, this ratio is fixed. In particular, this ratio is independent of the probabilities of obtaining a charged lepton of either sign from the cascade. One should note, however, that if the L-violating couplings are so large as to compete with the gauge couplings for the decay of sparticles other than the LSP, this result can change. But, flavour physics and neutrino physics experiments suggest that these Yukawa couplings would take rather small values if SUSY models are to explain the above phenomena.

In realistic situations, where we have to consider the experimental triggers, detector efficiencies etc., the ratio x can fluctuate around the predicted value of ~ 0.12. Unfolding these effects in an event by event basis is not an easy exercise, and we abstain from trying to do so. In Table 5.10 we present the ratio x obtained

Point	$\sigma_{SS3\ell} + \sigma_{MS3\ell}$ (fb)	$\sigma_{SS3\ell}$ (fb)	x
1a(1)	928.32	75.11	0.08
1a(2)	1084.26	110.06	0.10
1a(3)	228.24	27.51	0.12
1a(4)	149.47	14.20	0.10

Table 5.10.: The 3ℓ (signal+SM background) and SS3ℓ (signal) cross-sections at 14 TeV LHC after the $m_{eff} > 250$ GeV cut and the ratio x calculated including the SM background contribution. The total SM background in the 3ℓ channel after the above cut is 10.12 fb. Note that the predicted value of x in this case is ~ 0.12, which shifts somewhat after including the effects of lepton isolation, detection efficiencies, other cuts and the SM backgrounds. The agreement with the predicted value is within 20% in most cases.

by Monte Carlo simulations with proper cuts in different benchmark points with widely varying SUSY parameters. We see that to within 20% one always gets a ratio as predicted, thereby validating the above analysis. Thus we find that this ratio of SS3ℓ to the total trilepton production cross-section gives us dynamic information about the underlying SUSY theory, in particular the L-violating coupling involved and the Majorana nature of the decaying LSP.

What happens if we change the L-violating coupling? Note that, in the presence of a generic λ_{ijk}-type coupling a $\tilde{\chi_1}^0$ decays to two charged leptons and a neutrino. Only if one of these leptons is a tau, which in turn can decay hadronically, one can obtain an SS3ℓ signal. Therefore, one of the indices in $\{ijk\}$ has to be 3. Moreover, we find the ratio $x \simeq 0.12$ only for the none-zero coupling λ_{123}. The reason for this is that if $i = 3$ or $j = 3$ (which are equivalent due to the antisymmetry of λ_{ijk} in the indices i, j), then the $\tilde{\chi_1}^0$ can also decay to a ν_τ instead of a $\tau^\pm$, thereby changing the ratio. For example, for the set of couplings $\{131, 132, 231, 232\}$ we find this ratio to be approximately $x \sim 0.14$, while for the

set $\{121, 122\}$, $x = 0$, since no SS3ℓ events are expected in these cases .

The above analysis thus shows that the dynamic information of a Majorana $\tilde{\chi_1}^0$ decaying via $L_iL_jE_k^c$-type couplings can be captured in a quantity easily measurable at the LHC experiments. Since the cross-sections in the 3ℓ and SS3ℓ channels are rather large (see Table 5.10) at the 14 TeV LHC, one can acquire a reasonably good statistics within $1 - 5\,\text{fb}^{-1}$ of integrated luminosity. Therefore, these cross-sections can be measured and the ratio x calculated fairly accurately in the early periods of the 14 TeV run.

5.7.2. Neutralino LSP with λ'-type couplings

The case for $\tilde{\chi_1}^0$ LSP with λ'-type couplings is somewhat more complicated than that for the λ-type couplings. No unique prediction (which is independent of the other SUSY parameters) can be made there about the ratio x. One can, however, construct a similar ratio with four-lepton events. Subsequently, we obtain a linear relation between these two ratios, which is then independent of the parameters determining the cascade decays.

In the presence of a λ'-type coupling, a $\tilde{\chi_1}^0$ decays either to two quarks and a neutrino, or to two quarks and a charged lepton. SS3ℓ signals can arise in the second case. But now we have more ways in which one can obtain trilepton events. Let us define the fraction of cases in which a $\tilde{\chi_1}^0$ decays via $\tilde{\chi_1}^0 \to l^{\pm}q\prime q$ to be α. Now let us note the various possible ways of obtaining trilepton events in Table 5.11. The structure and meaning of the different entries in this table are same as explained in detail for Table 5.9.

Since α denotes the probability that a $\tilde{\chi_1}^0$ will decay leptonically, the fraction of cases a pair of $\tilde{\chi_1}^0$'s give rise to two leptons is α^2. Similarly, when both the $\tilde{\chi_1}^0$'s decay to neutrinos and quarks, we do not obtain any leptons from LSP decays. This happens in $(1-\alpha)^2$ fraction of trilepton events. And, finally, in the remaining $2\alpha\,(1-\alpha)$ fraction of cases, we obtain one lepton from the decay of the two LSP's. In the first case, when all three of the leptons come from the cascade, we do not obtain any SS3ℓ event, making the MS3ℓ fraction unity. In order to understand the second case, note that in Table 5.11, when two leptons come from the cascade, we define P_3 to be the probability of them being oppositely charged ($l^{\pm}l^{\mp}$). Thus, $(1 - P_3)$ is the probability of them being of same charge ($l^{\pm}l^{\pm}$). In such a case, in a trilepton event, evidently the third lepton comes from LSP decay.

No. of leptons (Cascade)	No. of leptons (LSP Decay)	Fraction of cases	SS3ℓ Fraction	MS3ℓ Fraction
3	0	$(1-\alpha)^2$	0	1
2	1	$2\alpha\,(1-\alpha)$	$\frac{1-P_3}{2}$	$\frac{1+P_3}{2}$
1	2	α^2	0.25	0.75

Table 5.11.: Fraction of trilepton events with different origins for the leptons, and the fractions of SS3ℓ and MS3ℓ events among them (see explanation in text).

In half of such events the lepton coming from LSP decay will also have the same sign, thereby giving rise to an SS3ℓ event. Thus the probability of obtaining an SS3ℓ event is $\frac{1-P_3}{2}$. Consequently, the probability for obtaining a MS3ℓ event is $\left(1-\frac{1-P_3}{2}\right) = \frac{1+P_3}{2}$. In the third case, where two of the leptons come from LSP decay, because of the Majorana nature of the decaying $\tilde{\chi_1}^0$ LSP, we get the corresponding fractions in the same way as in the previous sub-section, where we considered $\tilde{\chi_1}^0$ decay via λ-type terms.

In this case, therefore, we find the following formula for the ratio x defined in eqn. 5.4.

$$x = \alpha - \frac{3}{4}\alpha^2 - P_3\left(\alpha - \alpha^2\right) \tag{5.6}$$

Now, the ratio α is very weakly dependent on the sparticle mass spectra, especially the difference between the up and down-type squark masses entering the off-shell propagators in the 3-body $\tilde{\chi_1}^0$ decays. In most scenarios this difference is rather small, especially for the first two families. On the whole, α is close to 0.5 in most cases.

As mentioned before, there is a residual dependence of x on P_3, thereby making this ratio vary as the other SUSY parameters vary (also the parton distribution functions affect P_3). In order to eliminate P_3 and obtain a prediction that follows just from the Majorana nature of the $\tilde{\chi_1}^0$ and the L-violating coupling involved, we introduce another ratio y defined as

$$y = \frac{\sigma_{SS4\ell}}{\sigma_{SS4\ell} + \sigma_{MS4\ell}} \tag{5.7}$$

where $\sigma_{SS4\ell}$ and $\sigma_{MS4\ell}$ are the same-sign four-lepton and mixed-sign four-lepton cross-sections respectively.

To calculate y, we make a table similar to the one made for calculating x.

No. of leptons (Cascade)	No. of leptons (LSP Decay)	Fraction of cases	SS4ℓ Fraction	MS4ℓ Fraction
4	0	$(1-\alpha)^2$	0	1
3	1	$2\alpha\,(1-\alpha)$	0	1
2	2	α^2	$\frac{1-P_3}{4}$	$\frac{3+P_3}{4}$

Table 5.12.: Fraction of four-lepton events with different origins for the leptons, and the fractions of SS4ℓ and MS4ℓ events among them (see explanation in text).

Since, the fraction of cases for the different possibilities are only dependent on the number of leptons coming from LSP decays, the entries in the third column of Table 5.12 can be understood in the same way as in the trilepton case, which we explained before while discussing Table 5.11. In the first two cases, where four and three leptons come from the cascade respectively, the MS4ℓ fraction is 1, since we cannot get more than two same-sign leptons from the cascade. In the third case, we define P_3 as before. Since $(1 - P_3)$ is the probability to have a same-sign lepton pair from the cascade, in order to obtain a same-sign four lepton event, we need the other two leptons coming from LSP decay to be of the same-sign as that of the cascade leptons. Now, since the ${\tilde{\chi_1}}^0$ is a Majorana particle, when it decays leptonically, the probability to obtain a same charge lepton as in the cascade is $1/2$, and similarly for the second ${\tilde{\chi_1}}^0$, thus giving us a probability of $\frac{1-P_3}{4}$ to obtain an SS4ℓ event. The rest of the events are of MS4ℓ variety, which come with a fraction of $\left(1 - \frac{1-P_3}{4}\right) = \frac{3+P_3}{4}$. This completes the explanation of Table 5.12.

From Table 5.12 and eqn. 5.7 we find that

$$y = \frac{\alpha^2}{4} - \frac{\alpha^2 P_3}{4}. \tag{5.8}$$

The total SUSY production cross-section σ_{total} cancels out in the ratio as in the case for x. Combining these two equations for x and y, we can eliminate P_3 to obtain the following equation relating x and y:

$$x = \frac{\alpha^2}{4} + 4y\left(\frac{1}{\alpha} - 1\right) \tag{5.9}$$

This equation is therefore a prediction based just on the Majorana nature of the decaying $\tilde{\chi_1}^0$ LSP and the presence of λ'-type couplings. In order to verify the above claim and also to see the deviations due to lepton selection and isolation effects we note the values of x and y obtained in different benchmark points and compare them with the above prediction taking $\alpha \sim 0.5$ and present the results in Table 5.13.

Point	y^S_{MC}	x^S_{MC}	$x^S_{eqn.}$	y^{S+B}_{MC}	x^{S+B}_{MC}	$x^{S+B}_{eqn.}$
2(1)	0.024	0.147	0.159	0.018	0.111	0.135
2(2)	0.023	0.154	0.155	0.020	0.126	0.143
2(3)	0.027	0.144	0.171	0.021	0.102	0.147
2(4)	0.044	0.175	0.239	0.025	0.094	0.163

Table 5.13.: The ratios x and y after the $m_{eff} > 250$ GeV cut, before and after adding the SM background cross-sections. Here, y^S_{MC} and x^S_{MC} refer to the ratios x and y calculated only with the signal whereas y^{S+B}_{MC} and x^{S+B}_{MC} denote the ratios calculated adding up both the signal and the background cross-sections in the appropriate channels. $x^S_{eqn.}$ and $x^{S+B}_{eqn.}$ denote the values of x calculated using eqn. 5.9 taking $\alpha = 0.5$, with y^S_{MC} and y^{S+B}_{MC} as the respective inputs.

The entries of Table 5.13 have been explained in the caption of the table. The ratios x and y have been evaluated from cross-sections calculated for the 14 TeV LHC. As the total 3ℓ and 4ℓ cross-sections in the case of a $\tilde{\chi_1}^0$ LSP with λ'-type coupling are comparable to the SM backgrounds, the ratios x and y change after

adding the backgrounds. In order to show that we present the ratios both before and after adding the SM background cross-sections. In order to validate the prediction derived in eqn. 5.9, we take the Monte Carlo prediction for y as an input, and then calculate the value of x from eqn. 5.9, and denote it by $x_{eqn.}$. This $x_{eqn.}$ is then compared with x_{MC}, the value obtained from Monte Carlo. The rather excellent agreement between the entries in the third and fourth columns in Table 5.13 demonstrates the viability of our claim in eqn. 5.9. As noted before, here we have used the approximate value of 0.5 for α. We then again repeat the same calculation after adding the SM backgrounds in the 3ℓ and 4ℓ channels. Since the backgrounds are comparable to the signal in this case, the ratios change somewhat after the background addition, and the agreement between the prediction of eqn. 5.9 and the MC is not as good as with only the signal, which is expected. Also note that, in the benchmark points $2(2)$ and $2(4)$ we have the $\tilde{\chi_1}^{\pm}$ lighter than the $\tilde{e_L}$. This reduces the $\tilde{\chi_1}^{\pm}$ branching fraction to leptons, thereby leading to a reduction of trilepton and four-lepton events of same-sign and mixed-sign varieties. The lower branching fraction is compensated by the much larger total SUSY production cross-section in point $2(2)$. Point $2(4)$ thus suffers from lower number of multi-lepton events, and the accurate evaluation of the ratios x and y here would require much larger statistics. Also if SS3ℓ signals are indeed seen in the mass range of, say point $2(4)$, then the further reduction of backgrounds may be a pressing need in order to extract dynamics out of this signal.

5.7.3. Neutralino LSP with bi-linear couplings

In the presence of bi-linear L-violating couplings, the decay branching fractions of $\tilde{\chi_1}^0$ in different channels are dependent on various other soft SUSY-breaking parameters, too. Thus it is not possible to predict a specific equation which will be valid generically for all possible choices of the relevant parameters. Instead, we focus in a region where the $\tilde{\chi_1}^0$ decays either in the $W^{\pm}\mu^{\mp}/\tau^{\mp}$ or in the $Z\nu$ channel. This is largely the case when the slepton/sneutrino states have not-too-large mixing with the Higgs states [20]. In this case, we find an equation relating the x and y-variables which is very similar to the equation of straight line found for the case of $\tilde{\chi_1}^0$ LSP with λ'-type couplings (with a different slope for the straight line!). Since the detailed evaluation of the relevant branching fractions in different combinations of charged-lepton final states is straightforward but cumbersome, we just note down the final results in the following tables.

No. of leptons (Cascade)	No. of leptons (LSP Decay)	Fraction of cases	SS3ℓ Fraction	MS3ℓ Fraction
3	0	0.146	0	1
2	1	0.366	$\frac{1-P_3}{2}$	$\frac{1+P_3}{2}$
1	2	0.335	0.17	0.83
0	3	0.134	0	1

Table 5.14.: Fraction of trilepton events with different origins for the leptons, and the fractions of SS3ℓ and MS3ℓ events among them, in the case of a $\tilde{\chi_1}^0$ LSP with bi-linear L-violating couplings (see explanation in text).

No. of leptons (Cascade)	No. of leptons (LSP Decay)	Fraction of cases	SS4ℓ Fraction	MS4ℓ Fraction
4	0	0.146	0	1
3	1	0.366	0	1
2	2	0.335	$0.17 - 0.17P_3$	$0.83 + 0.17P_3$
1	3	0.134	0	1
0	4	0.020	0	1

Table 5.15.: Fraction of four-lepton events with different origins for the leptons, and the fractions of SS4ℓ and MS4ℓ events among them, in the case of a $\tilde{\chi_1}^0$ LSP with bi-linear L-violating couplings (see explanation in text).

From Table 5.14 we find that

$$x = 0.24 - 0.19P_3 \tag{5.10}$$

and similarly, from Table 5.15 we find an expression for y

$$y = 0.06(1 - P_3) \tag{5.11}$$

We can eliminate P_3 from equations 5.10 and 5.11, to obtain an equation of straight line relating x and y

$$x = 3.529y + 0.063 \tag{5.12}$$

As mentioned before, this equation is very similar to the equation obtained for the case of $\tilde{\chi_1}^0$ LSP with λ'-type couplings. The slope in the $x - y$ plane, however, is slightly different in this case.

Point	y^S_{MC}	x^S_{MC}	$x^S_{eqn.}$	y^{S+B}_{MC}	x^{S+B}_{MC}	$x^{S+B}_{eqn.}$
3(1)	0.012	0.096	0.107	0.012	0.088	0.105
3(2)	0.016	0.087	0.112	0.015	0.075	0.115

Table 5.16.: Same as in Table 5.13, for the case of bi-linear L-violation.

In Table 5.16, which is similar to Table 5.13, we present a comparison of the MC calculation and the prediction from eqn. 5.12 for x, with y calculated from MC as input. We find that the predictions agree with the MC calculations to within $\sim$ 20% or better. As for the λ' case, the prediction and MC calculations deviate a little bit more after adding the SM backgrounds, since the total signal cross-sections in the 3ℓ and 4ℓ channels are comparable to the backgrounds. Also, in this case as the total rates for multi-lepton events are rather small for the chosen benchmark points (with the squark and gluino masses $\sim$ 1 TeV), we need a much larger statistics in order to calculate the ratios accurately.

5.8. Summary and conclusion

In this chapter, we have described a detailed study of SS3ℓ and SS4ℓ signals in the context of the LHC, to arrive at a number of important conclusions. First, such signals are enhanced, to such a degree as to be appreciable even during the 7 TeV run (and also the 14 TeV run with low integrated luminosity), if there is (a) L-violation by odd units, and (b) the presence of self-conjugate fields. The

outstanding theoretical scenario meeting the above requirements is SUSY with R-parity violated via lepton number. Therefore, we strongly advocate the investigation of such signals, especially as they are complementary to signals with large missing E_T.

We have not only presented results for the mSUGRA scenario, but have gone beyond it and focused on different regions of the parameter space of a general SUSY model. It has been shown that sizeable SS3ℓ rates are expected over various regions of interest in the parameter space, so much so that upto a TeV in the scale of strongly interacting superparticle masses can be explored at the 7 TeV run itself. This in itself is quite remarkable for signals with such high multiplicity of leptons, and can be attributed to almost non-existent SM backgrounds. It is further shown that event rates of comparable magnitude are almost impossible to achieve in an L-conserving SUSY scenario of a general kind. This, we argue, further strengthens the motivation of studying same-sign multileptons.

The other really useful feature of SS3ℓ and SS4ℓ signals that we have emphasized is that they enable us to extract information on the dynamics of R-parity violation, namely, whether lepton number is violated through the λ, λ' or the bilinear terms. Using SS3ℓ and SS4ℓ event rates in conjunction with their mixed-sign counterparts, one is able to define certain ratios and their relationships which are typical of the type of R-parity violating terms, taken one at a time. More importantly, these ratios and their relations are largely independent of the SUSY spectrum and the nature of cascades, and depend centrally on the Majorana character of neutralinos, making our conclusions extremely general. We perform detailed simulation for a number of benchmark points to substantiate this claim. The simulations include the effects of experimental cuts as well the SM backgrounds for mixed-sign trileptons and four leptons.

Thus the overwhelming recommendation, coming out from the results presented in this chapter, is for a careful analysis of SS3ℓ and SS4ℓ signals at the LHC. Such analysis should be concurrent with the search for events with large missing energy, because of its complementary nature. This chapter, in conjunction with Chapter-4, completes our studies on identifying various low missing-energy scenarios at the LHC with the help of distinctive signals. We should mention that these signals are not only useful for the purpose of discovery, but can also be further utilized for distinguishing between various new physics possibilities giving rise to similar signatures at the LHC. Same-sign trileptons in particular can make

several cases of L-violating SUSY stand out compared to other models predicting low missing-energy. In addition, since the possibility of obtaining observable rates of SS3ℓ in R-parity conserving SUSY is very small, this can be considered as a "smoking gun" channel for L-violating SUSY in the context of supersymmetric models. We take up the problem of model discrimination in further detail in Chapter 6.

Bibliography

[1] V. D. Barger, W. Y. Keung and R. J. N. Phillips, Phys. Rev. Lett. **55**, 166 (1985); R. M. Barnett, J. F. Gunion and H. E. Haber, Phys. Lett. B **315**, 349 (1993); H. Baer, X. Tata and J. Woodside, Phys. Rev. D **41**, 906 (1990).

[2] W. -Y. Keung, G. Senjanovic, Phys. Rev. Lett. **50**, 1427 (1983).

[3] V. D. Barger and R. J. N. Phillips, Phys. Rev. D **30**, 1890 (1984).

[4] For ways of reducing backgrounds to SS3ℓ from mis-measurements and fakes, see, V. E. Ozcan *et al.*, J. Phys. G **36**, 095002 (2009).

[5] B. Mukhopadhyaya, S. Mukhopadhyay, Phys. Rev. **D82**, 031501 (2010).

[6] S. Mukhopadhyay and B. Mukhopadhyaya, Phys. Rev. D **84**, 095001 (2011).

[7] For a review see, for example, R. Barbier *et al.*, Phys. Rept. **420**, 1 (2005).

[8] K. Desch, S. Fleischmann, P. Wienemann, H. K. Dreiner, S. Grab, Phys. Rev. **D83**, 015013 (2011); B. Bhattacherjee, G. Bhattacharyya and S. Raychaudhuri, Phys. Rev. D **84**, 075006 (2011); P. Fileviez Perez, S. Spinner and M. K. Trenkel, Phys. Rev. D **84**, 095028 (2011); C. Grojean and R. S. Gupta, arXiv:1110.5317 [hep-ph].

[9] N. Arkani-Hamed *et al.*, JHEP **0207**, 034 (2002); H. C. Cheng and I. Low, JHEP **0408**, 061 (2004); J. Hubisz and P. Meade, Phys. Rev. D **71**, 035016 (2005).

[10] C. T. Hill and R. J. Hill, Phys. Rev. D **75**, 115009 (2007); Phys. Rev. D **76**, 115014 (2007).

[11] V. Barger, *et al.*, Phys. Lett. B **655**, 228 (2007); A. Freitas *et al.*, JHEP **0809**, 013 (2008); S. Mukhopadhyay *et al.*, JHEP **1005**, 001 (2010).

[12] I. Picek, B. Radovcic, Phys. Lett. **B687**, 338-341 (2010); K. Kumericki, I. Picek, B. Radovcic, arXiv:1106.1069 [hep-ph].

[13] Z. Sullivan and E. L. Berger, Phys. Rev. D **78**, 034030 (2008).

[14] M. L. Mangano *et al.*, JHEP **0307**, 001 (2003).

[15] T. Sjöstrand *et al.*, JHEP **0605**, 026 (2006).

[16] J. Pumplin *et al.*, JHEP **0207**, 012 (2002); M. R. Whalley *et al.*, arXiv:hep-ph/0508110.

[17] G. Aad *et al.* [The ATLAS Collaboration], arXiv:0901.0512 [hep-ex]; G. L. Bayatian *et al.* [CMS Collaboration], J. Phys. G **34**, 995 (2007).

[18] J. Alwall, M. Herquet, F. Maltoni, O. Mattelaer and T. Stelzer, JHEP **1106**, 128 (2011)

[19] M. Cacciari *et al.*, JHEP **0809**, 127 (2008).

[20] S. Roy and B. Mukhopadhyaya, Phys. Rev. D **55**, 7020 (1997); B. Mukhopadhyaya *et al.*, Phys. Lett. B **443**, 191 (1998); M. Hirsch *et al.*, Phys. Rev. D **62**, 113008 (2000).

[21] A. Datta, B. Mukhopadhyaya and S. Roy, Phys. Rev. D **61**, 055006 (2000).

[22] B. C. Allanach *et al.*, Phys. Rev. D **75**, 035002 (2007).

[23] A. Djouadi *et al.*, Comput. Phys. Commun. **176**, 426 (2007).

[24] M. Muhlleitner *et al.*, Comput. Phys. Commun. **168**, 46 (2005).

[25] A. Djouadi, M. M. Muhlleitner and M. Spira, Acta Phys. Polon. B **38**, 635 (2007).

[26] S. Mukhopadhyay and B. Mukhopadhyaya, in preparation.

[27] A. Pukhov, arXiv:hep-ph/0412191.

Part III.

Low Missing Energy New Physics: Discrimination at the LHC

Chapter 6.

Discriminating low missing-energy look-alikes at the LHC

6.1. Introduction

After devoting the previous two chapters to finding out specific signals which can be used to discover certain new physics scenarios, and to devising ways of reducing the corresponding standard model backgrounds, we now turn our attention to the problem of discriminating among these new physics scenarios which can fake each other by giving rise to similar signals at the LHC. As we have seen in Chapter-2, many of the proposed scenarios of new physics systematically predict a host of new particles occurring in correspondence with those present in the SM. In addition, the need to accommodate an invisible, weakly interacting particle qualifying as a dark matter candidate often invites the imposition of a Z_2 symmetry on the theory, which renders the lightest of the new particles stable. This leads to the prediction of large missing transverse energy (MET) at the LHC, due to the cascades of new particles ending up in the massive stable particle that eludes the detectors. Such MET (together with energetic jets, leptons etc.) goes a long way

in making such new physics signals conspicuous. Even then, however, one has to worry about distinguishing among different theoretical scenarios, once some excess over SM backgrounds is noticed. Thus one has the task of using the LHC data to differentiate among models like supersymmetry (SUSY), universal extra dimensions (UED) and littlest Higgs with T-parity (LHT), all of which are relevant at the TeV scale. With the SM particles supplemented with new, more massive ones having the same gauge quantum numbers (with only spins differing in the case of SUSY) in all cases, their signals are largely similar. The consequent problem of finding out the model behind a given set of signatures is often dubbed as the LHC inverse problem. The name was coined when it was shown first in the context of SUSY [1] that different choices of parameters within SUSY lead to quantitatively similar LHC signals. The efforts towards distinction were subsequently extended to the aforementioned different scenarios with large missing energy signature at the LHC [2–4].

Though the scenarios predicting MET signals are attractive from the viewpoint of explaining the dark matter content of the universe, and they also satisfy the electroweak precision constraints while keeping the new particle spectrum 'natural', the discrete symmetry ensuring the stability of the weakly interacting massive particles is almost always introduced in an *ad hoc* manner. For example, it is well-known that the superpotential of the minimal SUSY standard model (MSSM) can include terms which violate the conventionally imposed R-parity, defined as $R = (-1)^{(3B+L+2S)}$. If SUSY exists, the violation of R-parity cannot therefore be ruled out. Similarly, boundary terms in UED can violate the Kaluza-Klein parity usually held sacrosanct, and T-parity in LHT can be broken by the so-called Wess-Zumino-Witten anomaly term. While one is denied the simplest way of having a dark matter candidate when the Z_2 symmetry is broken, these are perfectly viable scenarios phenomenologically, perhaps with some alternative dark matter candidate(s). In SUSY, for example, the axino or the gravitino can serve this purpose even if R-parity is broken. And, most importantly, the different scenarios with broken Z_2 are as amenable to confusion as their Z_2-preserving counterparts, as far as signals at the LHC are concerned. The mostly sought-after final states (such as jets + dileptons) are expected from all of these scenarios, various kinematical features are of similar appearance, and in none of the cases does one have the MET tag for ready recognition, in clear contrast to scenarios with unbroken Z_2.

Side by side with the problem of large missing energy look-alike models, the disentanglement of 'low missing energy look-alikes' is thus an equally challenging issue, on which not much work has been done yet. Some criteria for distinction among this class of look-alikes are developed in this chapter [5]. Specifically, we consider four possible scenarios of new physics with low missing energy signature:

1. Supersymmetry with R-parity violation (SUSY-RPV)
2. Minimal universal extra dimensions (mUED) with KK-parity conserved (UED-KKC)
3. Minimal universal extra dimensions with KK-parity violated (UED-KKV)
4. Littlest Higgs model with T-parity violated by the Wess-Zumino-Witten anomaly term (LHT-TPV).

It should be noted that UED-KKC is also included in this study. This is because, as will be seen in the following sections, the peculiar features of the mUED spectrum (namely, a large degree of degeneracy) often leads to the lightest stable particle carrying very low transverse momentum. In addition, one often also has nearly back-to-back emission of the invisible particle pair. Consequently, the MET spectrum is rather soft over a large region of the parameter space, and the signals can be of similar nature as those of Z_2-violating scenarios. Hence we would like to emphasize that mUED with KK-parity conserved is a scenario which can be easily distinguished by its much softer MET spectrum from other models predicting a massive stable particle (like SUSY with R-parity), but might actually be confused with the other Z_2-violating scenarios.

We have repeatedly seen in the previous chapters that signals containing leptons have relatively less SM backgrounds compared to events with fully hadronic final states. We therefore focus on possible leptonic channels in the various models under consideration. One has to note, however, that it is difficult to devise model-independent cuts such that the SM backgrounds are reduced while keeping a significant fraction of the signal events intact for all the models. For example, strong cuts on the transverse momenta of the leptons cannot be applied in case of mUED as the leptons there are very soft in general, owing to the almost degenerate spectrum of the Kaluza-Klein excitations. This makes it difficult to reduce the SM backgrounds in the single lepton and opposite-sign dilepton channels (which have rather large irreducible backgrounds from $W+$ jets and

$t\bar{t}+$ jets respectively). Although same-sign dilepton and trilepton channels have relatively lower rates within the SM, they are not very suitable for the purpose of distinguishing between the above models. The main reason for this is that many otherwise conspicuous invariant mass peaks cannot be reconstructed in these channels. These invariant mass peaks, however, are very helpful in classifying the models. In addition, since one is now looking at situations where the new physics signals are *not* accompanied by large MET, rising above the SM backgrounds is a relatively harder task which is accomplished better with a larger multiplicity of leptons. Keeping this in mind, here we have tried to develop a procedure of model discrimination, depending on four-and higher-lepton signals as far as possible.

The four-lepton channel is viable in all the four models mentioned above, and such events can be used to extract out several qualitative differences among the models, including the presence or absence of mass peaks. Therefore, our study largely focuses on the four-lepton channel. Furthermore, since most cascades start with the production of strongly interacting heavier particles in these new theories, as we have seen in Chapter-2, generically we can obtain at least two hadronic jets in the signal. Apart from the four-lepton channel, we also use the presence (or absence) of signals with even higher lepton multiplicity as a discriminating feature. It is of course true that these methods of discrimination can often be applied only after sufficient luminosity has been accumulated. In this sense, our study differs from that of [2], where the inverse problem was considered not only for models with a very large MET signal, but also at a modest luminosity of $200\,\mathrm{pb}^{-1}$ only.

This chapter is organized as follows. The choice of relevant parameters in the various models considered (the main features of these models have been discussed in Chapter-2) and our general strategy and methods adopted in event generation at the LHC are summarised in section 6.2. We use this strategy to show some predictions in section 6.3 to convince the reader that the different scenarios indeed fake each other considerably at the LHC. Section 6.4 is devoted to a detailed study of kinematics of four-lepton final states, whereby a significant set of distinction criteria are established. In section 6.5, we discuss the usefulness of the channel with five or more leptons. Some scenarios over and above those covered here in details are qualitatively commented upon in section 6.6. We summarise and conclude in section 6.7.

6.2. Multilepton final states: signal and background processes

6.2.1. Event generation and event selection criteria

Before we establish that the models mentioned in the introduction (and described in Chapter-2) all qualify as look-alikes with low MET, and suggest strategies for their discrimination through multilepton channels, we need to standardise our computation of event rates in these channels. With this in view, we outline here the methodology adopted in our simulation, and the cuts imposed for reducing the SM backgrounds. The predicted rates of events for some benchmark points, after the cuts are employed, are presented at the end of this section.

As the production cross-section for strongly interacting particles is high at the LHC, we start with the production of these heavier 'partners' (having different spins for SUSY-RPV, and same spins in the remaining cases) of quarks and gluons at the initial parton level $2 \to 2$ scattering. Though in principle there are contributions to the multilepton final states from electroweak processes as well, they are subleading, and are left out in our estimate. In this sense, our estimates of the total cross-sections in various channels, are in fact lower bounds. Also, the observations made by us subsequently on final state kinematics are unaltered upon the inclusion of these subleading effects.

For our simulation of signal processes, in case of SUSY-RPV, we have used PYTHIA 6.421 [6] for simulating both the production of strongly interacting particles and their subsequent decays. Since the values of the L-violating couplings that we have taken are very small, they do not affect the renormalisation group running of mass parameters from high to low scale [7]. Therefore, The SUSY spectrum is generated with SuSpect 2.41 [8]. For UED, while the production is once again simulated with the help of PYTHIA, both KK-parity conserving and KK-parity violating decay branching fractions are calculated in CalcHEP 2.5 [9] using the model file written by [10] and then passed on to PYTHIA via the SUSY/BSM Les Houches Accord (SLHA) (v1.13) [11]. For UED-KKV, we have implemented the relevant KK-parity violating decay modes in CalcHEP. Finally, for LHT with T-violation the initial parton level hard-scattering matrix elements were calculated and the events generated with the help of CalcHEP. These events, along with the relevant masses, quantum numbers and decay branching fractions were

passed on PYTHIA with the help of the SLHA interface for their subsequent analysis. In all cases, showering, hadronization, initial and final state radiations from QED and QCD and multiple interactions are fully included while using PYTHIA.

To simulate the dominant SM backgrounds, events for the processes ZZ and $t\bar{t}$ were generated with PYTHIA. Backgrounds from $t\bar{t}Z$ have been simulated with the generator ALPGEN [12], and the unweighted event samples have been passed onto PYTHIA for the subsequent analysis.

We have used the leading order CTEQ6L1 [13] parton distribution functions. Specifically, for PYTHIA, the Les Houches Accord Parton Density Function (LHAPDF) [14] interface has been used. The QCD factorization and renormalization scales are in general kept fixed at the sum of masses of the particles which are produced in the initial parton level hard scattering process. If we decrease the QCD scales by a factor of two, the cross-section can increase by about 30%.

While the signal primarily used in our analysis is $4l + nj + \not{E}_T$ ($n \geq 2$), we have also considered events with five or more number of leptons in section 6.5. No restriction was made initially on the signs and flavours of the leptons. As we shall see subsequently, the 'total charge of leptons' can be used as a useful discriminator at a later stage of the analysis.

The different ways in which multilepton signals can arise in the various models under consideration have been described in Chapter-2. The principal backgrounds to the $4l + nj + \not{E}_T$ channel ($n \geq 2$) are ZZ/γ^*, $t\bar{t}$ and $t\bar{t}Z/\gamma^*$. Although in case of ZZ (where the two associated jets can come from ISR and FSR), there is no real source of MET if we demand a $4l$ signal (i.e., both the Z's have to decay leptonically), jet energy mismeasurement can give rise to some amount of fake MET.

The following basic selection cuts were applied for both the signal and the background [15, 16]:

Lepton selection:

- $p_T > 10$ GeV and $|\eta_\ell| < 2.5$, where p_T is the transverse momentum and η_ℓ is the pseudorapidity of the lepton (electron or muon).
- **Lepton-lepton separation:** $\Delta R_{\ell\ell} \geq 0.2$, where $\Delta R = \sqrt{(\Delta\eta)^2 + (\Delta\phi)^2}$ is the separation in the pseudorapidity–azimuthal angle plane.
- **Lepton-jet separation:** $\Delta R_{\ell j} \geq 0.4$ for all jets with $E_T > 20$ GeV.
- The total energy deposit from all *hadronic activity* within a cone of $\Delta R \leq 0.2$

around the lepton axis should be ≤ 10 GeV.

Jet selection:

- Jets are formed with the help of PYCELL, the inbuilt cluster routine in PYTHIA. The minimum E_T of a jet is taken to be 20 GeV, and we also require $|\eta_j| < 2.5$.

We have approximated the detector resolution effects by smearing the energies (transverse momenta) with Gaussian functions [15,16], as discussed in Chapter 3.3.

Note that, in addition to the basic cuts discussed above and the further cuts on the lepton p_T's described in the next sub-section, we also have used a cut on the invariant mass of the opposite sign (OS) lepton pairs formed out of the four-leptons. We have demanded that $M_{l^+l^-} > 10$ GeV for all the OS lepton pairs. This cut helps us in reducing backgrounds coming from γ^* produced in association with a Z-boson or top quark pairs. *We shall collectively refer to the basic isolation cuts and this cut on dilepton invariant masses as* **Cut-1**.

6.2.2. Numerical results for four-lepton events

Two benchmark points have been chosen for each of the look-alike models and it is seen that the four and higher lepton signals can rise well above SM backgrounds, thus forming the basis of further kinematic analyses. In order to show that our analysis is independent of the mass-scale of new physics involved, we have chosen two benchmark points with different mass spectra. Also, we should emphasize here that in the subsequent analysis we shall be using kinematic features of the final states predicted by the different models which are largely independent of the choice of parameters. This is precisely why we take two different benchmark points and demonstrate that the essential qualitative distinctions between the models do not change as we go from one point to another. *Thus our conclusions reflect distinction among the various low-MET models as a whole, and do not pertain to specific benchmark points.* The relevant parameters of these models and their values at the benchmark points are described below. For details about the models, we refer the reader to Chapter-2.

For SUSY-RPV, we have worked in the minimal supergravity (mSUGRA) framework. This is done just with an economy of free parameters in view, and it does not affect our general conclusions. In this framework, the MSSM mass spec-

trum at the weak scale is determined by five free parameters. Among them the universal scalar (m_0) and gaugino masses ($m_{1/2}$) and the universal soft-breaking trilinear scalar interaction (A_0) are specified as boundary conditions at a high scale (in this case the scale of gauge coupling unification), while the ratio of the vacuum expectation values of the two Higgs doublets (tanβ) and the sign of the Higgsino mass parameter (sgn(μ)) as defined in eqn. 2.2 are specified at the electroweak scale. In our analysis the electroweak scale has been fixed at $\sqrt{m_{\tilde{t}_1} m_{\tilde{t}_2}}$, where $\tilde{t}_1$ and $\tilde{t}_2$ are the two mass eigenstates of the top squarks respectively.

In case of the minimal universal extra dimension (mUED) model with conserved Kalutza-Klein (KK) parity (UED-KKC), the essential parameters determining the mass spectrum are the radius of compactification (R) and the ultra-violet cut-off scale of the theory (Λ). Although in mUED with KK-parity violated (UED-KKV) we have an additional parameter h, for small values of this parameter, R and Λ once again primarily determine the mass spectrum.

In the Littlest Higgs model with T-parity violation (LHT-TPV), the new T-odd quark and gauge boson masses are determined by two parameters: f and κ_q (see Chapter 2.3 for their precise definitions). Apart from that, an additional parameter κ_l appears in the T-odd lepton sector, which we have fixed to be equal to 1.0 throughout our study.

The choice of parameters for the different models are as follows:

1. **Point A:**
   - *SUSY-RPV*: $m_0 = 100$ GeV, $m_{1/2} = 250$ GeV, tan$\beta = 10$, $A_0 = -100$ and sgn(μ)> 0. The RPV coupling taken is $\lambda_{122} = 10^{-3}$. With these choices, we find the sparticle masses relevant to our study as (all in GeV) $m_{\tilde{g}} = 606$, $m_{\tilde{\chi_1}^0} = 97$, $m_{\tilde{\chi_1}^\pm} = 180$, $m_{\tilde{d}_L} = 568$, $m_{\tilde{t}} = 399$, $m_{\tilde{e_L}} = 202$, $m_{\tilde{\nu_{eL}}} = 186$.
   - *LHT-TPV*: $f = 1500$ GeV, $k_q = 0.285$. With these choices, we find the T-odd particle masses relevant to our study as (all in GeV) $u_H = 603$, $d_H = 605$, $A_H = 230$, $W_H = Z_H = 977$.
   - *UED-KKC*: $R^{-1} = 475$ GeV and $\Lambda = 20R^{-1}$. With these choices of UED-KKC parameters, the masses of relevant KK-particles are given by (all in GeV), $m_{g_1} = 609$, $m_{Q_1} = 568$, $m_{Z_1} = 509$, $m_{W_1} = 509$, $m_{l_1} = 489$ and $m_{\gamma_1} = 476$.

- *UED-KKV*: For UED-KKV, the values of R^{-1} and Λ are chosen to be same as in the case of UED-KKC. The value of the KK-parity violating parameter h is set to 0.001.

2. **Point B:**
   - *SUSY-RPV*: $m_0 = 100$ GeV, $m_{1/2} = 435$ GeV, $\tan\beta = 5$, $A_0 = 0$ and sgn(μ)> 0. The RPV coupling taken is $\lambda_{122} = 10^{-3}$. With these choices, we find the sparticle masses relevant to our study as (all in GeV) $m_{\tilde{g}} = 1009$, $m_{\tilde{\chi_1}^0} = 176$, $m_{\tilde{\chi_1}^\pm} = 331$, $m_{\tilde{d_L}} = 927$, $m_{\tilde{t}} = 695$, $m_{\tilde{e_L}} = 309$, $m_{\tilde{\nu_{eL}}} = 300$.
   - *LHT-TPV*: $f = 2375$ GeV, $k_q = 0.285$. With these choices, we find the T-odd particle masses relevant to our study as (all in GeV) $u_H = 956$, $d_H = 957$, $A_H = 368$, $W_H = Z_H = 1549$.
   - *UED-KKC*: $R^{-1} = 800$ GeV and $\Lambda = 20R^{-1}$. With these choices of UED-KKC parameters, the masses of relevant KK-particles are given by (all in GeV), $m_{g_1} = 1025$, $m_{Q_1} = 956$, $m_{Z_1} = 851$, $m_{W_1} = 851$, $m_{l_1} = 824$ and $m_{\gamma_1} = 800$.
   - *UED-KKV*: For UED-KKV, the values of R^{-1} and Λ are chosen to be same as in the case of UED-KKC. The value of the KK-parity violating parameter h is set to 0.001.

For LHT-TPV, UED-KKC and UED-KKV the Higgs mass has been fixed at 120 GeV. The top quark mass has been taken as 175 GeV in our study. In LHT-TPV, the value of κ_l has been kept fixed at 1. The choices of f and κ_q have been made in order to match the mass scale of the strongly interacting particles in LHT with those of the other models (these particles are predominantly produced in the initial hard scattering at the LHC). We should note here that this could have also been achieved with other different choices of these parameters, and we have remarked about their implication in section 6.4.2.

Table 6.1 shows the signal and SM background cross-sections for the $4l+ \geq 2j + \not{E}_T$ channel at LHC running with $\sqrt{s} = 14$ TeV after Cut-1 and additional cuts on lepton p_T's. The signal cross-sections are shown for the two above different choices of parameters in each model. On the whole, it is evident from the table that our event selection criteria assure us of enough background-free events in each case. The backgrounds look somewhat challenging for LHT-TPV for benchmark point B. However, one still can achieve a significance (defined as $S/\sqrt{B}$, S

and B being respectively the number of signal and background events) of 5σ with an integrated luminosity of 30 fb^{-1}. For point A, $5\,\text{fb}^{-1}$ is likely to be sufficient for raising the signal way above the backgrounds, and attempting discrimination among various theoretical scenarios via kinematical analysis.

We also show the sensitivity of the signals of the different scenarios to gradually tightened p_T cuts on the leptons. Clearly, the close degeneracy of the spectrum in UED-KKC makes the leptons softer. Thus the signal events fall with stronger cuts imposed on the relatively softer leptons. Although such cuts applied during the offline analysis can be useful in discriminating the UED-KKC scenario from the rest, one has to use this yardstick with caution. This is because the situation can change with different values of the UED parameters R^{-1} and Λ (as can be seen from point B). While they also change the KK excitation masses together with changing the mass-splitting, the estimate of masses from data for UED is not reliable, for reasons to be discussed in the next section. We therefore suggest some kinematical criteria that bypass this caveat.

6.3. On what ground are the models look-alikes?

In addition to the fact that all the suggested models have appreciable cross-section in the four lepton channel (and also in various other channels that we are not considering for model-discrimination for reasons described in the introduction), in order to ascertain that these models are indeed look-alikes, we first show that certain kinematic distributions, like MET or effective mass have very similar features in these scenarios of new physics. To begin with, we note that with similar masses of the strongly interacting new particles (squarks and gluinos for SUSY-RPV, q_1 and g_1 for the two variants of UED, and q_H for LHT-TPV), the MET distributions look similar.

The missing transverse energy in an event is given by

$$\not{E}_T = \sqrt{\left(\sum p_x\right)^2 + \left(\sum p_y\right)^2}. \tag{6.1}$$

Here the sum goes over all the isolated leptons, the jets, as well as the 'unclustered' energy deposits.

Point A				
p_T^l Cuts (GeV)	SUSY-RPV (fb)	LHT-TPV (fb)	UED-KKC (fb)	UED-KKV (fb)
(10,10,10,10)	9450.91	21.09	163.36	14008.93
(20,10,10,10)	9447.87	21.09	129.29	13990.97
(20,20,10,10)	**9354.09**	**20.96**	**75.13**	**13819.24**
(20,20,20,10)	8486.90	19.66	30.73	11781.96
(20,20,20,20)	5013.02	12.90	7.16	7697.5
Point B				
(10,10,10,10)	756.00	1.71	26.24	872.94
(20,10,10,10)	756.00	1.71	25.83	872.74
(20,20,10,10)	**755.22**	**1.71**	**22.81**	**868.90**
(20,20,20,10)	736.43	1.66	14.73	804.96
(20,20,20,20)	555.70	1.22	4.77	520.27
SM Backgrounds				
	ZZ/γ^*	$t\bar{t}$	$t\bar{t}Z/\gamma^*$	Total
(10,10,10,10)	2.18	0.51	0.87	3.56
(20,10,10,10)	2.18	0.51	0.87	3.56
(20,20,10,10)	**2.17**	**0.43**	**0.87**	**3.47**
(20,20,20,10)	2.06	0.17	0.79	3.02
(20,20,20,20)	1.42	0.09	0.55	2.06

Table 6.1.: Cut-flow table showing the change in $4l+ \geq 2j + \not{E}_T$ cross-section as we gradually increase the cuts on the lepton p_T. The p_T cuts shown within the brackets are ($p_T^{l_1}$, $p_T^{l_2}$, $p_T^{l_3}$, $p_T^{l_4}$) where l_1, l_2, l_3 and l_4 are the four leptons ordered according to their p_T's. The signal (point A and point B) and the SM background cross-sections quoted are for $\sqrt{s} = 14$ TeV. For all our subsequent analysis of four-lepton events, we have used the (20,20,10,10) cut. *We shall refer to this cut, applied in addition to Cut-1, as* **Cut-2**.

The MET distributions for the four scenarios under study are shown in Figure 6.1. The similarity of the MET distributions is obvious in all the four cases, including UED-KKC. For UED-KKC, as mentioned before, the reason behind this is the close degeneracy of the spectra. As a result, in this model the two γ_1's produced at the end of the cascades on the two sides have little transverse momentum, and quite often they are also back-to-back in the transverse plane. Consequently, the net MET is considerably reduced, in spite of the γ_1 being a massive particle. Thus UED-KKC is as much of a look-alike with SUSY-RPV and LHT-TPV as UED-KKV.

The confusion among the look-alikes from MET distributions is expected to be more for similar values of the masses of the strongly interacting new particles. Since the direct measurement of mass at LHC is not easy, a measured quantity that often bears the stamp of these masses is the so-called effective mass. It is defined as the scalar sum of the transverse momenta of the isolated leptons and jets and the missing transverse energy,

$$M_{eff} = \sum p_T^{jets} + \sum p_T^{leptons} + \not{E}_T, \tag{6.2}$$

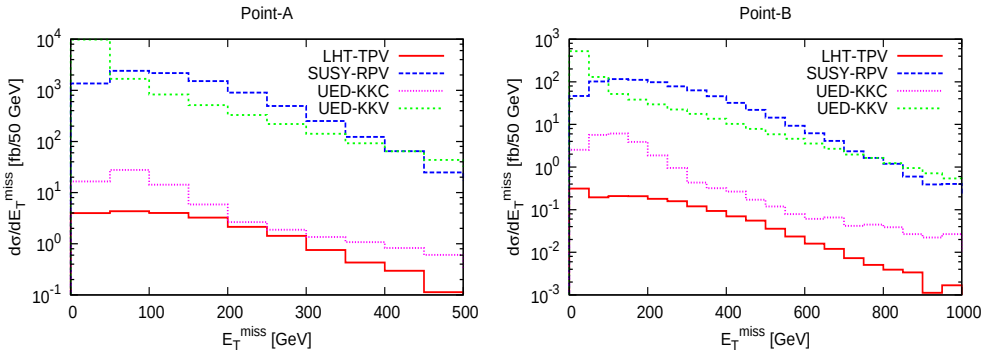

Figure 6.1.: Missing E_T distribution in various models for point A (left figure) and point B (right figure), at $\sqrt{s} = 14$ TeV after Cut-2.

Note that although usually M_{eff} carries the information about the mass scale of the particles produced in the initial parton level hard scattering, this is not true in all cases. Specifically, it is well-known that for a mass spectrum which is very closely spaced, M_{eff} largely underestimates the relevant mass-scale, the reason being very similar to that for the MET distribution being low in UED-KKC.

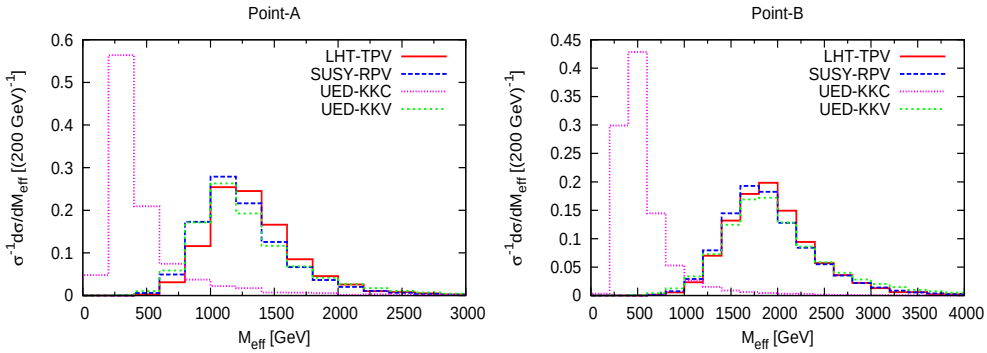

Figure 6.2.: Normalized effective mass distribution in various models for point A (left figure) and point B (right figure), at $\sqrt{s} = 14$ TeV after Cut-2.

If an excess is seen in the $4l + nj + \not{E}_T$ ($n \geq 2$) channel, fingers can be pointed at the several models mentioned before. Figure 6.1 is an example where the MET distributions show similar behaviour when the strongly interacting heavy particles in all of the four aforementioned models under consideration have similar masses. We thus conclude that all the four models clearly qualify as missing energy look-alikes. The minor differences that exist are difficult to use as discriminators, as these can be masked by features of the detector as well as systematic errors. In Figure 6.2, we also present the M_{eff} distributions for all these models, for the same 'mass scale' of $\sim$ 600 GeV (1000 GeV) for point A (point B). One finds that all the models except UED-KKC have a peak in the M_{eff} distribution at around twice the mass-scale (i.e., $\sim$ 1200 GeV for point A). For point A in UED-KKC, the distribution peaks at around 300 GeV. Similar features are also observed for point B.

This fact, if correlated with the total cross-section, can perhaps be used to single out the UED-KKC model from the remaining three. However, one can still vary the excited quark and gluon masses in UED-KKC to match both the MET distributions for other models with a 600 GeV mass-scale. In order for this to happen, however, R^{-1} has to be as large as about 3 TeV. This would not only lead to very low total cross-section but also imply a scenario that is ruled out due to overclosure of the universe through γ_1.

However, while similar MET distribution but much softer M_{eff} distribution can single out UED-KKC, similar distributions in both variables but very low

cross-sections can be noticed in special situations in the other models as well. For example, one can have RPV SUSY with both the λ-and λ'-type interactions, with the later being of larger value, thus suppressing the decay of the lightest neutralino into two leptons. In such a case, with $m_{\tilde{q}} \simeq m_{\tilde{g}} \simeq 600$ GeV, the MET as well as M_{eff}-distributions will be very similar as earlier, but the cross-section may be down by a large factor.

The above example shows that there is a pitfall in using total rate as a discriminant. Keeping this in view, we choose our benchmark points with similar masses for all the models but look for other kinematical features where the differences show up.

6.4. Analysis of $4l$ events

6.4.1. Four-lepton invariant mass distribution: two classes

In the table containing rates of four-lepton final states, we have allowed all the leptons to be of either charge. While we keep open the option of having all charge combinations, in this and the next two subsections we concentrate on those events where one has two positive and two negatively charged leptons. The issue of 'total charge of the set of leptons' and its usefulness in model discrimination is taken up section 6.4.4.

For the $4l + nj + \not{E}_T$ channel (with $n \geq 2$), the first distribution that we look into is that of the four-lepton invariant mass (M_{4l}). From Figure 6.3 we can see that, based on the M_{4l} distribution the models can be classified into two categories, 1) those with a peak in the M_{4l} distribution and 2) those without any such peak.

In SUSY-RPV, there is no single bosonic particle decaying, via cascade, to four leptons. Hence, no invariant mass peak is expected in this model and the M_{4l} distribution has a very broad shape, as we see in Figure 6.3. As discussed earlier, in the example taken, the four leptons here come from the RPV decays of the neutralino and the RPC decays of the chargino.

Similarly, in UED-KKC the four leptons come from the two cascade decay chains and not from a single particle. In this case, the decay of a Z_1 gives two leptons of opposite charge and same flavour in each chain. Note that the range in which M_{4l} takes values for UED-KKC is rather restricted, as can be seen in

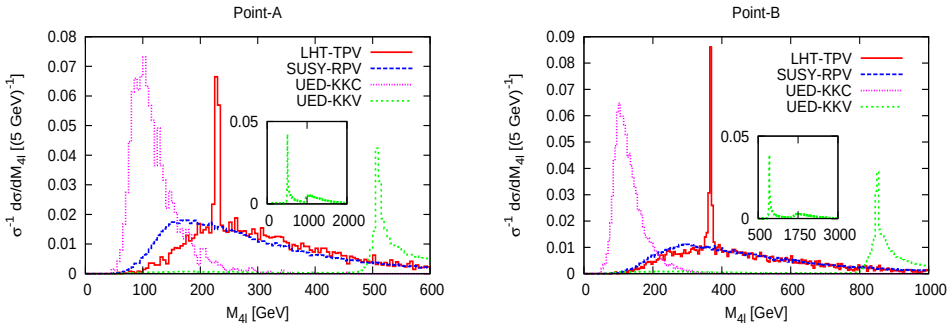

Figure 6.3.: Normalized invariant mass distribution of four leptons (M_{4l}) in the different models for point A (left figure) and point B (right figure), at $\sqrt{s} = 14$ TeV. The insets show the full range of M_{4l} for UED-KKV. The distributions have been plotted after Cut-2.

Figure 6.3. We can understand this in the following manner. Let us denote the four-momenta of the two leptons coming from one chain by p_1 and p_2, and those of the other two from the second chain by p_3 and p_4. Then, an approximate upper bound on M_{4l} can be obtained as follows:

$$\begin{aligned} M_{4l}^2 &= (p_1 + p_2 + p_3 + p_4)^2 \\ &= (p_1 + p_2)^2 + (p_3 + p_4)^2 + 2(p_1 + p_2).(p_3 + p_4) \end{aligned} \tag{6.3}$$

Now,

$$(p_1 + p_2)^2 \leq \frac{(M_{Z_1}^2 - M_{L_1}^2)(M_{L_1}^2 - M_{\gamma_1}^2)}{M_{L_1}^2} \tag{6.4}$$

A similar bound is also applicable to $(p_3 + p_4)^2$. Finally, we can approximate

$$2p_1.p_3 = 2(E_1E_3 - \vec{p_1}.\vec{p_3}) \simeq 2E_1E_3(1 - cos\theta_{13}) \leq 4E_1E_3 \tag{6.5}$$

Here θ_{13} is the angle between $\vec{p_1}$ and $\vec{p_3}$. Hence, we can finally approximate the upper bound on M_{4l} for UED-KKC as

$$M_{4l} \leq \sqrt{2\frac{(M_{Z_1}^2 - M_{L_1}^2)(M_{L_1}^2 - M_{\gamma_1}^2)}{M_{L_1}^2} + 4[E_1E_3 + E_1E_4 + E_2E_3 + E_2E_4]} \tag{6.6}$$

The first term within the square-root has the numerical value of about 2400 GeV^2 for point A in UED-KKC. Because of the unknown boost of the partonic centre of

mass frame, we cannot put any definite upper bound on the p_T's of Z_1 and L_1, and therefore the maximum possible values of the lepton energies E_i are also undetermined. Still, as very little energy is available at the rest frame of the decaying KK-excitations (once again because of low mass-splittings), E_i cannot be very large. This is the reason we expect M_{4l} for UED-KKC to take values in a somewhat restricted range.

For UED-KKV, we observe a very sharp peak in the M_{4l} distribution around $\sim$ 510 GeV (850 GeV) which is the mass of Z_1 for point A (point B). The four leptons in this case come from the cascade decay of a Z_1 to a lepton pair and a γ_1 followed by the KKV decay of the γ_1 to another pair of leptons. There is of course a long tail in the M_{4l} distribution here coming from the cases where all four of the leptons do not come from the decay of a single Z_1. For example, they can come from the leptonic decay of the two γ_1's via KK-parity violating interactions. We demonstrate this full range in the insets of Figure 6.3. It is, however, important to note that, in these cases, M_{4l} mostly exceeds M_{γ_1} when two of the leptons come from γ_1 decay and the two others come from the cascade. On the other hand, the invariant mass is greater than $2M_{\gamma_1}$ when the four leptons come from the decay of two γ_1's. This is why we observe an excess after around 1 TeV (1.6 TeV) for point A (point B) in the insets of Figure 6.3. As long as we have a γ_1 LKP with KK-parity violating interactions, this very clear peak, followed by a hump, observable in the M_{4l} distribution is a very important feature of UED-KKV.

Finally in LHT-TPV, we see in Figure 6.3 a very sharp peak superposed in a broad overall distribution. The reason for this is that in the example taken, most of the four-lepton events are due to the decay of an A_H to W^+W^- followed by the leptonic decays of the W's. These events will not give rise to any invariant mass peak. But, there is a fraction of events where one A_H decays to a ZZ pair which then in turn can decay to four-leptons. This will give rise to a peak in M_{4l} as we see in Figure 6.3. Note that, the branching fraction of an A_H of mass 230 GeV to a pair of Z-bosons is around 22% while it is 77% to a pair of W's. Over and above that, the branching fraction of $W^\pm$ to charged leptons is greater than that of Z. This accounts for the spread of events away from the peak, as seen in Figure 6.3. One may also note that, in general, fewer 4-lepton events are expected in this model from leptonic cascades of the Z_H. This is because, for our choice of parameters, Z_H has the largest branching ratio in the hA_H channel.

Based on the above considerations, LHT-TPV and UED-KKV fall into category-

1 while SUSY-RPV and UED-KKC belong to category-2. Note that, this classification for LHT-TPV is valid only for $A_H \geq 120$ GeV, so that it has sufficient branching fraction for $ZZ^{(*)}$. We shall discuss the other cases later in subsection 6.4.2.

Our task now is to distinguish between the look-alike models within each category. We do so in the following subsections.

6.4.2. Pairwise dilepton invariant mass distribution of the four leptons

One can go a little further in the task of model discrimination by combining the information from M_{4l} plots with distributions in the invariant mass distribution M_{ij} $(i, j = 1, 2)$ of the OS lepton pairs. Taking events with two pairs of opposite-sign leptons, we first order the leptons of each sign in the descending order of transverse momentum. In order to be sufficiently general in our analysis, no constraint on the flavour of the leptons is imposed while pairing them up. This is because, in SUSY-RPV, flavours of the leptons coming from neutralino decays are not correlated in general, apart from constraints coming from the antisymmetry in the first two indices of the λ_{ijk}-type terms in the superpotential. Thus in general we can form four possible pairs of opposite sign (OS) leptons.

For the models belonging to *category-2*, i.e., SUSY-RPV and UED-KKC, the M_{ij} distributions show no peaking behaviour. But, we see in the insets of Figure 6.4 that the M_{ij} distributions for UED-KKC show a prominent edge at $\sim$ 35 (50) GeV for point A (point B). We note that in 50% of the cases, the lepton pairs come from the same decay chain starting with a Z_1 (as described in detail in the context of angular correlation between the lepton-pairs in subsection 6.4.3). Therefore, an invariant mass edge is expected at the value given by $\sqrt{(M_{Z_1}^2 - M_{L_1}^2)(M_{L_1}^2 - M_{\gamma_1}^2)/M_{L_1}^2}$, which comes out to be 32.36 (50.95) GeV for point A (point B).

For the SUSY-RPV point under consideration, we also see in Figures 6.4 and 6.5 an edge in the invariant mass distributions of two OS leptons near the corresponding neutralino mass. But as the two leptons in the pairs we consider have equal probability of coming from either the same chain or two different chains, the mass-edge in the distributions is smeared by the "wrong combinations". If one forms OS leptons pairs with a very small opening angle between them, the neutralino mass-edge will become very sharp. As the lightest neutralino mass can be as low as 46 GeV [17], the position of the invariant mass edge for UED-

KKC and SUSY-RPV will not be very different for neutralino masses close to this bound. However, for neutralino masses higher than $\sim$ 100 GeV, the edge positions will be quite different, as in UED-KKC the value obtained cannot be that large in any allowed region of the parameter space.

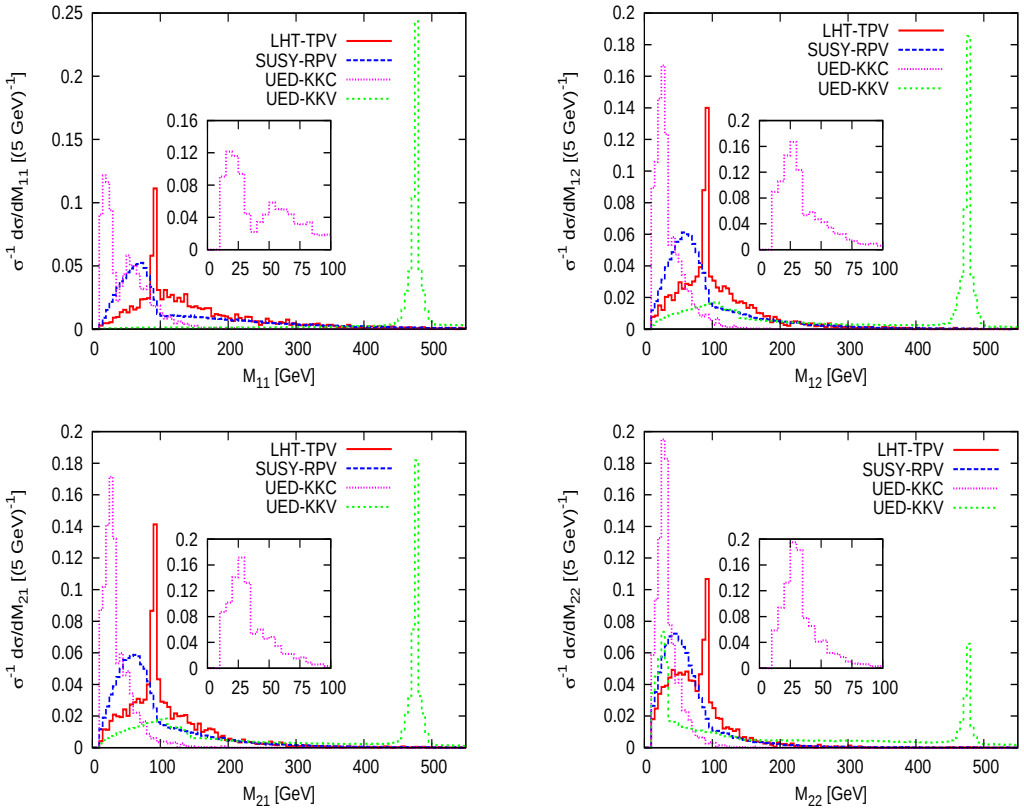

Figure 6.4.: Normalized invariant mass distribution of OS lepton pairs formed out of the four leptons with total charge zero. The above distributions are for point A, at $\sqrt{s} = 14$ TeV, after Cut-2. The insets are shown in order to clearly identify the position of the invariant mass edge for UED-KKC.

In case of models belonging to *category-1*, we can see from Figures 6.4 and 6.5 that the distributions for UED-KKV show a clear peak at the same value of M_{ij} for all the four possible cases. The peak is at the mass of γ_1 which is 475 (800) GeV for point A (point B). The two OS leptons coming from the decay of a γ_1 are expected to be of high transverse momentum, thereby constituting the majority of (11) pairs. Therefore, the peak height is very large for the M_{11} distribution. As we

gradually consider OS combinations of softer leptons, the peak height reduces . This is because, most of the softer leptons come from intermediate stages of the cascade, and invariant mass distributions involving them will just give rise to a broad overall distribution. Therefore, in UED-KKV, as long as the LKP is the heavy photon, such an invariant mass peak is an unmistakable feature of the model. Here, one should also note that the position of the OS dilepton peak is always different from the position of the four-lepton peak as we obtain in UED-KKV. The difference, although not very large, can be observed at the LHC given the fact that the four-lepton channel is a rather clean one. Looking at Figures 6.3 and 6.4 we find that for point A, the M_{4l} peak is roughly at 509 GeV (M_{Z_1}) and the M_{ij} peaks are at 475 GeV (M_{γ_1}). Hence the difference between the values of these two peak positions, which in this case is around 34 GeV, is large enough to be measurable within the experimental resolutions at the LHC. Moreover, note that, these two peaks appear in two different distributions making the resolution even easier. Similar considerations apply for point B, too.

In the example considered here, the corresponding distributions for LHT-TPV also show a clear peak at the mass of the Z-boson ($\sim$ 90 GeV), as we can see from Figures 6.4 and 6.5. The Z-peak is superposed over a broad M_{ij} distribution coming from leptons from W's. Note that for point A, the branching fraction of $A_H \to ZZ$ is 22% and the corresponding branching fraction $A_H \to W^+W^-$ is 77%. Therefore, relatively fewer dilepton pairs come from the decay of a Z-boson and hence the fraction of events under the Z-peak is smaller compared to the total distribution. For point B, as the $A_H \to ZZ$ branching fraction increases to 35%, the peak at M_Z is even more prominent over the l^+l^- continuum coming from W^+W^-. This, however, is not generic to LHT-TPV. As discussed in detail in Chapter 4, as far as the decays of A_H is concerned, there are essentially three possible cases for this model [18, 19]. For lower masses ($M_{A_H} \lesssim 120$ GeV, $f \lesssim 800$ GeV) the decay of A_H is dominated by the loop-induced two-body modes into fermions (case-1), whereas for higher masses ($M_{A_H} > 2M_W, f > 1070$ GeV) the two-body modes to gauge boson pairs dominate (case-3). For intermediate masses, both the two-body and three-body modes compete (in the three-body mode we have one off-shell $W^\pm$ or Z) (case-2). The points we have analysed here (point A and B), belong to case-3. For case-1 one would obtain a very clear peak in the OS dilepton invariant mass distribution but no peak in M_{4l}, while in case-2 a peak is expected in both OS dilepton and four-lepton distributions at the same

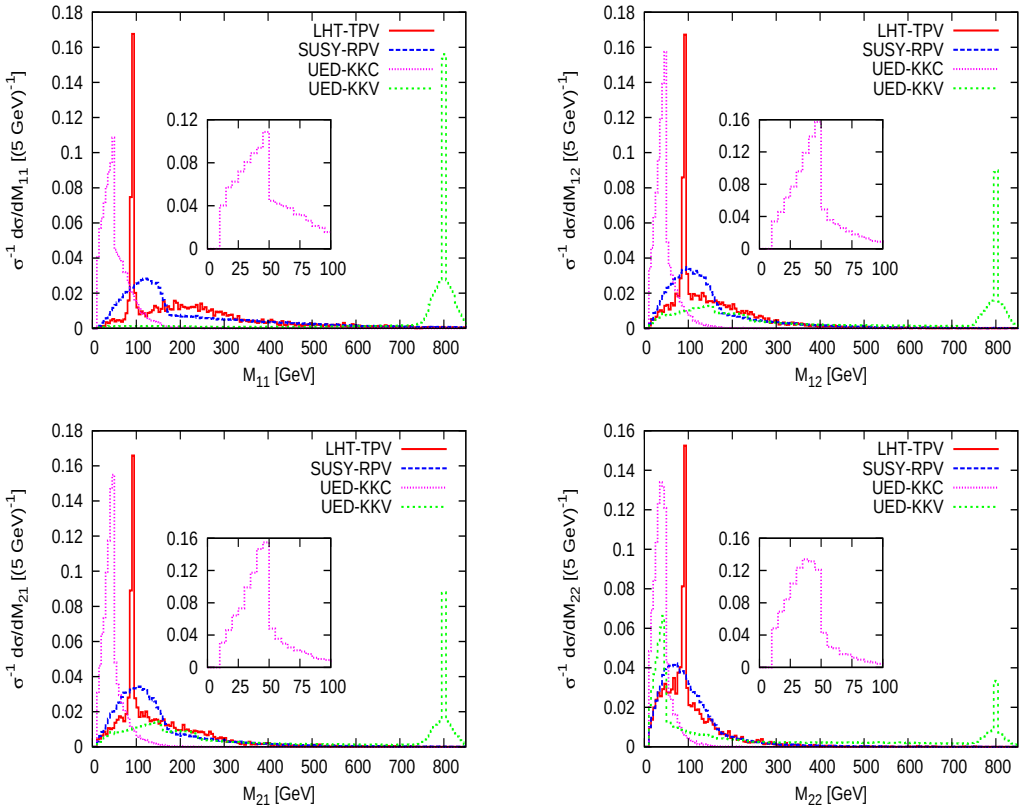

Figure 6.5.: Same as Figure 6.4, for point B.

mass-value. Therefore, case-1 will give rise to a situation where LHT-TPV belongs to category-2, but it will be distinguishable from SUSY-RPV and UED-KKC by its dilepton peak. And in case-2, LHT-TPV would belong to category-1, but it can still be distinguishable from UED-KKV by the fact that the OS dilepton and four-lepton peaks will be at the same mass-value for LHT-TPV, but at different values for UED-KKV. Moreover, in case -2, 120 GeV $\lesssim M_{A_H} \lesssim$ 160 GeV, and no peak is expected in UED-KKV at such a low value of the dilepton invariant mass. For details on the reconstruction of such peaks above SM backgrounds in LHT-TPV, we refer the reader to Chapter 4. Thus, we note that the features of OS dilepton invariant mass distributions, if used in conjunction with other important kinematic characteristics, can help in discriminating models belonging to different categories.

In addition to the invariant mass distributions of the different possible OS

dilepton pairs formed out of the four leptons, it might also be useful to look into pairwise correlation of the different M_{ij}'s as shown in Figure 6.6. In this figure, for the purpose of illustration, we show the correlation of (M_{11}, M_{12}) and (M_{11}, M_{22}) for the various models at point A on an event-by-event basis (at $\sqrt{s} = 14$ TeV after Cut-2). We can see from Figure 6.6 that for the models where we observe peaks in the M_{ij} distributions, the (M_{11}, M_{12}) correlation plot shows two typical lines parallel to the M_{11} and M_{12} axes at the values of the peak-position (around 475 GeV for UED-KKV and 90 GeV for LHT-TPV). On the otherhand, for the models showing an edge in the M_{ij} distributions we see from the scatter plots that the values of M_{ij} are mostly concentrated within the upper-bound given by the position of the edge (around 100 GeV for SUSY-RPV and 35 GeV for UED-KKC).

If both the OS dilepton pairs 11 and 22 come from a γ_1 in UED-KKV or a Z-boson in case of LHT-TPV, then M_{11} and M_{22} will have the same value (with an error-bar, due to detector effects etc.) in the corresponding event. That's why we expect a "blob" in the (M_{11}, M_{22}) plane as can be seen from Figure 6.6 for UED-KKV and LHT-TPV (centred around M_{γ_1} and M_Z respectively). For UED-KKC or SUSY-RPV, the boundedness of M_{ij}'s is once again reflected by the "box-like" distribution, the spread away from the boxes being significantly lesser than for the (M_{11}, M_{12}) case, as the leptons in the pair 22 are much softer. As we have four possible OS lepton pairings as explained before, one can have six different correlation plots between them. But all the essential features remain the same as in the two correlation plots we show for the various models.

6.4.3. Pairwise angular correlation of the four leptons

In this subsection, we consider the correlation in the opening angle between the lepton pairs. The pairs have been formed out of the four leptons following the same prescription as used in the previous subsection.

In Figures 6.7 and 6.8 we have presented distributions of the cosine of the opening angle between the OS lepton pairs for point A and point B respectively. The opening angle is calculated in the lab frame and is defined by the relation

$$cos\theta_{ij} = \frac{\vec{p}_i.\vec{p}_j}{|\vec{p}_i||\vec{p}_j|} \; ; \quad i,j = 1,2 \tag{6.7}$$

where $\vec{p}_i$ and $\vec{p}_j$ stand for the momenta of positive and negatively charged leptons

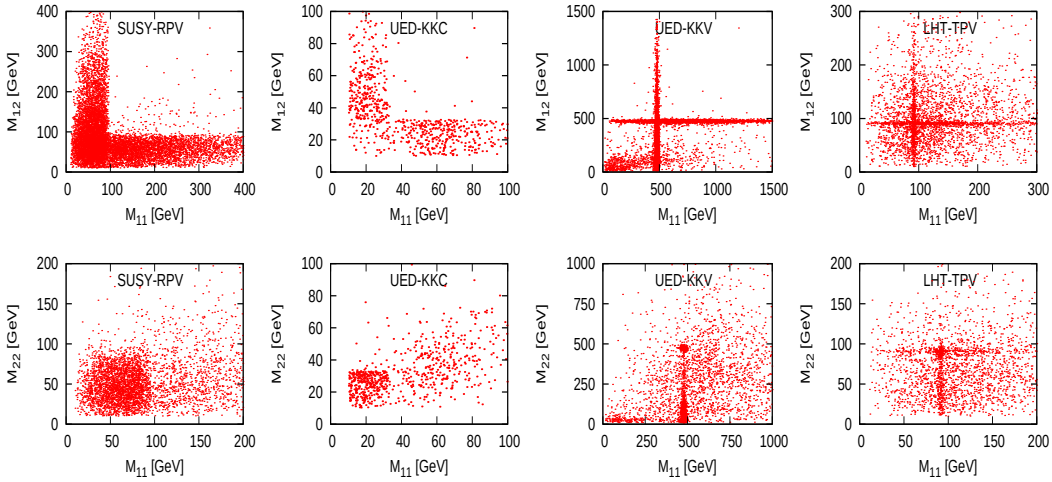

Figure 6.6.: Pairwise correlation of opposite-sign dilepton invariant mass on an event-by-event basis for point A in various models at $\sqrt{s} = 14$ TeV, after Cut-2. We have shown two of the six possible correlations, the essential features in the rest being the same.

respectively.

In order to quantify the difference between the various models in the distribution of $cos\theta_{ij}$, we define the following asymmetry variable:

$$A_{ij} = \frac{\int_0^{+1} \frac{d\sigma}{dcos\theta_{ij}} d(cos\theta_{ij}) - \int_{-1}^{0} \frac{d\sigma}{dcos\theta_{ij}} d(cos\theta_{ij})}{\int_0^{+1} \frac{d\sigma}{dcos\theta_{ij}} d(cos\theta_{ij}) + \int_{-1}^{0} \frac{d\sigma}{dcos\theta_{ij}} d(cos\theta_{ij})}. \tag{6.8}$$

As we are considering the normalized distribution of $cos\theta_{ij}$ here, the denominator of A_{ij} as defined in Equation 6.8 will be 1. In Table 6.2 we show the values of A_{ij} in the different models under consideration.

Let us first consider the *models belonging to category-2*. We can see from Figures 6.7 and 6.8 that for SUSY-RPV, the distribution of $cos\theta_{ij}$ tends to peak towards $+1.0$. This is because the fraction of OS lepton pairs which are coming from the decay of a sufficiently boosted single neutralino tend to be highly collimated. The rest of the combinations (which include two leptons coming from two separate decay chains, or one coming from a chargino and another from a neutralino decay) will have OS leptons which are largely un-correlated. Thus we can see a overall flat distribution of $cos\theta_{ij}$ with a very significant peaking towards $+1.0$. For the same reason, the values of A_{ij} in SUSY-RPV in Table 6.2 are

Point A				
Variable	SUSY-RPV	LHT-TPV	UED-KKC	UED-KKV
A_{11}	0.46	0.37	0.17	-0.11
A_{12}	0.44	0.28	0.34	0.06
A_{21}	0.44	0.28	0.34	0.07
A_{22}	0.32	0.15	0.12	0.08
Point B				
A_{11}	0.39	0.38	0.16	-0.24
A_{12}	0.37	0.33	0.18	-0.02
A_{21}	0.38	0.33	0.16	5.27×10^{-4}
A_{22}	0.22	0.18	0.11	0.03

Table 6.2.: Asymmetry variable (A_{ij}), as defined in eqn. 6.8, in the different models for point A and point B. The values quoted are at $\sqrt{s} = 14$ TeV, after Cut-2.

larger than in the other models for all i, j. We should note here that the boost of the neutralino is large, thanks to the substantial mass splitting among the gauginos usual in mSUGRA. In a generic MSSM model, the splittings might become smaller, thereby rendering the neutralinos less boosted and the distributions of $cos\theta_{ij}$ less sharply peaked towards $+1.0$.

For UED-KKC, we have two possibilities while forming the OS lepton pairs - the two leptons can either come from the same decay chain or they can come from two separate decay chains. In the former case, we expect the two OS leptons to have a smaller opening angle in general. This is because, they come from the decay chain $Z_1 \rightarrow l^+l^-\gamma_1$, where the parent Z_1 will be carrying the boost of the initially produced Q_1 . As the leptons themselves have very low p_T's in the rest frame of the Z_1, this boost of the Z_1 will make them collimated to an extent. For the second possibility, the leptons are, in many cases, nearly back-to-back as they come from the cascade decay of two Z_1's which for a significant fraction of events lie in two different hemispheres of the detector. For point A, the mass splittings are quite small between the $n = 1$ KK-excitations, whereas for point B, they are relatively larger. Since we have demanded two of the leptons to have p_T greater than 20 GeV, it is very likely from the point of view of UED mass splittings that for point A, in a larger fraction of events, both of the hard leptons will not come out from the same decay chain . Therefore, in a significant number of events, the combinations (12) and (21) are expected to be from the same chain, whereas the (11) and (22) pairs will involve both the decay chains. This leads us to expect the cosθ_{12} and cosθ_{21} distributions to be more peaked towards $+1.0$ than towards -1.0, while the cosθ_{11} and cosθ_{22} distributions have slight peaking near both $+1.0$ and -1.0. It can be readily verified that Figure 6.7 is in conformity with these observations. Similarly, we see from Table 6.2 that (for point A) the values of $A_{12}(= 0.34)$ and $A_{21}(= 0.34)$ are relatively higher and positive, implying significant asymmetry with more events having cos$\theta >$ 0. We also note that $A_{11}(= 0.17)$ and $A_{22} = (0.12)$ indicate more symmetric distributions for cosθ_{11} and cosθ_{22} as discussed above. This asymmetry, however, is no longer expected if the mass-splittings become larger, as then the OS lepton pairs can come with equal probability from both the chains. We observe this feature in case of point B in Figure 6.8 and also in Table 6.2. Therefore, in UED-KKC, the distribution of cosθ_{ij} is in general *much less asymmetric towards* $+1.0$ as compared to SUSY-RPV.

Thus, based upon the above features, one should be able to distinguish between SUSY-RPV and UED-KKC. We shall see in what follows that there are also other features like the total charge of the four leptons, or the ratio of five or higher lepton to four-lepton cross-sections which can act as useful discriminators between the models belonging to category-2.

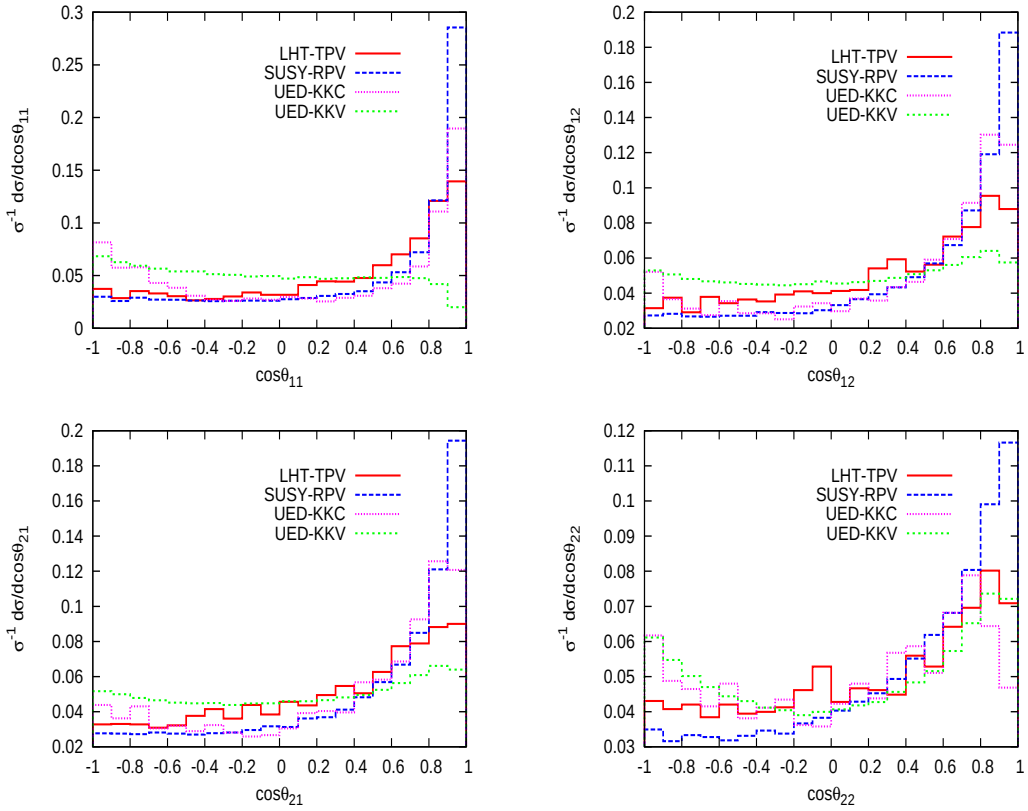

Figure 6.7.: Normalized distribution of $\cos\theta_{ij}$ in the different models for point A at $\sqrt{s} = 14$ TeV after Cut-2.

Next we consider the *models belonging to category-1*. In case of UED-KKV, the two OS leptons of highest p_T come in most cases from the decay of a γ_1 which itself has a very low p_T to start with. So, in the rest frame of γ_1, the two leptons will almost be back-to-back, leading to the slight peaking of $cos\theta_{11}$ towards -1.0 as seen from Figures 6.7 and 6.8. This interesting feature of UED-KKV is also reflected in the value of $A_{11} = -0.11$ (-0.24) for point A (point B). The distributions for $\cos\theta_{12}$ and $\cos\theta_{21}$ on the other hand are very flat indicating that these leptons have no angular correlation between them. This is not unexpected, since the combinations (12) and (21) will generally be formed when one of the leptons (the harder one with index 1) comes from the decay of γ_1, and the other, softer one, from the intermediate stages of the cascade (mostly from the decay of Z_1, W_1 or L_1). Therefore, A_{12} and A_{21} are close to zero as can be seen from Table 6.2. Finally, we see that the distribution for $\cos\theta_{22}$ shows a peaking behaviour towards

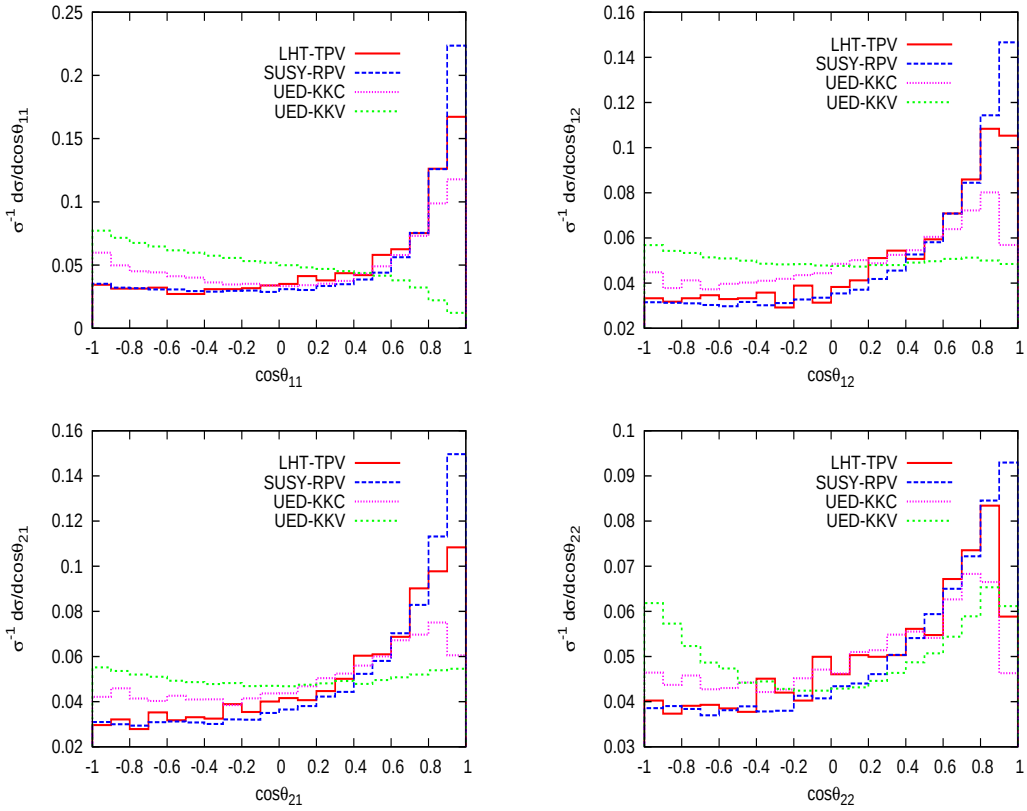

Figure 6.8.: Normalized distribution of $\cos\theta_{ij}$ in the different models for point B at $\sqrt{s} = 14$ TeV after Cut-2.

both $+1.0$ and -1.0. This can be understood from the fact that the two softest leptons almost always come from the intermediate stages of the cascade where they emerge from either the decays of Z_1 and W_1. A large fraction of Z_1-initiated events gives rise to collimated leptons (giving rise to the peaking towards $+1.0$, while a significant fraction of events where the leptons come from W_1 will have them coming out in opposite directions (responsible for the peaking towards -1.0.

Finally, from all the distributions of $\cos\theta_{ij}$ and the values of A_{ij} it is clear that the LHT-TPV model has features similar to SUSY-RPV. In particular, as the leptons come from the decays of a boosted A_H (via intermediate W^+W^- or ZZ states), they tend to be collimated. The collimation here is somewhat less than as in SUSY-RPV because of the fact that for the chosen parameters (point A), the squark (gluino)-neutralino mass difference ($\sim 471(509)$ GeV) is much larger than the q_H-A_H mass difference (~ 375 GeV).

Thus while both UED-KKV and LHT-TPV might give rise to clear peaks in the M_{4l} distribution, they show *entirely different behaviour* as far as the angular correlation between the OS lepton pairs is concerned. This, therefore, can act as a very good discriminator between these models belonging to category-1. In the following subsections, we shall look into some more variables that can be used to further clarify the distinction between these two models, especially when different types of mass-spectra in LHT-TPV tend to obliterate the $4l$ mass peaks so spectacular for our chosen benchmark points.

We should note here that there is a dip observable in the $\cos\theta_{ij}$ distributions towards the last bin near $+1.0$ for UED-KKC and LHT-TPV. This dip, however, is not seen in the $\cos\theta_{11}$ distribution. This is stemming from the fact that we have demanded all OS lepton pairs to have an invariant mass greater than 10 GeV. Now, when the lepton p_T's are not very high themselves, the invariant mass becomes very small when the angle between the leptons tends to zero. These events, therefore, have been removed by the above cut, giving rise to the observed dip. As for the (11) combination the leptons are much harder, the lepton pairs always pass the invariant mass cut, and this feature does not appear for this case.

6.4.4. Total charge of the four-leptons

Here we consider the variable total charge (Q) of the four leptons obtained in the general channel $4l+ \geq 2j + \not{E}_T$. Q can take values in the set {-4,-2,0,2,4}. In Figures 6.9, 6.10 we see the distribution of Q for the different models. We observe that UED-KKC clearly stands out as in this case the four leptons come from two cascade decay chains starting with Z_1's leading to $Q = 0$ for all the events. For the RPV coupling considered for point A, the lightest neutralino in SUSY-RPV always decays to a pair of leptons and a neutrino. If no other leptons come from the cascade, these four leptons will have a total charge $Q = 0$. On the other hand, if some additional leptons come from the decays of charginos or sleptons in the cascade, the lepton multiplicity in those events will be higher than four. It is however possible in a certain fraction of events to have a pair of leptons (coming from the decay of a single boosted neutralino) to be so highly collimated that they do not pass the lepton-lepton separation cut. These events might lead to a total charge $Q = \pm 2$. For LHT-TPV different combinations of W and Z decays can lead to four-lepton events. Hence, the expected values of Q are (-2,0,2). For UED-KKV,

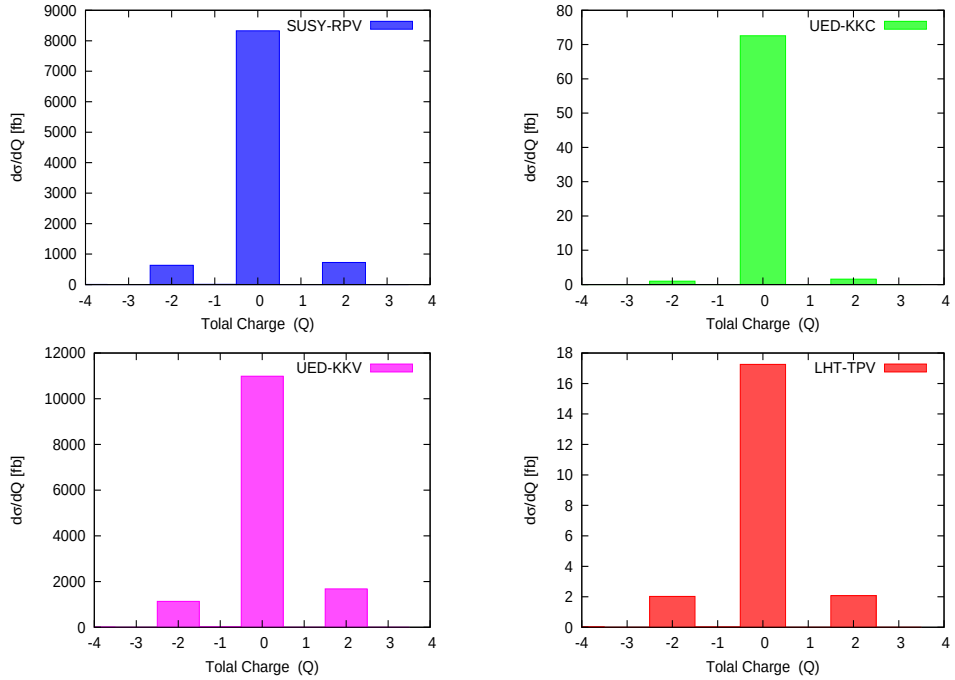

Figure 6.9.: Total charge distribution of the four-leptons in the different models: for point A, at $\sqrt{s} = 14$ TeV, after Cut-2.

the leptons coming from the decay of γ_1 are always oppositely charged. But, it is possible to obtain W_1's of either charge from the cascades, giving rise to same-sign lepton pairs, over and above those coming from γ_1. This leads to $4l$ events with $Q = \pm 2$. Hence, essentially, from the distribution of Q, the UED-KKC model can be separated from the rest.

6.5. Five or higher lepton events

For all of the models discussed here, additional leptons, over and above those coming from sources discussed in the previous subsections, can come from various stages in the cascades. In Table 6.3, the rates for final states with five or more leptons are presented for our chosen benchmark points. The p_T cut has been uniformly maintained at 10 GeV for each lepton. The ratios of the five or higher lepton event rates to those for four-leptons are also presented. The SM backgrounds for channels with lepton multiplicity greater than four are negligible.

The rates for such added profusion of leptons depend on the respective

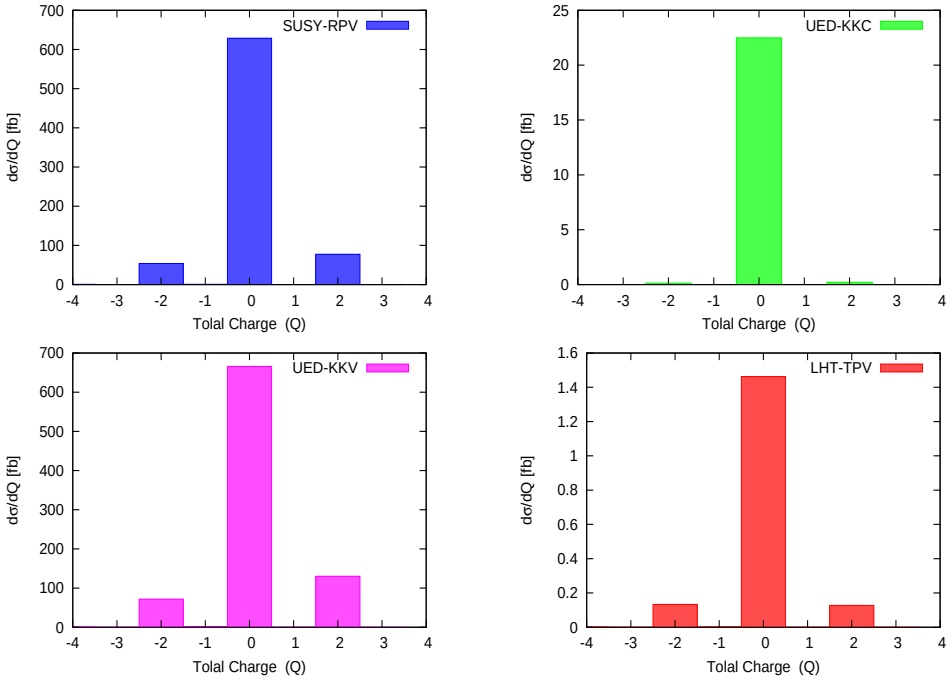

Figure 6.10.: Same as Figure 6.9, for point B.

spectra. The deciding factor here is the leptonic branching ratio for Z_2-odd particles at intermediate stages of the cascade. In this respect, UED-KKC and LHT-TPV fare worse. For UED-KKC, five-lepton events are not expected from the production and decays of the $n = 1$ KK-particles. Hence, the very small number of events with lepton multiplicity higher than four come from the decays of B-mesons, pions or photons. For LHT-TPV, with our choice of parameters, there are few additional leptons coming from the intermediate steps in the cascade. Therefore, in most of the $5l$ events found, the leptons are entirely coming from the decay of the two A_H's produced. One should note that this rate will increase for other choices of parameters, especially when the T-odd gauge bosons and the T-odd leptons are lighter than the T-odd quarks. For the SUSY-RPV examples considered, a proliferation of multilepton events is a well-known fact, and that is reflected in the high value of $\frac{\sigma(\geq 5l)}{\sigma(4l)}$. For point B, the ratio is higher (0.6) than for point A (0.35). This is because, as can be seen in section 6.2.2, in the former case, the SUSY mass spectrum is such that the chargino can decay to sleptons/sneutrinos, whereas in the later case such decays are not allowed by phase-

Point A			
Model	$\sigma(4l)$ in fb	$\sigma(\geq 5l)$ in fb	$\frac{\sigma(\geq 5l)}{\sigma(4l)}$
SUSY-RPV	9450.91	3285.85	0.35
UED-KKC	163.36	1.57	0.01
UED-KKV	14008.93	4015.64	0.29
LHT-TPV	21.09	2.82	0.13
Point B			
SUSY-RPV	756.00	450.96	0.60
UED-KKC	26.24	0.12	0.005
UED-KKV	872.94	287.05	0.33
LHT-TPV	1.71	0.24	0.14

Table 6.3.: Cross-section of four and five or more lepton events and the ratio $\frac{\sigma(\geq 5l)}{\sigma(4l)}$ for the different scenarios under consideration. The values tabulated are for point A and point B after isolation cuts and $p_T^l > 10$ GeV for all leptons, at $\sqrt{s} = 14$ TeV.

space considerations. This leads to a higher branching fraction of obtaining a lepton from the cascade, thereby leading to relatively larger rates for events with higher lepton multiplicity in point B. For, UED-KKV, the ratio does not change significantly as we change the mass-scale. Therefore, we conclude that from this ratio, one can always single out the UED-KKC model. In the other models, there is enough room to change the ratios by adjusting the mass-spectra suitably.

6.6. Other possibilities

In addition to the kinds of new particle spectrum considered above, other possibilities of low missing energy look-alikes may offer themselves for detection as

well as discrimination at the LHC. A few illustrative cases are discussed below.

In L-violating SUSY, we have a host of other possibilities. We considered the case of a neutralino LSP with a λ-type RPV coupling in our analysis. In the presence of λ'-type couplings instead, a neutralino will decay to two quarks and a charged lepton/ neutrino. Hence, the rate of four-lepton events will decrease. In addition, we shall not see the asymmetric peaking behaviour observed in the $cos\theta_{ij}$ distributions, too, since the lepton-pairs in this case will not be coming from the decay of a single boosted particle. Similarly, the edge in the dilepton invariant mass distributions will also not be present. There are, however, two features which distinguish this scenario from the rest. Firstly, the total charge distribution will now show a significant increase for $Q = \pm 4$. Secondly, with one lepton coming from each lightest neutralino during the SUSY cascades in two chains, a pair of same-sign dileptons occurs frequently at the end of the decay chains. Since the gluino, too, is of Majorana nature, being thereby able to produce charginos of either sign, there will be a surge in same-sign trilepton (SS3ℓ) events observed [21]. We have studied this scenario in detail in Chapter 5. In this connection, it should be mentioned that large rates of SS3ℓ can be used to distinguish several cases of L-violating SUSY with other models predicting low MET, as in those models we expect very low rates of SS3ℓ, as seen for the case of LHT-TPV in Chapter 5.6. SS3ℓ, in conjunction with SS4ℓ and their mixed-sign counterparts, can also be used to distinguish between different L-violating cases within SUSY, as has been seen in Chapter 5.7.

A stau LSP scenario with λ-type couplings will also have similar implications. Here, stau will decay to a lepton and a neutrino. If we have a stau LSP with λ'-type couplings instead, the 4l-signal will be suppressed, as the stau will decay to two quarks in this case. We also note that in presence of relatively larger values of λ'-type couplings, there is a region of the mSUGRA parameter space where the sneutrino can also become an LSP [7,20]. However, the sneutrino in this case will decay to a pair of quarks thus reducing the possibility of having four leptons in the final state. Finally, we also remark that in the presence of bilinear R-parity violating terms, if we choose the RPV parameters to be consistent with the observed neutrino mass and mixing patterns, the neutralino LSP can decay to $W\mu$, $W\tau$ or $Z\nu$ [22]. Hence, four-lepton events will again be viable with a peak at M_Z in the OS dilepton invariant mass distributions. But there will not be any peak in the corresponding M_{4l} distribution. This last feature thus seems to be generically

true in SUSY-RPV.

In the framework of a minimal UED model with KK-parity conservation, γ_1 is the LKP and characteristic signatures of this scenario were discussed throughout this article. The mUED model is based on the simplifying assumption that the boundary kinetic terms vanish at the cut-off scale Λ. This assumption restricts the mUED spectrum in such a way that the splittings among different KK excitations are small enough to result in soft final state particles and thus low missing E_T. As discussed in Chapter 2.2, the boundary terms receive divergent contributions and thus require counterterms. The finite parts of these counterterms remain undetermined and are therefore free parameters of the theory. This additional freedom could be exploited to end up with an unconstrained UED (UUED) scenario with several different possibilities:

- Particular combinations of the aforementioned free parameters can remove the degeneracy of the mUED mass spectrum. This results in harder leptons and jets in the final state and thus gives rise to a harder missing-E_T distribution. Such a version of the UED model no longer falls in the category of *low missing energy look-alikes*. The corresponding criteria for large missing-E_T scenarios will have to be applied in this situation [3].
- The values of the additional parameters could be chosen in such a way that even though the mass spectrum remains degenerate as in the case of mUED, the mass of ν_1 becomes smaller than M_{γ_1}. This leads to a scenario with ν_1 as the LKP and therefore, a possible candidate for cold dark matter. In this case, the γ_1's produced at the end of decay cascades will further decay into $\nu\nu_1$ pairs, resulting in similar phenomenology as in the case of mUED explored in this work. However, the four-lepton event rate in this case will be significantly reduced due to the fact that Z_1 mostly decays to $\nu\nu_1$ pairs, as this channel will now have enhanced phase-space available as compared to lL_1.
- One can also have such a combination of parameters that only the positions of Z_1 and $W_1^{\pm}$ in the $n = 1$ mass spectrum are altered. The first possibility is that Z_1 and $W_1^{\pm}$ are heavier than the $n = 1$ quarks. In such situations, $n = 1$ quarks will decay into qlL_1 via tree-level 3-body modes. L_1 subsequently decays into $l\gamma_1$ and combining the two cascade decay chains, one can then obtain four-lepton signals. However, the opposite-sign dilepton invariant mass distributions will not show any invariant mass edge in this scenario.

The other possibility is that Z_1 and $W_1^{\pm}$ may become lighter than the $n = 1$ leptons. Here, the possible decay modes of interest are $Z_1 \to ll\gamma_1$ and $W_1^{\pm} \to l\nu\gamma_1$. Phenomenologically, this scenario will again be quite similar to the mUED cases we have studied.

In the framework of UED-KKV, the masses of the KK-fermions have a small dependence on the value of the KK-parity violating coupling h. As shown in Ref. [23], as we increase the value of h, the KK-fermion masses decrease. As the $n = 1$ quarks are much heavier than Z_1 and $W_1^{\pm}$ in mUED with KK-parity conserved, the presence of non-zero KK-violating coupling h does not lead to any appreciable change in the excited quark masses vis-a-vis those of the remaining particles. Therefore, the decay patterns of the $n = 1$ quarks remain the same. However, for smaller R^{-1}, singlet $n = 1$ leptons and the γ_1 are almost degenerate. Therefore, in addition to having a smaller R^{-1}, if we have a larger value of h, singlet $n = 1$ leptons may become lighter than γ_1. For example, this can happen for $R^{-1} = 500$ GeV and $h > 0.01$. Here, the only possible decay channel available for these singlet $n = 1$ leptons is via the KK-parity violating mode to a SM lepton of the same flavour and a Z/γ^*. The phenomenology of this scenario will be significantly different from the one we have considered so far with smaller values of h ($h \sim 0.001$) and a γ_1 LKP, and is therefore an interesting possibility for further studies.

In LHT-TPV, as we have two free parameters κ_q and κ_l which determine the masses of the T-odd quarks and leptons, the possibility of obtaining a fermionic LTP exists. In such cases, via the T-parity breaking terms, these fermions might decay to standard model particles. As observed in Ref. [18], there are two possible ways in which these fermionic LTP's can decay. As the WZW term breaks T-parity only in the gauge sector directly, a T-odd lightest fermion can decay by a three-body mode mediated by a virtual T-odd gauge boson. There is also the possibility of having loop-induced two-body decay modes. Therefore, the major decay channels are $f_H \to Zf$, $f_H \to W\tilde{f}$ and $f_H \to A_H^* f$. In the last case, the off-shell A_H might again decay to four-leptons via ZZ, but there will not be any peak in the M_{4l} distribution. On the other hand, if the LTP is a T-odd charged lepton, one can observe a spectacular five-lepton peak. The other possible decay modes will also lead to $4l$ and $5l$ events in varied rates, although the quantitative predictions of these will require us to determine the relative importance of the three-body and the loop-induced two body decay modes of f_H.

6.7. Summary and conclusions

We have considered four characteristic scenarios which can pass off as low missing energy look-alikes at the LHC. After convincing the reader that UED-KKC in its minimal form, in spite of containing a stable invisible particle, often falls in this category, we have studied the contribution of each scenario to events with four or more leptons. Since total rates alone, at the four-lepton level at least, can mislead one in the process of discrimination, we have resorted to kinematic features of final states in the different cases.

The first of these is the four-lepton invariant mass distribution. On this, we have found that the models get divided into two categories, depending on whether the four leptons show an invariant mass peak or not. While LHT-TPV and UED-KKV are in the first category, SUSY-RPV and and UED-KKC belong to the second one, thus offering a clear distinction.

For distinguishing between models within each category, we have used three observable quantities, namely, angular correlation and invariant mass of opposite-charge lepton pairs, and the total charge of the four observed leptons. It is found that angular correlations as well as the total charge causes SUSY-RPV to stand out quite clearly with respect to minimal UED-KKC. UED-KKV, too, stands out distinctly from the others, as far as angular correlations are concerned. This, however, still leaves room for discrimination. This happens, for example, where LHT-TPV has such a spectrum that the heavy photon LTP does not decay dominantly into four leptons. The distinction of this scenario with SUSY-RPV and UED-KKC is still possible using the pairwise invariant mass distribution of oppositely charged dileptons. We have also found that the relative positions of the dilepton vs. four-lepton invariant mass peaks, and the existence of an 'edge' in the dilepton invariant mass distribution lead to useful discriminating criteria. In addition, the ratio of five or higher lepton event rates to those for four leptons sets UED-KKC apart from the other scenarios.

As mentioned before, we haven't paid particular attention so far to the flavour content of the four leptons. In SUSY-RPV, depending upon the L-violating coupling chosen, the flavour content will change. However one can discover a pattern in the fraction of events with $4e$, 4μ, $2e2\mu$, $3e1\mu$ or $1e3\mu$, for specific RPV couplings (here e stands for the electron or positron and μ stands for the muon or anti-muon, and, for example, $3e1\mu$ means a four-lepton event with 3 e's and 1

μ). For the λ_{122} coupling that we chose for our analysis, we obtain, as expected, around 47.5% events to be of $1e3\mu$-type, whereas $2e2\mu$ and 4μ being $\sim 25\%$ each. No events are expected to be of $3e1\mu$ or $4e$-type. This is certainly a notable feature, but as observed above, these flavour ratios will change if we change the L-violating coupling. For UED-KKC one will always obtain $4e$, 4μ or $2e2\mu$-type events, while for UED-KKV all flavour combinations are possible. For LHT-TPV, depending upon the point of parameter space one is in, all flavour combinations are once again possible with varying fractions. Thus, although flavour content of the leptons can sometimes be useful, they might not be a very robust feature of the models, except for the case of UED-KKC.

We have also made a set of qualitative observations on other related scenarios such as RPV via λ'-type or bilinear terms, situations with stau or sneutrino LSP, UED-KKC with an unconstrained particle spectrum and different LTP (LKP) in LHT-TPV (UED-KKV). The qualitative changes that some of these scenarios entailed have been pointed out. On the whole, while the various theoretical models in their 'minimal' forms offer clear methods for distinction, a confusion can always be created in variants of the models with various degrees of complications. The same observation holds also for theories predicting large missing E_T. Thus one may perhaps conclude that, while some striking qualitative differences await one in the approach from 'data to minimal theories', there is no alternative to an analysis of the mass spectrum, possibly linking spin information alongside, if one really has to exhaust all possibilities that nature may have in store. Furthermore, the availability of data with high statistics, enabled by large accumulated luminosity, is of great importance. All this is likely to keep the highly challenging character of the LHC experiment alive till the last day of its run.

Bibliography

[1] N. Arkani-Hamed, G. L. Kane, J. Thaler and L. T. Wang, JHEP **0608** (2006) 070.

[2] J. Hubisz, J. Lykken, M. Pierini and M. Spiropulu, Phys. Rev. D **78**, 075008 (2008).

[3] A. Datta, G. L. Kane and M. Toharia, arXiv:hep-ph/0510204.

[4] P. Meade and M. Reece, Phys. Rev. D **74**, 015010 (2006); L. T. Wang and I. Yavin, JHEP **0704**, 032 (2007); M. M. Nojiri and M. Takeuchi, Phys. Rev. D **76**, 015009 (2007); C. Kilic, L. T. Wang and I. Yavin, JHEP **0705**, 052 (2007); A. Datta *et al.*, Phys. Lett. B **659**, 308 (2008); G. Hallenbeck *et al.*, Phys. Rev. D **79** (2009) 075024; A. Belyaev *et al.*, Pramana **72**, 229 (2009); B. Bhattacherjee *et al.*, Phys. Rev. D **81** (2010) 035021.

[5] K. Ghosh, S. Mukhopadhyay, B. Mukhopadhyaya, JHEP **1010**, 096 (2010).

[6] T. Sjöstrand *et al.*, JHEP **0605**, 026 (2006).

[7] B. C. Allanach *et al.*, Phys. Rev. D **75**, 035002 (2007).

[8] A. Djouadi *et al.*, Comput. Phys. Commun. **176**, 426 (2007).

[9] A. Pukhov, arXiv:hep-ph/0412191.

[10] A. Datta, K. Kong and K. T. Matchev, arXiv:1002.4624 [hep-ph].

[11] J. Alwall *et al.*, arXiv:0712.3311 [hep-ph]; P. Skands *et al.*, JHEP **0407**, 036 (2004).

[12] M. L. Mangano *et al.*, JHEP **0307**, 001 (2003).

[13] J. Pumplin *et al.*, JHEP **0207**, 012 (2002).

[14] M. R. Whalley, D. Bourilkov and R. C. Group, arXiv:hep-ph/0508110. `http://projects.hepforge.org/lhapdf/`

[15] G. Aad *et al.* [The ATLAS Collaboration], arXiv:0901.0512 [hep-ex]; G. L. Bayatian *et al.* [CMS Collaboration], J. Phys. G **34**, 995 (2007).

[16] Bruce Mellado, private communication.

[17] C. Amsler *et al.* [Particle Data Group Collaboration], Phys. Lett. **B667**, 1 (2008).

[18] A. Freitas, P. Schwaller and D. Wyler, JHEP **0809**, 013 (2008).

[19] S. Mukhopadhyay, B. Mukhopadhyaya and A. Nyffeler, JHEP **1005**, 001 (2010).

[20] M. A. Bernhardt *et al.* Phys. Rev. D **79** (2009) 035003.

[21] B. Mukhopadhyaya, S. Mukhopadhyay, Phys. Rev. **D82**, 031501 (2010). S. Mukhopadhyay and B. Mukhopadhyaya, Phys. Rev. D **84**, 095001 (2011).

[22] S. Roy and B. Mukhopadhyaya, Phys. Rev. D **55**, 7020 (1997); B. Mukhopadhyaya, S. Roy and F. Vissani, Phys. Lett. B **443**, 191 (1998); M. Hirsch *et al.*, Phys. Rev. D **62**, 113008 (2000).

[23] B. Bhattacherjee, Phys. Rev. D **79** (2009) 016006.

Chapter 7.

Summary and conclusions of the thesis

The physics of electroweak symmetry breaking and the possible existence of new physics beyond the standard model are being thoroughly probed at the Large Hadron Collider (LHC). One distinguishing criterion for new physics, often used in these searches, is a large amount of missing transverse energy, carried away by massive stable particles. However, this criterion may not be fulfilled in a number of well-motivated theoretical scenarios. In this thesis, we have considered several such situations, their characteristic signatures in the form of multiple leptons, and the criteria for distinguishing among various scenarios of this kind. In this connection, we have emphasized the usefulness of one type of signals, namely, same-sign trileptons and four-leptons, not only as a clean discovery mode for new physics but also as a probe to the underlying dynamics of supersymmetry with lepton number violation.

In Chapter 1, we have briefly reviewed the standard model, and both theoretical and experimental motivations for trying to find out new physics beyond it. We describe several possible scenarios of new physics in Chapter 2, namely supersymmetry, minimal universal extra-dimensions, and little Higgs models. In each case, we also discuss how the often imposed Z_2 symmetries, which make

the lightest among the predicted set of new particles stable, can be violated. The final chapter in the introductory part, Chapter 3, discusses the salient features of the LHC, typical components of a collider detector and also some important kinematic variables used in hadron collider physics.

In the second part of the thesis we discuss the identification of certain low missing-energy scenarios at the LHC, by devising distinctive signals which are also less prone to SM backgrounds. In Chapter 4, we consider the discovery of low mass resonances in the littlest Higgs model with T-parity violation. In the presence of the T-parity violating Wess-Zumino-Witten (WZW) anomaly term, the otherwise stable heavy photon A_H in the Littlest Higgs model with T-parity (LHT) decays to either SM gauge boson pairs, or to SM fermions via loop diagrams. We make a detailed study of the collider signatures where the A_H can be reconstructed from invariant mass peaks in the opposite sign same flavour dilepton or the four-lepton channel. This enables us to obtain information about the fundamental symmetry breaking scale f in the LHT and thereby the low-lying mass spectrum of the theory. We also discuss the SM backgrounds that arise in these channels in detail, and devise ways to reduce them. We find that using these signals, it is possible to cover a large part of the typical parameter space of LHT. For example, at the $\sqrt{s} = 14$ TeV LHC and with an integrated luminosity of $30\,\text{fb}^{-1}$, one can probe a scale of f up to 1.5 TeV and T-odd quark masses almost up to 1 TeV. In this region of the parameter space, the mass of the reconstructed A_H ranges from 66 GeV to 230 GeV.

In Chapter 5, we point out that same-sign multilepton events, not given due attention yet for new physics search, can be extremely useful at the LHC. After showing the easy reducibility of the standard model backgrounds, we demonstrate the viability of same-sign trilepton (SS3ℓ) signals for R-parity breaking supersymmetry, at both 7 and 14 TeV. We find that same-sign four-leptons (SS4ℓ), too, can have appreciable rates. Same-sign trileptons are also expected, for example, in little Higgs theories with T-parity broken by anomaly terms. For the case of lepton-number (L) violating supersymmetry (SUSY), we demonstrate the efficacy of these signals for both minimal supergravity as well as a more general phenomenological SUSY model. Furthermore, we show that it is extremely unlikely to ever achieve similar rates in R-parity conserving SUSY. In addition, we show how SS3ℓ and SS4ℓ, in conjunction with the mixed-sign trilepton and four-lepton channels, can be used to extract dynamical information about the un-

derlying SUSY theory, namely, the Majorana character of the decaying lightest neutralino and the nature of L-violating couplings. We define suitable variables and relationships between them which can be verified experimentally and which are largely independent of the SUSY production cross-sections and the cascade decay branching fractions. These theoretical predictions are validated by Monte Carlo simulations including detector and background effects.

In the final part of the thesis, in Chapter 6, we present a study on the so-called LHC inverse problem. The problem of discriminating possible scenarios of TeV scale new physics with large missing energy signature at the LHC has received some attention in the recent past. We have considered the complementary, and yet unexplored, case of theories predicting much softer missing energy spectra. As there is enough scope for such models to fake each other by having similar final states at the LHC, we have outlined a systematic method based on a combination of different kinematic features which can be used to distinguish among different possibilities. These features often trace back to the underlying mass spectrum and the spins of the new particles present in these models. As examples of "low missing energy look-alikes", we consider supersymmetry with R-parity violation, universal extra dimensions with both KK-parity conserved and KK-parity violated and the littlest Higgs model with T-parity violated by the Wess-Zumino-Witten anomaly term. Through detailed Monte Carlo analysis of the four and higher lepton final states predicted by these models, we show that the models in their minimal forms may be distinguished at the LHC, while non-minimal variations can always leave scope for further confusion.